EMANUELE ROCCIA

BROADBAND QUANTUM LIGHT: FROM SOURCE ENGINEERING TO QUANTUM METROLOGY

UNIVERSITÁ DEGLI STUDI ROMA TRE

DOTTORATO DI RICERCA IN SCIENZADELLA MATERIA,
NANOTECNOLOGIE E SISTEMI COMPLESSI

PH.D. THESIS

Broadband quantum light: from source engineering to quantum metrology

EMANUELE ROCCIA

SUPERVISOR: PROF. MARCO BARBIERI
PH.D. COORDINATOR: PROF. FABIO BRUNI

PUBLICATIONS

This thesis is based upon the following publications and pre-prints:

- *Entangling measurements for multiparameter estimation with two qubits*, E. Roccia, I. Gianani, L. Mancino, M. Sbroscia, F. Somma, M. G. Genoni, M. Barbieri, Quantum Sci. Technol. (2017)

- *What Hong-Ou-Mandel interference says on two-photon frequency entanglement*, M. Barbieri, E. Roccia, L.Mancino, M. Sbroscia, I.Gianani, F. Sciarrino, Scientific Reports 7 (2017)

- *Monitoring dispersive samples with single photons: the role of frequency correlations*, E. Roccia, M. G. Genoni, L. Mancino, I. Gianani, M. Barbieri, M. Sbroscia, Quantum Measurements and Quantum Metrology 4 (1), 64-69 (2017)

- *Heralded generation of high-purity ultrashort single photons in programmable temporal shapes*, V. Ansari, E. Roccia, M. Santandrea, M. Doostdar, C. Eigner, L. Padberg, I. Gianani, M. Sbroscia, J. M. Donohue, L. Mancino, M. Barbieri, C. Silberhorn, Optics express 26 (3), 2764-2774 (2018)

- *Multiparameter approach to quantum phase estimation with limited visibility*, E. Roccia, V. Cimini, M. Sbroscia, I. Gianani, L. Ruggiero, L. Mancino, M. G Genoni, M. A. Ricci, M. Barbieri, Optica 5 (10), 1171-1176 (2018)

- *Assessing frequency correlation through a distinguishability measurement*, M. Sbroscia, I. Gianani, E. Roccia, V. Cimini, L. Mancino, P. Aloe, M. Barbieri, Optics letters 43 (16). 4045-4048

(2018)

The updated and complete list of publications can be found on arXiv.org

CONTENTS

LIST OF FIGURES

LIST OF TABLES

ACRONYMS

APD Avalanche Photo-Diode

BBO Beta Barium Borate

BIPM International Bureau of Weights and Measures

BS Beam Splitter

CRB Cramer Rao Bound

CS Control-Sign

CW Continuous Wave

DOF Degree Of Freedom

FI Fisher Information

FPGA Field Programmable Gate Array

FWHM Full Width at Half Maximum

HOM Hong-Ou-Mandel

HWP Half Wave Plate

JSA Joint Spectral Amplitude

JSI Joint Spectral Intensity

MSE Mean Square Error

PBS Polarised Beam Splitter

PDC Parametric Down-Conversion

PDF Probability Density Function

POVM Positive Operator Valued Measure

PPBS Partially Polarised Beam Splitter

QCRB Quantum Cramer Rao Bound

QET Quantum Estimation Theory

QFI Quantum Fisher Information

QWP Quarter Wave Plate

SLD Symmetric Logarithmic Derivative

SLM Spatial Light Modulator

SM Single Mode

SNSPD Superconducting Nanowire Single Photon Detector

SQL Standard Quantum Limit

TM Temporal Mode

INTRODUCTION

The coming of quantum mechanics in the last century has represented one of the biggest revolutions of Physics and technology thereafter. The exploitation of quantum discoveries for the radical amelioration of currently technology provides one of the tantalising challenges of our time, in response to the Moore's law that cannot escape from the bounds of the quantum reality itself. Citing the *Quantum Manifesto*: "previously untapped aspects of quantum theory are ready to be used as a resource in technologies with far-reaching applications, including secure communication networks, sensitive sensors for biomedical imaging and fundamentally new paradigms of computation".
Since light is increasely becoming a valuable carrier for modern communication, the upgrade to its quantum counterpart, *quantum optics*, seems to be in the same way one of the better proposal to implement in the future quantum technology. Going down this road in last decade many photon-based approaches have been attempted, with the deployment of *single photons* in order to transfer all the basic elements of quantum communication in the optical language. However, this new perspective of quantum technology needs also solid supports, assuring the efficiency and control of photonic devices, such as single-photon sources.

In this thesis I examined the possibility of assessing frequency correlations occurring in a probabilistic two-photon generation event, the *parametric down-conversion*, through the use of quantum metrological approach. In order to well understand the current techniques for identification and measurement of spectral entanglement, a first exploration has been performed with pulse-shaping strategy through the use of spectral resolutive instruments. However, for nearly continuous wave pump light, things become quite more demanding, in terms of frequency resolution.
Hence the needs of using quantum metrology schemes in order to find those methods aiming at circumvent such issue. After the

comprehension of the opportunities provided by the multi parameter estimation approach on the characterisation of dispersive materials, a combination of metrological techniques, proofing that it constitutes a valuable tool in order to solve the spectral correlation assessment, even in future developments.

1 SINGLE-PHOTON TECHNOLOGIES

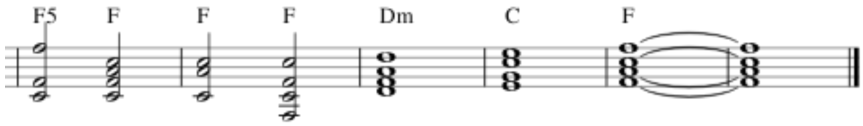

— Also sprach Zarathustra, R. Strauss

1.1 INTRODUCTION

Since 1900, when Max Planck laid the foundations of the *quantum theory of light* [1], the exploitation of radiation for quantum experiments has been widely investigated both in the research world and subsequently for the implementation of novel technologies. The notion of *quantum nature of light* has been firstly approached by Philipp Lenard in 1902, who linked the *frequency* of light and the *energy* of electrons emitted by gases ionisation experiment [2], apparently in opposition with the Maxwell wave theory which predicts that the electron energy would be proportional with the light *intensity*. This idea was then pioneered by Albert Einstein [3], that introduced the concept of *energy discretisation* nature of electromagnetic energy, which can be decomposed on integer multiples of the fundamental quantum energy, equal to the frequency of light multiplied by the Planck's constant. So that, the Einstein description of photo-electric experiment, started the innovative view, unexplored up to that time, of the so-called *dualism nature* of electromagnetic radiation, that is corpuscular and wave-like at the same time.

After a formal quantisation of the electromagnetic field performed

by Dirac [4], who showed that the wave-like properties of light field can be conjugated with the concepts of creation and destruction of photons, many works explored the quantum nature of light, *e.g.* Brown-Twiss interferometer [5], permitting to describe the matter-radiation interaction first with semiclassical theory while subsequently with full quantum theory, after the invention of laser by Maiman [6]. Over the years, interferometry plays a key role for the investigation of the first excited state of the quantised radiation field which contains only one quantum of energy [7–9]: the *single photon*. Indeed, the observation of the *antibunching* property of light appears right away a phenomenon that is truly due to the quantum mechanical nature of radiation. In turn, the discovery of single photon states has led to the fundamental task of how to generate them. Many approaches have been explored, *e.g. quantum dots* constituting nearly on-demand single photon sources [10–12], or heralded photon pair sources, based for example on *parametric down-conversion* (PDC) process [13–16], as well as attenuated light beams [17–19], used for many applications in *quantum communication* until today, like *quantum key distribution* protocols. However, heralded photon pair phenomenons suffer from the issue due to the nature of generation process itself, explored for the first time looking at interference in the Hong-Ou-Mandel (HOM) arrangement [8]: the photon *indistinguishability*. While path and polarisation problem of non-distinguishability has been accomplished easily by the use of linear optics, *spectral correlations* between PDC-photons, caused by energy and momentum conservation laws, results to be more challenging [20–25].

In this Chapter I will summarise the state of art relating to this question, exploring the physics behind the generation of such frequency correlations. First, there is a brief overview on main concepts behind the quantum mechanics formalisation. After that, it is reported the differences between single photon states compared to the other states of light in terms of their statistics before a short outline of the major techniques for single photon generation. At the end, it is being addressed the spectral correlation problem and some proposals for its resolution.

1.2 QUANTUM OPTICS

Dirac formalism for the quantisation picture of light represented a turning point for the exploitation of quantum properties of photons for information and communication purposes. The traditional approach to quantum formalism can be performed due to the possibility of identify the electro-magnetic radiation by *coordinates* and *quantum momenta*. Without exploring all the proof steps, it is possible to assert that, starting from the classical mechanics for Maxwell equations, the electro-magnetic field can be associated to a collection of independent *harmonic oscillators*, each one associated to a certain mode corresponding to a wave vector $\mathbf{k}$ and polarisation direction $\lambda = 1, 2$ [26].

Due to this oscillator representation, it is possible to quantised the radiation field by looking at the well-known quantum expression of *harmonic oscillator Hamiltonian* with a given frequency ω, considering firstly a single mode excitation,

$$\hat{\mathcal{H}} = \hbar\omega\left(\hat{a}^\dagger\hat{a} + \frac{1}{2}\right), \tag{1}$$

where $\hbar = h/2\pi$ and h is the original Planck constant.
In the Eq.1 we introduced the operators $\hat{a}^\dagger$ and $\hat{a}$ which are called, respectively, the *creation* and *destruction* operators for the harmonic oscillator which possess the commutation property,

$$[\hat{a}, \hat{a}^\dagger] = \hat{a}\hat{a}^\dagger - \hat{a}^\dagger\hat{a} = 1, \tag{2}$$

The "role" of these operators is simple but efficient to understand. Let $|n\rangle$ be an energy eigenstate of the hamiltonian $\hat{\mathcal{H}}$, called *number state* or *Fock state*, with eigenvalue E_n as the amount of energy of the n-th level, so that

$$\hat{\mathcal{H}}|n\rangle = \hbar\omega\left(\hat{a}^\dagger\hat{a} + \frac{1}{2}\right)|n\rangle = E_n|n\rangle. \tag{3}$$

It is easy to demonstrate [26] that the action of $\hat{a}^\dagger$ and $\hat{a}$ on the state $|n\rangle$ provokes an increase or decrease of the energy level, respectively. In fact, we note that

$$\hat{a}^\dagger|n\rangle = \sqrt{n+1}|n+1\rangle, \tag{4}$$

with a new energy $E_{n+1} = E_n + \hbar\omega$ for the creator operator, while

$$\hat{a}|n\rangle = \sqrt{n}|n-1\rangle, \tag{5}$$

with energy $E_{n-1} = E_n - \hbar\omega$ for the destruction operator.
These properties highlight the fundamental concept behind quantum theory of light. As we can see from the Hamiltonian in Eq.1 and from $\hat{a}^\dagger$ and $\hat{a}$ properties, the electromagnetic field can assume only *discrete* values of energy, whose lowest value is known as *quantum vacuum energy* or *zero-point energy* of such an oscillator ($E_0 = 1/2(\hbar\omega)$), and the first level of excitation differ from the vacuum by a $\hbar\omega$ amount of energy, that is also the basic quanta of light field, the *photon*. One can assert that creation and destruction operators can be utilised for those processes where there is a radiative emission or absorption by atoms or matter in general. It is possible to define the action of $\hat{a}^\dagger$ as a representation of the physical occurrence where a photon is generated with energy $\hbar\omega$; vice versa, $\hat{a}$ acting on a n-photon state, constitutes the destruction one photon from the system, absorbing a $\hbar\omega$ unit of energy.

Thus, quantum description of photon emission and absorption has been considered to act as a quantum cavity with the excitation of discrete values of energy on a fixed mode. However, it is possible to extend such representation, looking at those cases where more than one different modes can be excited from the cavity. So that, the electromagnetic field is quantised by the association of quantum harmonic oscillator considering each mode $\mathbf{k}\lambda$ excited in the quantisation cavity, leading to the more complete destruction and creation operator expressions,

$$\begin{aligned} \hat{a}_{\mathbf{k}\lambda}|n_{\mathbf{k}\lambda}\rangle &= \sqrt{n_{\mathbf{k}\lambda}}|n_{\mathbf{k}\lambda}-1\rangle, \\ \hat{a}^\dagger_{\mathbf{k}\lambda}|n_{\mathbf{k}\lambda}\rangle &= \sqrt{n_{\mathbf{k}\lambda}+1}|n_{\mathbf{k}\lambda}+1\rangle, \end{aligned} \tag{6}$$

that now can be interpreted as the absorption and emission, respectively, of one photon of energy $\hbar\omega_k$ in mode $\mathbf{k}\lambda$. The different

cavity modes are independent, so that the commutation relation described in Eq.2 can be generalised as,

$$[\hat{a}_{\mathbf{k}\lambda}, \hat{a}^{\dagger}_{\mathbf{k}'\lambda'}] = \delta_{\mathbf{k},\mathbf{k}'}\delta_{\lambda,\lambda'}. \tag{7}$$

In conclusion, it is possible to excite L radiation modes, and all these result to be independent from each other, leading to a more general description of total field quantum state, that can be written as a product as a product of individual mode states,

$$|n_{\mathbf{k}_1 1}, n_{\mathbf{k}_1 2}, n_{\mathbf{k}_2 1}, \ldots, n_{\mathbf{k}_l 2}\rangle = \bigotimes_{i=1}^{L} \bigotimes_{\lambda_j=1}^{2} |n_{\mathbf{k}_i \lambda_j}\rangle. \tag{8}$$

By defining the operations that cause absorption or emission of photons in such way, we are assuming that the light beams are time-independent, omitting all the possible time evolutions that can occurs during generation, detection or interactions. In fact, all real light beams do not continue for ever, but rather they exhibit time variations on time scales comparable to the observation times in many practical experiments. In particular, it often happens that quantum light is generated in the form of short optical pulses, affecting the spectra shape which covers an extended range of frequencies instead of being monochromatic. Such scenario requires a representation that taken into account the excitation of an infinite range of modes of the optical system. Moreover, the quantisation of electromagnetic field embracing this extension can be performed by a set of modes characterised by a continuous wavevector, leading to the *continuous-mode* description of quantum theory of light, and permitting to move from the sum of all possible modes $\sum_{\mathbf{k}}$ to the integral $1/\Delta\omega \int d\omega$, choosing the frequency continuous variable ω instead of wavevector $\mathbf{k}$.

In this depiction, we need to extend the definition of number states mentioned before, now bearing in mind that a photon state must have the form of a pulse, or a succession of pulses, with energy and intensity spreaded over the infinite propagation axis, or analogously over the time axis. So that, it is convenient to described single and multiple photon states with their spectral amplitude function $\xi(\omega)$ satisfying the normalisation conditions,

$$\int d\omega |\xi(\omega)|^2 = \int dt |\xi(t)|^2 = 1, \tag{9}$$

that is valid both for the frequency and time domain, by Fourier transformation.
Under this conditions, assuming parallel beams with plane wavefronts and single polarisation, the destruction and creation operators, $\hat{a}_k$ and $\hat{a}_k^\dagger$, now do not represent the absorption or emission of a single-mode photon state but a *photon wavepacket*, defined as,

$$\begin{aligned} \hat{a}_\xi^\dagger &= \int d\omega \xi(\omega) \hat{a}^\dagger(\omega) = \int dt \xi(t) \hat{a}^\dagger(t), \\ \hat{a}_\xi &= \int d\omega \xi(\omega) \hat{a}(\omega) = \int dt \xi(t) \hat{a}(t), \end{aligned} \tag{10}$$

where we introduced the continuous-mode creation and destruction operators at frequency ω, $\hat{a}(\omega)$ and $\hat{a}^\dagger(\omega)$.
As a result, the number states formulation evolves in their continuous-mode counterpart defined as,

$$|n_\xi\rangle = \sqrt{n!}\left(\hat{a}_\xi^\dagger\right)^n |0\rangle, \tag{11}$$

where $|0\rangle$ is the continuous-mode vacuum state.
Thanks to the wavepacket representation, it is possible to anticipate that spectral correlations play a central role for the determination of single-photon states, thing that will become much more clear afterwards, with the introduction of auto-correlation function, which will define the statistics of the light.

1.2.1 *Quantum information*

Treating photons as quantum entities has given rise the suggestion of their utilisation as attractive tools for the realisation of optical devices capable to exploit their quantum properties. Furthermore the coming of *quantum information theory* in early 1980s has sped up the investigation of photonics platforms in order to support the large amount of protocols produced by this novel studies.
Such theory started in 1982, when Richard Feynman raised the

issue that there seemed to be some fundamental difficulties while simulating physical systems subjected to the quantum mechanics by the use of classical computers [27]. As a possible answer he suggested that building *quantum computers* would allow us to avoid those difficulties. This idea has given rise to a whole new branch of science, *i.e.* quantum information, that combines the well-established concepts of classical information theory with the laws governing the quantum world. With the advent of quantum information, new notions as *superposition* and *entanglement* have been introduced, near to some remarkable challenging algorithms, like the problem of finding the prime factors of an integer, discovered by Shor in 1994 [28, 29] or the problem of conducting a search through some unstructured search space, solved by Grover in 1996 [30].

The hearth of quantum information holds in the extension of the unit of classical information and classical computation, the *bit*, in its quantum counterpart, the *quantum bit* or *qubit*. It can be described generally as a superposition vector $|\psi\rangle \in \mathbb{H}$ living in the Hilbert space $\mathbb{H}$ [31],

$$|\psi\rangle = \alpha|0\rangle + \beta|1\rangle, \tag{12}$$

where $\{|0\rangle, |1\rangle\}$ constitutes quantum logical basis, and where α and β are complex numbers such that $|\alpha|^2 + |\beta|^2 = 1$.
With the introduction of qbits, we can exploit them in order to describe quantum systems whose state is not completely known. When such state evolves stochastically, at a given moment it can be represented by an *ensemble of pure states* $\{p_i, |\psi_i\rangle\}$, where p_i is the probability of the system being in the particular pure state $|\psi_i\rangle$ ($\sum_i p_i = 1$). So that, a *density matrix* operator can be associated to such ensemble by the expression,

$$\rho = \sum_i p_i |\psi_i\rangle\langle\psi_i|, \tag{13}$$

that satisfied three fundamental conditions:

- *Hermitian condition* ($\rho = \rho^\dagger$).

- *Unitary trace condition* ($\mathrm{Tr}[\rho] = 1$).
- *Positivity condition* ($\langle\varphi|\rho|\varphi\rangle \geqslant 0, \forall|\varphi\rangle \in \mathbb{H}$).

The density operator approach, represented as a probabilistic mixture of pure states, constitutes a suitable tool capable to discriminate *pure* states, satisfying the $\mathrm{Tr}[\rho^2] = 1$ condition, against *mixed* states, having the $\mathrm{Tr}[\rho^2] < 1$ condition, that describe a mixture of different pure states.

Another advantage due to the use of density matrices involves in the possibility of practical description of large dimensionality quantum systems, *i.e.* quantum *composite systems*. Such states, living in the tensor product of the Hilbert spaces of the component physical systems, are associated to the density matrix, which is express in the form $\rho^N = \otimes_{n=1}^{N} \rho^{(n)}$, where $\rho^{(n)}$ denotes the single-particle density matrix. Within the expansion of Hilbert space dimension, single states constituting the composite system, could be strongly correlated each other, giving rise to the unique quantum property called *entanglement*. Taking into account the form of composite density matrix, an ensemble of quantum state is defined entangled, or non separable, if it cannot be mathematically written as a sum of pure product states $\rho^N = \sum_i p_i \otimes_{n=1}^{N} \rho^{(n)}$, where p_i-s are the probabilities of the product states, with $\sum_i |p_i|^2 = 1$ [32].

1.3 SINGLE PHOTONS: HOW CAN WE DISCRIMINATE THEM?

We introduced the quantum perspective on light, identified it with discrete blocks of energy called photons. However, radiation detection results to be a more demanding procedure than one might think. To clarify this point, the challenge does not comprise only the nature of photodetection devices that, however, cover an important function for the measurement procedure. Even using an ideal photomultiplier, capable to discriminate every single photon that irradiate its collective mask, the character of the light beam lies in the intrinsic photon statistics of the radiation itself, whose fluctuations change significantly according to the stream of photon *bunch* we collect.

The first approach to energy statistics from the electromagnetic radiation was discussed by Wilhelm Wien before the intervention of Planck in 1901 [33], which completed and formalised the previous conjecture leading to the famous *Planck law* of *black-body radiation*. Considering a single radiation mode within the cavity at angular frequency ω and at a temperature T, the probability of finding n photons, emitted by a hot body, called *thermal light*, can be expressed as

$$P_{th}(n) = \frac{\exp(-n\,\hbar\omega/k_B T)}{\sum_n^{\infty} \exp(-n\,\hbar\omega/k_B T)}, \tag{14}$$

where k_B is the Boltzmann constant. For our purposes, it is convenient to describe the distribution in Eq.14 in terms of the mean photon number,

$$\langle n\rangle = \frac{1}{\exp(\hbar\omega/k_B T) - 1}, \tag{15}$$

which reads as,

$$P_{th}(n) = \frac{1}{\langle n\rangle + 1}\left(\frac{\langle n\rangle}{\langle n\rangle + 1}\right), \tag{16}$$

which is the so-called *Bose-Einstein distribution*.
From this depiction, some consideration may be addressed by looking at the broadness of such distribution, which relies on its *variance*,

$$(\Delta n)^2_{th} = \sum_n^{\infty} (n - \langle n\rangle)^2 P_{th}(n) = \langle n\rangle + \langle n\rangle^2, \tag{17}$$

that is considerably larger than the one for *Poissonian distribution* (identified by the relation $(\Delta n)^2_P = \langle n\rangle$), falling in the category of the so-called *super-Poissonian* statistics of light, that holds all the distributions whose variances are larger than their mean values.

1.3.1 *Photon statistics from* $g^{(2)}$ *measurement*

The exploration of the black-body radiation case leads to the determination of a meaningful tool which establishes the statistics nature of light beam by examining photon number fluctuations. As we noticed, thermal radiation determines the very chaotic nature of light, because of its huge width-scale with the number of photons, *i.e.* the light intensity, compared to the Poissonian behavior. In general, the valuation of light statistics allows us to determine the degree of *bunching* of a stream of photons and their correlations.
Thus, the intensity-fluctuation test requires an appropriate measurement able to sense the correlations of certain radiation field. Such method can be found on the interferometric proposal by Hanbury Brown and Twiss [5], which express the correlation of two optical intensities in terms of *second-order coherence*. Despite the simple experimental scheme, consisting of symmetrical 50:50 beam splitter and a coincidence detection at its outputs, it accounts a valuable strategy for photon-nature discrimination while testing an unknown light source, by calculating the probability distribution of the output photon pair with time intervals τ. For a low photon flux and a relatively short coherence time, such probability distribution is a good approximation of the *degree of second-order temporal coherence*, $g^{(2)}(\tau)$, also known as *auto-correlation function* and defined as,

$$g^{(2)}(\tau = 0) = \frac{\langle \hat{a}^\dagger \hat{a}^\dagger \hat{a}\hat{a} \rangle}{\langle \hat{a}^\dagger \hat{a} \rangle^2}, \tag{18}$$

for a zero-delay interval $\tau = 0$. For sake of simplicity we now utilise the single-mode formalism, while the extension to the multimode one implies only some considerations on the spectral shape of light beam, leading to the same conclusions revealed below.
By observing the Eq.18, one can note that some actions on the light beam intensity, as attenuation or boosting, *does not* affect the auto-correlation function, that is, however, strictly linked to the statistic nature of the light beam. Indeed, recalling the destruction and creation operators commutation property in Eq.2, and intro-

ducing the *number operator* $\hat{n} = \hat{a}^\dagger \hat{a}$, the $g^{(2)}(0)$ function can be expressed as,

$$g^{(2)}(0) = \frac{\langle \hat{n}(\hat{n}-1)\rangle}{\langle \hat{n}\rangle^2} = 1 + \frac{(\Delta n)^2 - \langle \hat{n}\rangle}{\langle \hat{n}\rangle^2}, \tag{19}$$

where the photon number variance is defined as $(\Delta n)^2 = \langle \hat{n}^2\rangle - \langle \hat{n}\rangle^2$. Thus, in the auto-correlation function they appeared the main quantities which define a light statistics distribution, the number of photons *mean value* and their *variance*.
Having already investigated the statistics properties of chaotic light, we now focusing the other two states of light and their statistics: *coherent states* and *number states*. The first one falls under the category of classical electromagnetic radiation, but having a fixed phase. Such states include the well-known *laser emission*, that preserves the above mentioned properties as well as a constant flux of photons and lack of intensity fluctuations. In quantum formalism, it is often denoted by $|\alpha\rangle$. Without exploring all the mathematics behind the demonstration, coherent states presents a variance $(\Delta n)^2_P = \langle \hat{n}\rangle$, that is linked linearly with the mean photon number, which is a peculiarity of *Poisson statistics*. Indeed, the probability of finding n photons in the mode is expressed by the Poissonian distribution,

$$P_{coh}(n) = |\langle n|\alpha\rangle|^2 = e^{-\langle \hat{n}\rangle} \frac{\langle \hat{n}\rangle^n}{n!}. \tag{20}$$

The consequent auto-correlation function for coherent light beams can be calculated and results to be $g^{(2)}_{coh}(0) = 1$; somehow, such value is representative of a cut-off line that separates classical light statistics from *non-classical* ones, due to the high neatness nature of coherent states, despite being classical. Indeed all the light statistics having $(\Delta n)^2 < \langle \hat{n}\rangle$, called *sub-Poissonian*, are considered even more stable than the coherent case, exhibiting a narrower photon number distribution, that in several cases can be considered Dirac delta-like number of photons distribution. This phenomenon is a marker of purely quantum optical effect, namely photon *anti-bunching*.

Using statistics dictionary, this implies that there is no uncertainty in the photon number, whose variance therefore vanishes, $(\Delta n)^2 = 0$; so that, the expectation value of the photon number is simply $\langle \hat{n} \rangle = n$, and the degree of second-order coherence follows trivially from Eq.19,

$$g^{(2)}_{num}(0) = 1 - \frac{1}{n}. \tag{21}$$

Looking at this the $g^{(2)}_{num}(0)$, it is easy to notice that if the light source emits purely with a single-photon statistics, $n = 1$, it vanishes. Such outcome turns out to be intuitive considering the autocorrelation experimental Brown-Twiss interferometer explained before; in fact, imagining a single photon as an indivisible particle, it can be not splitted while interacting with the beam-splitter, so that it can only get out on one of the two output side, provoking a lack of coincidence rate, *i.e.* $g^{(2)}_{num}(0) = 0$.

1.4 SINGLE PHOTON SOURCES

We observed that from a $g^{(2)}(0)$ measurement it is possible to establish the intrinsic statistics of light. Such statistics may occur as a completely chaotic way, with thermal states, as a coherent wave, or in a purely quantum status, which is accurately determined by a n-photon system. Ideally, a *single-photon source* should produce a single photon at any arbitrary time defined by the user, where the probability of emitting a single photon is 100%, meanwhile the probability of multiple-photon emission is 0%, with a corresponding indistinguishable photon emission, and a repetition rate that is arbitrarily fast (limited only by the temporal duration of the single-photon pulses, perhaps). Thus we are dealing with the so-called *deterministic* or "*on-demand*" source.

However, the concept of generating single-photon wavepackets whose leading-edge time can be chosen at will has been developed only in the beginning of 2000s by Lounis and Moerner exploiting single-molecule emission [34]. Indeed most of on-demand sources can be grouped together in the so-called "*single-emitter*"

category, that is characterised be the two-level emission scheme: due to the radiation-matter interaction, such systems are able to emit single quanta of light by exciting, with an external control radiation, a system which has an atomic-like hamiltonian that can be described as discrete transition, whose falling from the excitation level to the ground state create a single photon with an energy $E_{gap} = \hbar\omega$ equal to the two-level gap.
This category includes a large variety of systems: from *single atoms* [35–37], which are designed to work in the strong-coupling regime of cavity quantum electrodynamics, where the single photon profoundly impacts the dynamics of the atom-cavity system and the optical cavity greatly enhances single-photon emission into a single spatial mode with a Gaussian transverse profile, to *single molecules* [38–41] and single ions [42–44], that exploited the vibrational energy level system and having a Λ-type energy-level configuration (*i.e.*, with two ground states and one excited state) respectively. Deterministic sources can be found also in more complex structures of matters, as *semiconductor quantum dots* [45–47], created by self-assembling process forming tiny islands of smaller-band-gap semiconductor embedded in a larger-band-gap semiconductor, or *color centers* [48, 49], that exploit for example the optical transition of nitrogen-vacancy, formed by a substitutional nitrogen atom and a vacancy at an adjacent lattice position in diamond.

1.4.1 *Parametric down-conversion*

Before the coming of deterministic sources, the concept of single-photon radiation has been already discussed and experimentally observed by another class of light beam emissions: *heralded* or *probabilistic* single-photon sources. These sources are based on *photon-pair emission* which is probabilistic; as suggested from the name, the leading-edge time of single-photon wavepackets is known by the observation of the other photon of a pair, that in modern quantum optics language is said that *heralds* the emission of the first one. Originally performed for the experimental demonstration of *non-locality* with a *Bell's test*, Freedman and Clauser developed the first prototype of *single photon-pair* source with an atomic cascade

of calcium [50]. Widely studied and improved over time [9, 51], heralded single-photon sources established themselves with the discovery of photon-entanglement property exploiting *parametric down-conversion* (PDC) [14, 52].
The overall process is sketched in Fig.1: a strong *pump* light field is propagating through a medium possessing a $\chi^{(2)}$ nonlinearity. During this interaction one of the pump photons decays into a photon pair, where we label the individual photons *signal* and *idler*. One of the two photons is subsequently detected to herald the presence of its partner, the signal photon, effectively generating a source of heralded single photons.

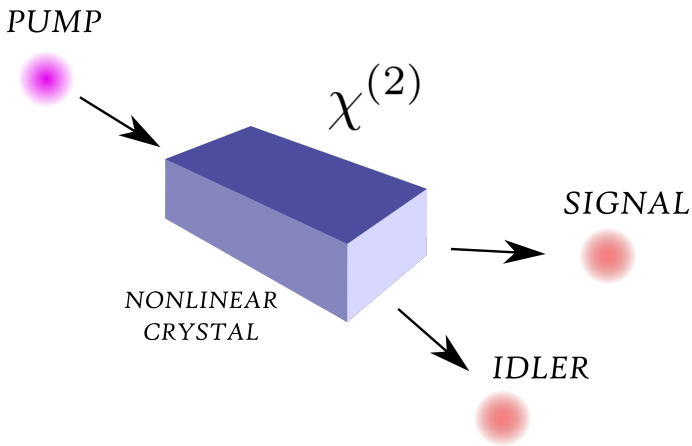

Figure 1: Parametric down-conversion generation of single-photon pair scheme.

Such phenomenon takes also the name of *three-wave mixing*, and it is allowed while the *energy conservation* is verified, *i.e.* the frequencies match,

$$\omega_p = \omega_s + \omega_i, \tag{22}$$

as well as the *momentum* is conserved in the non-linear crystal, *i.e. phase-matching condition*,

$$\mathbf{k}_p = \mathbf{k}_s + \mathbf{k}_i, \tag{23}$$

as shown schematically in Fig.2.

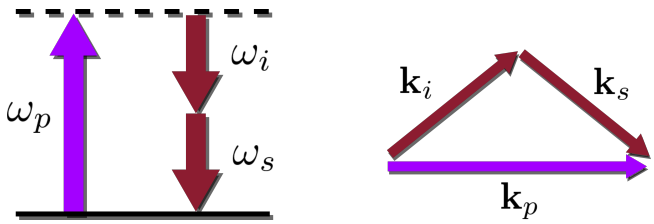

Figure 2: Energy conservation and phase-matching condition scheme in a degenerate parametric down-conversion process.

Due to the dispersion laws, isotropic crystals have not the necessary requirements for the PDC-generation; otherwise, the parametric conversion is allowed for the anisotropic materials, in which fields with different polarizations experience different refractive indices [53]. For *uniaxial crystals*, PDC-emission occurs by exploiting the *birefringence* nature of the bulk source, *i.e.* the difference of refractive indices between the crystal optical axis and one of its orthogonal, by knowing the dispersion relations of these crystals, which is the exact wavelength and temperature dependence of the refractive indices, usually available in the form of empirical *Sellmeier equations*; the plane containing the optical axis and the pump wave vector is called the principal plane, and we denote a light beam polarized orthogonally to that plane the ordinary (o) and the beam polarized within that plane the extraordinary (e) beam. Uniaxial crystals are widely used in quantum optics and the peculiarity relies on their two possible phase-matching *types*: type-I phase matching is possible for an extraordinary pump splitting into two ordinary PDC photons, $e \rightarrow o + o$, while type-II PDC can be achieved for $e \rightarrow o + e$.
This is the case of bulk crystals, that are still the main system of choice for the generation of multi-photon states in pulsed-pump PDC; however, low brightness due to the transversal walk-off constitutes an impediment restricting the useful length of a bulk crystal and thus limiting the photon-pair yield. So that, other approaches have been investigated: it is the case of *periodically-poled* crystals, based on *quasi phase-matching*, the simplest form of which is a periodically alternating orientation of the crystal domain, caus-

ing a consistent intensity growth of generated photon-pair that propagates collinearly through the crystal.

1.5 THE CORRELATION CHALLENGE

The high advantage of using on-demand sources is that of providing a single photon state at a chosen time. However, the experimental implementation presents very challenging issues. The main one is the stability: the atomic-like systems described above are very sensitive to thermal fluctuations and some of them have the very first energy levels easily occupied even at very low temperatures (few Kelvin degrees). These compromise the purity of single-photon emission, as well as not well-defined energies due to the boundary conditions, *e.g.* the structure of the semiconductor cavity for quantum dots [12, 54]. Another example of difficulty is the hardness of collecting single-photon radiation emitted from single molecules or single ions, giving rise to the creation and implementation of complex structures in order to reduce the loss due to the radial emission [55].

In this scenario, PDC sources acting as a very suitable strategy for single-photon generation, even at room temperature, and having a very accurate directional emission due to the phase-matching condition; thus the combination of momentum and energy conservation should assure the goodness of photon-pair emission, without caring about the above mentioned obstacles. However, during the definition of PDC generation we just assumed that the three-wave interference occurs for monochromatic light beams; this means that the unique spectral relation between the two-emitted single photons relies on the frequency relation we observed in Eq.22. Such assumption in a real scenario is difficult to achieve, due to the broad spectrum of the pump laser that is in many cases unavoidable even being narrowed. While such a pump irradiates a PDC source, all its monochromatic components are affected both by the energy conservation and phase-matching constrains; especially the last condition is connected directly to the dispersive properties of the PDC-crystal which has a different response de-

pending on the color of light. This produce a photon-pair whose spectral shapes could generally be *entangled*: imagining the PDC-generation as an optical quantum cavity, this occurrence can be consider as well as a multitude of pairs of single emitters, each one generating its own temporal/spectral mode. The results is a production of heralded photons which have an highly *multi-mode* nature, generally with numerous and highly correlated modes [56–58]. Diverse approaches can be performed in order to reduce the number of modes, and consequently the degree of spectral correlation, such as choosing a nonlinear medium with the correct dispersion characteristics, or with a proper filter on the photon-pair or even by shaping the pump pulses that caused the down-conversion, as we will observe later in this work.
So that, the detection of spectral multi-mode states on PDC events become fundamental for the establishment of frequency-entanglement, and it can be efficiently performed by determining the joint spectral amplitude (JSA), *i.e.* the joint probability for a spectral measurement of the two photons. However, such measurement requires the implementation of frequency-resolved coincidence detection, with an unavoidable trade-off between spectral resolution and counting rate in any given frequency bin, which might be an hard challenge, experimentally. For this reason, alternative suitable methods should be explored, trying to avoid the implementation hardness described above; for example, it is demonstrated that the Hong-Ou-Mandel interference is sensitive to spectral correlations, so that looking at its characteristic dip, one can extrapolate some information about the spectral structure of the two-photon state, even if not complete because of its independence from the spectral phase [20].

However, other ways may be explored in order to solve this challenge, in order to characterise the frequency entanglement by exploiting some particular spectral interactions; some of them has been investigated later in this manuscript, where we combine the strong correlation between spectrum and dispersion with a valuable tool for the improvement of measurement accuracy, the *quantum metrology*. In such case, multi-parameter approach helps us to extract the required amount of information on spectral correlation,

by looking at the *dispersion cancellation* phenomenon, that reduce the encountered noise due to spectral relation of the photon-pair emitted by a PDC source.

2

HERALDED GENERATION OF HIGH-PURITY ULTRASHORT SINGLE PHOTONS IN PROGRAMMABLE TEMPORAL SHAPES

"Merely by existing and evolving in time - by existing -
Any physical system registers information, and by evolving
In time it transforms or processes that information."
— The computational universe, S. Lloyd

2.1 INTRODUCTION

As discussed in the previous Chapter, sources based on PDC have granted a simple solution to heralded single-photon generation used for decades for the implementation of efficient photonics platform for quantum information and communication purposes. Furthermore, the occurrence of spectral correlation and its impact has been also mentioned; the characterisation of single-photon devices and their efficiency passes through the study and control of frequency entanglement. A complete engineering of such sources relies on the two above mentioned *conservation laws* governing the PDC-sources, which relates the *energies* and *wave-vectors* of generated photon-pairs with the ones of the intense pump beam of light that starts the parametric conversion process. Many works explored diverse techniques in order to enhance the photon distinguishability by HOM interference [59] and a more efficient source-brightness [60, 61].
One of most challenging studies on last decades provides for the investigation of *spectral correlations* occurring for the photon-pair generated by PDC sources. Despite this phenomenon usually represents a side effect, which prevents the photon purity and indistinguishability, essential requirements for efficient protocol applications in quantum computation and communication [62, 63], recently it has been shown that it can be exploited for a large

amount of profitable utilisation, *e.g.* quantum logical basis encoding exploiting temporal modes of single photon states [64–66].

In this Thesis, we explore the possibility of handle the spectral wave-functions of single photons generated by a PDC source implemented with a in-house fabricated waveguides, in order to produce a well-controlled phase-matching function with a tailored dispersion, using a shape apparatus which produces pump pulses with arbitrary spectral phase, in order to assure an improvement to nearly pure single photon states by reducing the presence of frequency entanglement.

2.2 TEMPORAL MODES

In quantum information processing within photonics platform, the *polarisation* degree of freedom (DOF) provides the most widely applied one for many years, permitting to simulate experimentally a large amount of quantum protocols and algorithms, due to the facility of management by means of using of linear optical elements, such as beam splitters, wave plates and detectors. Another DOF explored recently is the *orbital-angular-momentum* state of light, which has been exploited as a useful basis for encoding information even though the difficult match with existing single-mode fiber networks.

During the last decades the energy, *i.e. frequency*, DOF has been exploited for several experiments, which has been used as resource for quantum information science, capable to constitute a suitable tool as a logical basis encoding system as well as an adequate scheme for improving the quality of single photon sources. Because time and frequency are conjugate variables one can define a set of overlapping but orthogonal broadband wave-packet modes by the name *temporal modes* (TMs). For coherent beams of light or single-transverse mode guided wave geometry, it has been demonstrated that TMs form a *complete basis* which constitutes an arbitrary state in the energy degree of freedom [67]; so that, for a fixed polarisation and transverse field distribution, the quantum

state of a single photon can be defined as a coherent superposition of single-photon states in different monochromatic modes [62],

$$|A_j\rangle = \frac{1}{2\pi}\int d\omega\, f_j(\omega)\hat{a}^\dagger(\omega)|0\rangle, \tag{24}$$

where we sum for all the continuum spectrum. In Eq.24 we introduced the operator $\hat{a}^\dagger(\omega_i)$, which creates a monochromatic wave packet at frequency ω_i, and $f_j(\omega)$ that is complex spectral amplitude of the wave packet.
On the time "point of view", it is possible to express the same state a coherent superposition over many "creation times", by the use of Fourier transform,

$$|A_j\rangle = \int dt\, \tilde{f}_j(t)\hat{a}^\dagger(t)|0\rangle \equiv \hat{A}_j^\dagger|0\rangle, \tag{25}$$

where $\tilde{f}_j(t)$ is the temporal shape of the wave packet and where we use the definitions,

$$\begin{aligned}\hat{a}^\dagger(\omega) &= \int dt\, e^{i\omega t}\hat{a}^\dagger(t),\\ \hat{a}^\dagger(t) &= \frac{1}{2\pi}\int d\omega\, e^{-i\omega t}\hat{a}^\dagger(\omega).\end{aligned} \tag{26}$$

In this representation, we establish a new creation operator $\hat{A}_j^\dagger$, which creates the wave-packet state $|A_j\rangle$ from the vacuum $|0\rangle$.
An example of TM basis consists of the family of *Hermite-Gauss* functions of frequency, that can be usually associated to the quantum logical basis $\{|0\rangle, |1\rangle, \ldots, |d\rangle\}$, forming a carrier of information in a d-dimensional Hilbert space, called *qudit*. Generally, one can express a wave packet of single-photon quantum state $|\Psi\rangle$ as a superposition in a basis of TMs,

$$|\Psi\rangle = \sum_j^\infty c_j\hat{A}_j^\dagger|0\rangle, \tag{27}$$

where c_j are complex-value coefficients.
In order to fulfill the over mentioned matching between TMs and the quantum logical basis, the elements of TM basis are orthogonal with respect to a frequency and time integral,

$$\frac{1}{2\pi}\int d\omega\, f_j^*(\omega) f_k(\omega) = \int dt\, \tilde{f}_j^*(t)\tilde{f}_k(t) = \delta_{jk} \tag{28}$$

2.2.1 *TMs on PDC processes*

We now discuss the TMs structures of three wave mixing PDC phenomenon, where a *pump* laser horizontally polarised generates two photons that we identify as *signal* (horizontal polarisation) and *idler* (vertical polarisation); in particular the state of type-II PDC process describing the generated signal and a idler photon at frequency ω_s and ω_i respectively reads,

$$|\Psi_{PDC}\rangle = \int d\omega_s d\omega_i f(\omega_s,\omega_i)\hat{a}_H^\dagger(\omega_s)\hat{a}_V^\dagger(\omega_i)|0\rangle_H|0\rangle_V, \tag{29}$$

where $\hat{a}_H^\dagger(\omega_s)$ and $\hat{a}_V^\dagger(\omega_i)$ are the creation operators of signal and idler photons at horizontal (H) and vertical (V) polarisation. The function $f(\omega_s,\omega_i)$ in Eq. 29 establishes the so-called *joint-spectral amplitude* (JSA) function that is defined as

$$f(\omega_s,\omega_i) = \alpha(\omega_s,\omega_i)\phi(\omega_s,\omega_i), \tag{30}$$

where $\alpha(\omega_s,\omega_i)$ is the *pump distribution*, which includes the energy conservation condition and the spectrum of the pump pulses, and $\phi(\omega_s,\omega_i)$ is the *phase-matching function*. As mentioned before, $\phi(\omega_s,\omega_i)$ sets the achievable relation between the pump pulses and the generated signal and idler photons accordingly to the momentum conservation law in Eq.23, and depends strongly to the physical properties of the material, such as *dispersion*.
In principle $f(\omega_s,\omega_i)$ depends to the propagation direction of the generated photon-pair; here we assume that idler and signal photons propagate collinearly, permitting us to suppress the direction labels on the Eq.30. The pump distribution depends strictly to the frequency shape of the pump pulses in use for the PDC generation, while the phase-matching function is related to the group velocity the two photons encounters by arranging the crystal dispersion. The handling of the first function is the typical approach

which holds the *4-f line* set-up that permits to control the spectral shape of pump laser; since the $\phi(\omega_s, \omega_i)$ is correlated to the nature of the device used as PDC-source, in particular to the ordinary and extraordinary refractive indices of the medium, it requires an accurate engineering on the growth process of such crystals. A recent experimental approach provides for the possibility of using periodically-poled crystals, assembled into integrated photonics devices via waveguides in order to achieve an optimal dispersion; such a procedure represents one of the most utilised techniques assuring a properly tuning of phase-matching function.

2.3 SPECTRAL CORRELATIONS

Generally, one can decompose the JSA function in Eq.30 into two sets of TM basis functions $\{\psi_n(\omega_s)\}$ and $\{\phi_n(\omega_i)\}$ [57, 64, 68],

$$f(\omega_s, \omega_i) = \sum_n \sqrt{\lambda_n}\psi_n(\omega_s)\phi_n(\omega_i), \tag{31}$$

where λ_n, $\psi_n(\omega_s)$ and $\phi_n(\omega_i)$ follows the integral eigenvalue equations,

$$\begin{aligned} \lambda_n\psi_n(\omega_s) &= \int d\omega_i d\omega' f(\omega_s, \omega_i) f^*(\omega', \omega_i)\psi_n(\omega'), \\ \lambda_n\phi_n(\omega_i) &= \int d\omega_s d\omega' f(\omega_s, \omega_i) f^*(\omega_s, \omega')\phi_n(\omega'), \end{aligned} \tag{32}$$

satisfying the normalisation condition $\sum_n \lambda_n = 1$.

The formulation in Eq.31 is the so-called *Schmidt decomposition*, and defines a suitable tool which establish the *factorability* of JSA function, *i.e.* a method in order to find the spectral *degree of entanglement* of the photon-pair; in particular, the down-converted two-photon state is separable if there is only one term on the left side of Eq.31, see Fig.3. So that, such state can be written as,

$$|\Psi_{PDC}\rangle = \sum_n \sqrt{\lambda_n}\hat{A}_n^\dagger \hat{B}_n^\dagger |0\rangle_H |0\rangle_V, \tag{33}$$

where the effective creation operators $\hat{A}_n^\dagger$ and $\hat{B}_n^\dagger$ are given in terms of the TM functions $\psi_n(\omega_s)$ and $\phi_n(\omega_i)$ as,

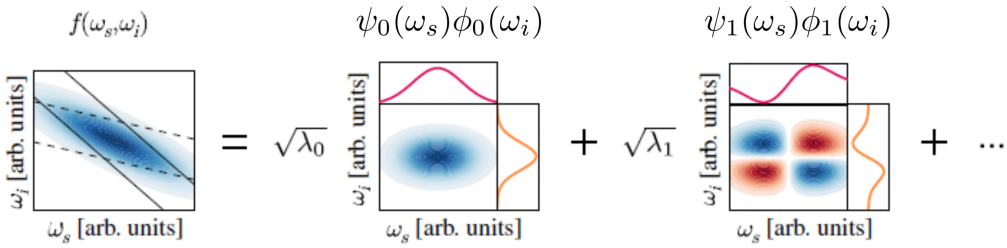

Figure 3: Representation of PDC process with Schmidt decomposition [64].

$$\begin{aligned}\hat{A}_n^\dagger &= \int d\omega_s \psi_n(\omega_s)\hat{a}_H^\dagger(\omega_i),\\ \hat{B}_n^\dagger &= \int d\omega_i \phi_n(\omega_i)\hat{a}_V^\dagger(\omega_i).\end{aligned} \tag{34}$$

In this representation, one can establish a *cooperativity parameter*, defined in terms of Schmidt eigenvalues,

$$K = \frac{1}{\sum_n \lambda_n^2}, \tag{35}$$

which provides the effective number of temporal modes in the state. It is possible to demonstrate[57] that the above mentioned operators $\hat{A}_n^\dagger$ and $\hat{B}_n^\dagger$ are strongly correlated due to the Schmidt decomposition in Eq.31; so that, performing a *second-order correlation* measurement of unheralded signal or idler photons,

$$\begin{aligned}g_s^{(2)}(\tau=0) &= \frac{\langle :(\sum_n \hat{A}_n^\dagger \hat{A}_n)^2 :\rangle}{\langle \sum_n \hat{A}_n^\dagger \hat{A}_n\rangle^2},\\ g_i^{(2)}(\tau=0) &= \frac{\langle :(\sum_n \hat{B}_n^\dagger \hat{B}_n)^2 :\rangle}{\langle \sum_n \hat{B}_n^\dagger \hat{B}_n\rangle^2},\end{aligned} \tag{36}$$

permits us to express the relation,

$$g_{s,i}^{(2)}(0) = 1 + \sum_n \lambda_n^2 = 1 + \frac{1}{K}. \tag{37}$$

For sake of simplicity, in this Thesis we focus on the so-called *purity* quantity,

$$P = 1/K = g^{(2)}(0) - 1, \tag{38}$$

that characterises the amount of factorability of the PDC photon-pair; for the case of a pure spectral state with $K = 1$, both signal and idler photons exhibits thermal photon number statistics corresponding to $g^{(2)}(0) = 2$.

2.4 PUMP-PULSE SHAPING

A complete control on the TM shape in a PDC-process, and in particular assessing a factorable JSA function, is a key requirement in order to improve the mode matching between individual sources which represents one of the benchmarks of quantum computing and communication multiplexing source-based technologies [63, 69, 70]. The possibility of reaching this task passes via a minimisation of spectral correlations between the PDC generated photons, *i.e.* a high degree of purity P.

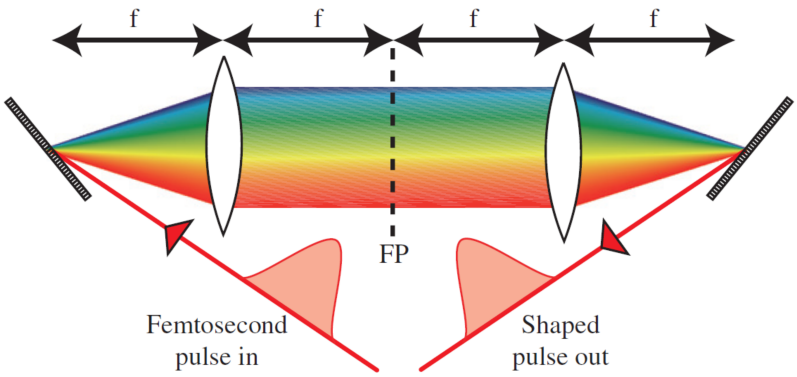

Figure 4: 4-f line scheme as pulse-shaper [71].

A possible strategy increasing the spectral purity of PDC process relies on shaping properly one of the photons generated [71]; experimentally, one can perform such temporal modelling by spectral modulation of the photon which can be achieved by a *4-f line*

set up, see Fig.4.
Such scheme is composed by two diffraction gratings and two lenses; initially each spectral component of broadband input photon is angularly dispersed by the first grating, then focused then is focused by the first lens to small diffraction spots in the *Fourier plane* where all the spectral components are spatially separated and focused; by inserting a proper mask in such plane one can modify the optical path for each spatial component (which corresponds to a specific frequency element) and thus shape the output pulse. Then a second combination of lens (or curved mirror) and grating allows the recombination of all the frequencies into a single collimated beam. Introducing this shape method to the PDC-generated photons, however, introduces loss and the rate of photon-pair is significantly reduced.

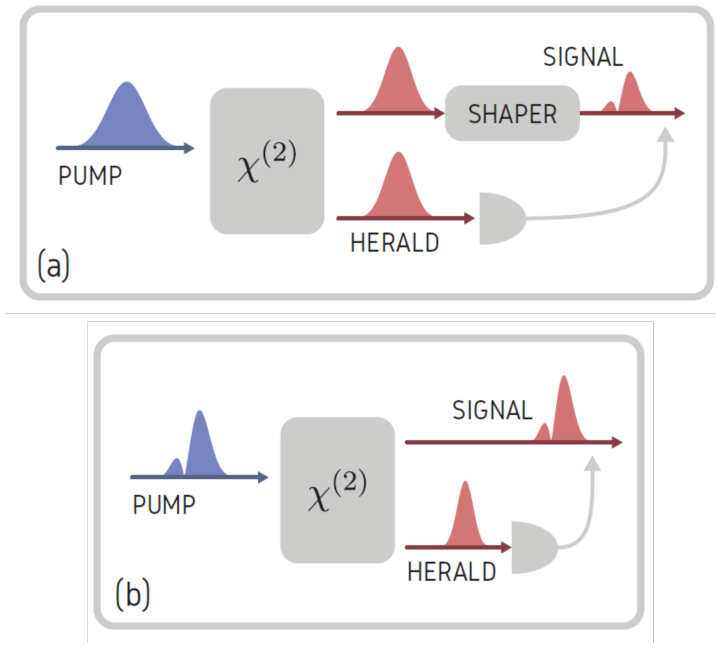

Figure 5: Scheme of experimental apparatus based on two different pulse-shaper approach: a) shaping on of the PDC-generated photons pulses; b) shaping the pump pulses.

In this Chapter we illustrate a novel approach to the pulse-shaping method, by modelling the shape of the pump pulses gen-

erating the PDC process instead of the heralded photons under appropriate phase-matching conditions, permitting to generate heralded photons which inherit the temporal shape of the pump pulse, see Fig.5.

2.4.1 *Experimental apparatus*

In Fig.6 we describe the apparatus scheme used for this experiment. First, we prepare the ultrashort pump pulses for the PDC process at 670 nm by generating the *second harmonics* of a tunable optical parametric oscillator which is at 1340 nm. The shaper consists by the previously mentioned 4-f line scheme; pump pulses are diffracted by a holographic grating with 2000 lines per mm, and then is reflected by cylindrical silver mirror in order to propagate collinearly all the spectral component to the two-dimensional reflective liquid crystal on silicon *spatial light modulator* (SLM); such device ensure the possibility of control independently the optical path of the beam in each pixel (the effective 2-D area of the SLM mask has 790×600 pixels), and consequentially giving a spectral phase for each spectral component irradiating the SLM device. A magnifying telescope is placed before the pulse-shape apparatus in order to match the size of each frequency component with the pixels of SLM to get an optimal resolution.
The resolution of 4f-setup is 35 pm that is enough permitting to prepare Hermite-Gauss-shaped pulses up to fourth order with 2 nm of *full width at half maximum* (FWHM) for the Gaussian profile, with an initial 6 nm bandwidth of our pump laser system. In order to collect the shaped beam after the shaper system, SLM reflects that at a slightly different angle which displaces the reflected beam vertically, permitting to collect the beam with a *D-shaped mirror*.

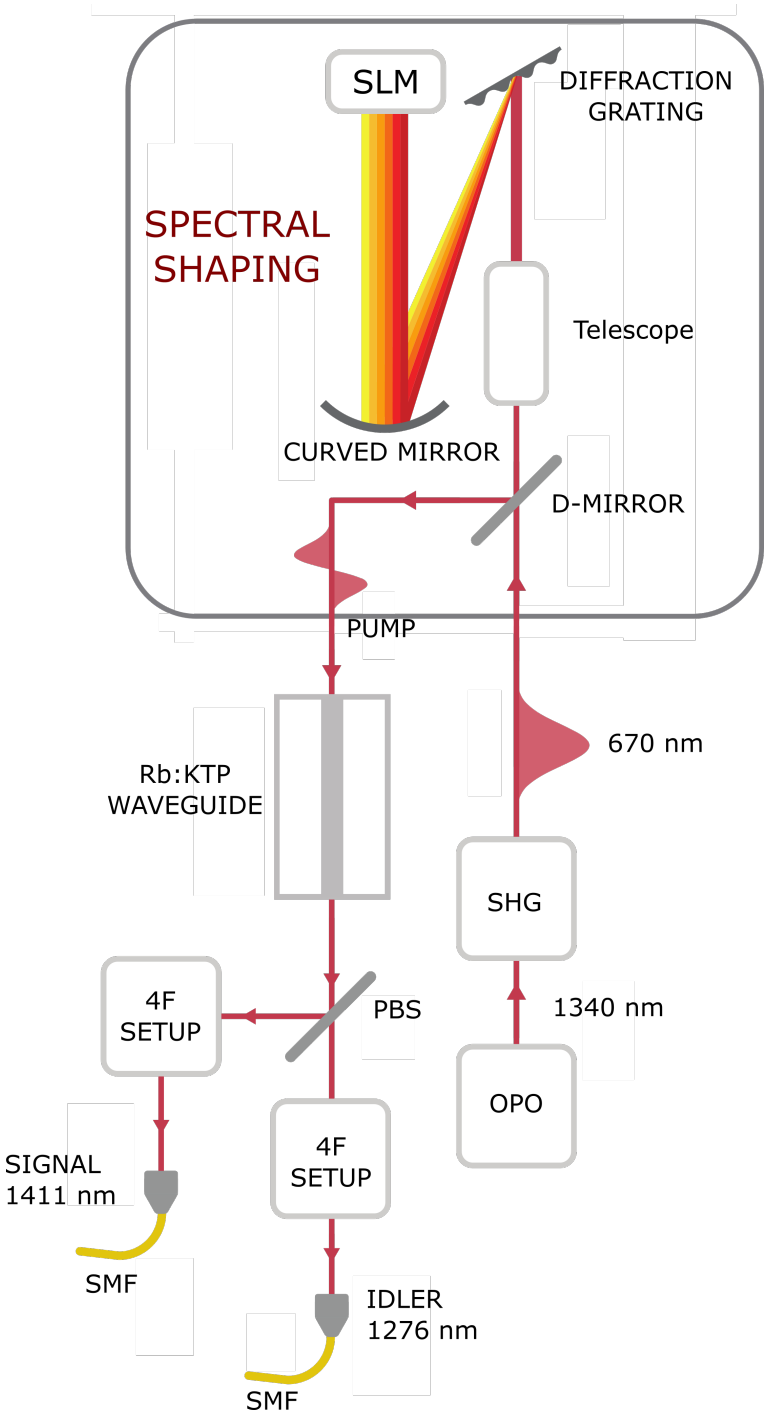

Figure 6: Experimental setup of TM controlling in a PDC process via pump-pulse shaping.

2.4.2 *Integrated source*

The main character of the experiment is the PDC-integrated source; it is based on a 16 mm long in-house built Rb:KTP waveguide with a nominal width of 3 μm and depth of 5 μm, designed to be spatially single-mode over the whole telecom range (~ 1500 nm) for both TE and TM polarisations. Such condition was explored before analytically, exploiting a phasematching with matched group-velocities of pump and signal fields, called *asymmetric group-velocity matching condition*, that occurs for a pump wavelength of 670 nm and a signal and idler wavelengths of 1411 nm and 1276 nm, respectively.
Interesting analysis are performed to the spectrum of photon-pair emitted with Gaussian frequency-shaped pump pulses; such measurement is conducted to the idler photon with the use of 4f-setup in the monochromator device, with a spectral resolution of 0.2 nm. The theoretical investigation suggests that the spectrum of idler photon follows the shape of phase-matching function $\phi(\omega_s, \omega_i)$; however, the measured spectrum (blue line in Fig.7) provides some relevant discrepancies respect on the expected behavior (grey line).

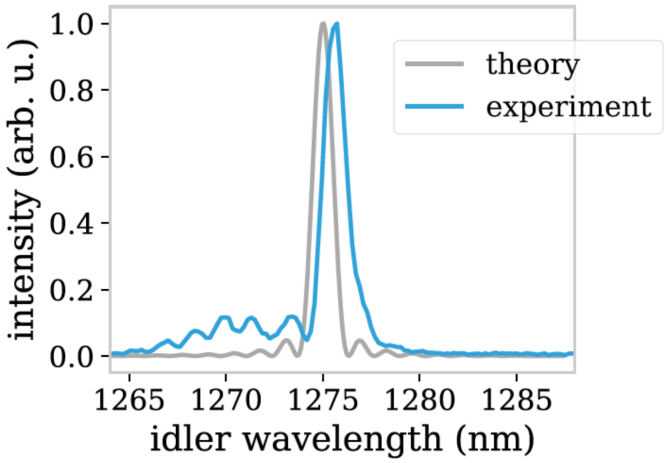

Figure 7: Theoretical and experimentally measured phasematching functions phasematching function $|\phi(\omega_s, \omega_i)|$.

This artifact can be explained by considering the inhomogeneities inside the waveguide; indeed, spatial distortions changing locally the width or depth make the waveguide channel non-uniform, *i.e.* the effective refractive index is not constant long the direction of propagation, distorting the phase-matching function that become generally broader. This phenomenon can be explained by considering little homogeneous portions of the waveguide; the overall phase-matching distribution then is a sum of all of these segments, which represents a coherent mixture of many sinc-functions with different widths and central frequencies that could cause the presence of unwanted asymmetric side-lobes, see Fig.7. Such features imply a reduction of spectral purity and the fidelity of single photon shaping. In order to avoid this loss, we choose to implement a filtering system on the idler photon, that allows to completely remove these side-lobes. The filtering system is performed by a 4f-line system where a slit-mask is placed on the Fourier plane, which permits to cut the undesired side-lobes; for the idler photon, the spectral filtering has a width of 3 nm.
In order to reduce spatial losses, we use a aspheric lens with a focal length of 8 mm to couple the pump laser to the waveguide. The coupling efficiencies of the modes emitted by the waveguide into the standard single-mode telecom fiber are measured using bright simulation laser tuned at the central frequencies of the PDC photons; the coupling efficiencies are 65% and 60% for idler and signal photons, respectively. The 4-f setups used as filters for both PDC-generated photons have a total transmission of 26% and 30% for signal and idler photons, respectively, due principally to a low diffraction efficiency of the diffraction gratings. The photons are finally collected with fiber-coupled superconducting nanowire single photon detectors (SNSPD) (Photon Spot) with system detection efficiencies of 41% at 1276 nm and 55% at 1411 nm.

2.5 JSI AND AUTO-CORRELATION RESULTS

In order to measure the order of factorability of the PDC process in this Chapter we perform a measurement of *joint spectral intensity* (JSI), *i.e.* the modulus square of the JSA function $|f(\omega_s, \omega_i)|^2$,

and auto-correlation function $g^{(2)}(0)$.
JSI measurement can performed by the use of a monochromator in the idler arm and a time-of-flight spectrometer in the signal arm [72]. For the frequency shape detection we use a 4.3 km long highly dispersive fiber (the total dispersion is equal to 0.3 ns/nm) which permits to map the spectrum into the temporal profile. This is resolvable directly in time on SNSPDs, which have a timing resolution of 70 ps, and a spectral resolution of about 0.2 nm.

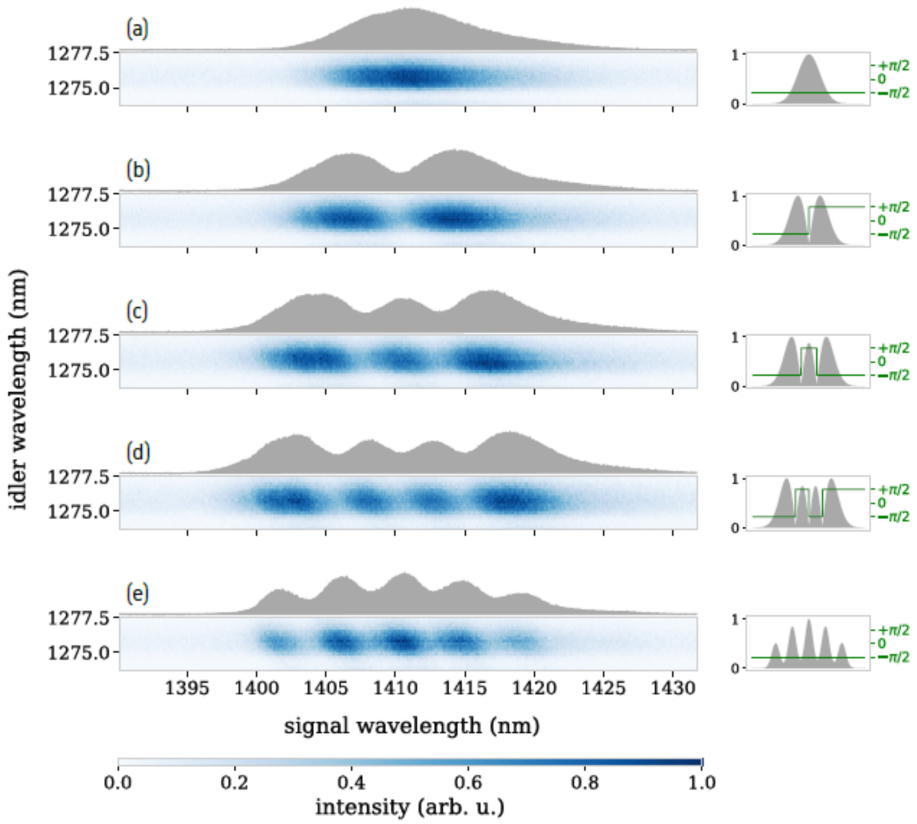

Figure 8: JSI measurements for different spectral-pump shapes.

We measured the JSIs, shaping the spectrum of pump pulses in the first four Hermite-Gauss modes and five frequency bins, plotted in Fig.8. The marginal spectral distributions of the signal photon is shown in grey above the JSI graphs, and the pump mode

of each JSI is figured on the right side, where the grey area is the spectral amplitude end the green line is the spectral phase induced by the SLM device. Schmidt number inferred from these JSIs is then calculated by decomposition of its eigenvalues, using a numerical singular value decomposition algorithm. The Schmidt numbers for a 5.0 nm broad pump pulses results $K_a = 1.01$, $K_b = 1.01$, $K_c = 1.02$, $K_d = 1.02$, and $K_e = 1.02$ following the labels on Fig.8, respectively for Gaussian, 1st-order Hermite-Gaussian, 2nd-order Hermite-Gaussian, 3rd-order Hermite-Gaussian, and frequency bins spectral profiles.

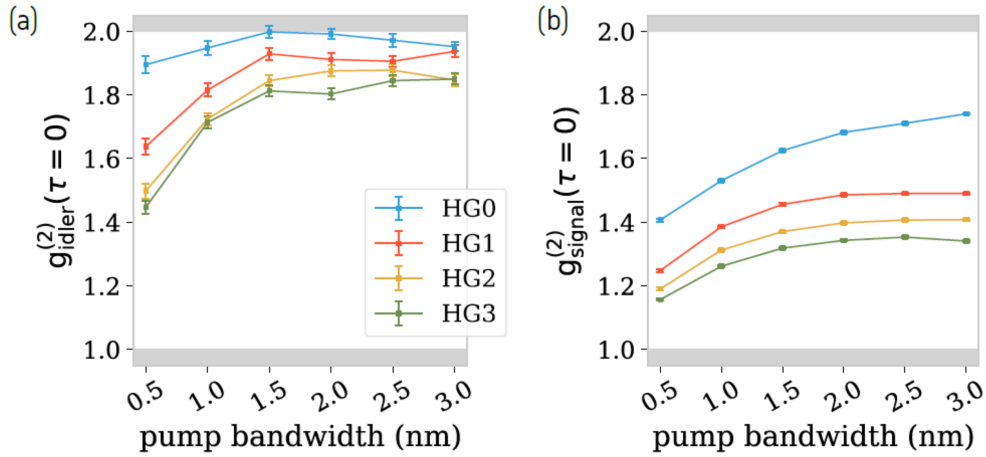

Figure 9: Second-order correlation function $g^{(2)}(0)$ experimental values for idler (a) and signal (b) with different pump bandwidth and different orders of Hermite-Gaussian modes. The error bars for the $g^{(2)}(0)$ in the signal plot are smaller than the markers.

Despite the JSI measurement constitutes an important tool extrapolating information about the spectral correlation of PDC photons, it can not discriminate the spectral phase of the photons and is also limited by the resolution of the spectrometers. Otherwise, as mentioned before, the auto-correlation function $g^{(2)}(0)$ of signal or idler provides a better measurement of photon-pair correlations, permitting to descriminate a single-mode PDC state with $g^{(2)}(0) = 2$ against highly multimode state with $g^{(2)}(0) \simeq 1$. Ex-

perimentally, $g^{(2)}(0)$ can be obtained by detecting the coincidence rate of one photon PDC-generated before splitting it with a 50 : 50 fiber coupler.

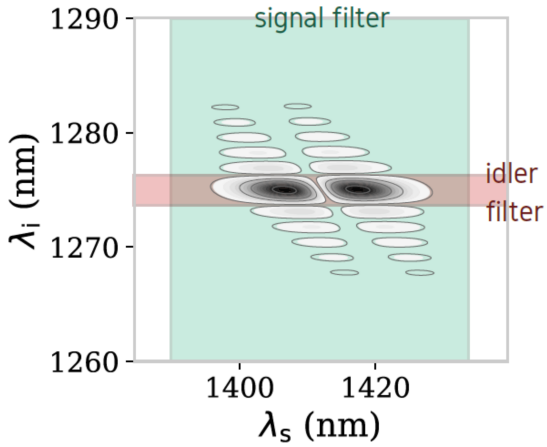

Figure 10: Contour plot of the theoretical joint spectral amplitude function combined with the bandpass filters acting at remove the phasematching sidelobes. The widths of filters in signal and idler arms are 45 nm and 3 nm, respectively.

In Fig.9 it is shown the experimental results of auto-correlation function for both photons depending on pump pulses in different orders of Hermite-Gauss modes and bandwidths ranging from 0.5 nm to 3.0 nm. As a preliminary consideration, one can assert that the $g^{(2)}(0)$, and consequentially the purity P described in Eq.38, becomes lower when the complexity structure of pump spectral-mode is higher, proportionally to its bandwidth. Such observation helps us to read properly the plots in Fig.9; indeed, for narrow-bandwidth pump pulses, the measurement is more sensitive to energy-correlation fluctuations, due to the exploitation of a short spectral range, which leads to a lower value of auto-correlation function values. Furthermore, it is possible to notice that increasing the order of Hermite-Gauss modes, which exhibits a more complex spectral feature according to the order number, the frequency correlation between idler and signal is improved, *i.e.* the

$g^{(2)}(0)$ function is lower. In Table 1 there are the highest values of auto-correlation measured for the idler photon, with a 1.5 nm broad pump, for different spectral shapes.

HG0	HG1	HG2	HG3
1.99 ± 0.02	1.93 ± 0.02	1.85 ± 0.02	1.81 ± 0.02

Table 1: Experimental values of auto-correlation function $g^{(2)}(0)$ at different frequency shapes: Gaussian (HG0), 1st-order Hermite-Gauss (HG1), 2nd-order Hermite-Gauss (HG2),3rd-order Hermite-Gauss (HG3).

The $g^{(2)}(0)$ measured to the signal arm, plotted in Fig.9 (b) is significantly lower respect to the idler one; the reason of such worsening can be find on the presence of previous mentioned side-lobes on the in-house fabricate KTP waveguide phase-matching function. As observed in the theoretical simulation of JSA contour plot in Fig.10, one can efficiently cut such noise on the idler photon by spectral filtering, while this is not possible for the signal photon. Even though the signal photons are themselves less pure, the high $g^{(2)}(0)$ of the idler ones suggests that shaped signal photons are considered highly pure when heralded by an idler detection.

2.6 CONCLUSIONS

In this experiment it has been shown a pulse-shaping approach on a PDC process, capable to produce spectrally pure heralded single photons. PDC-photon pair are generated in arbitrary temporal modes by shaping the pump pulses and optimising the dispersion of KTP in-house fabricated waveguides. The JSI measured verifies that the spectral shape of pump pulses is imparted to the signal photon, under proper phase-matching conditions. The frequency purity of this method has been verified by auto-correlation measurement $g^{(2)}(0)$, which depends strongly to the drawn feature and the bandwidth of pump spectral shape.

This method, in the quantum communication and computing frame-

work, represents a suitable tool which utilise sources capable to emit heralded single-photons on arbitrary TM basis in telecommunication band, avoiding the problem of loss due to the shaper apparatus, though partially. However, as notice during this chapter, frequency post-selection plays a fundamental role; indeed, it has been underlined that the use of filtering systems pre-detection was necessary in order to fix spectral noises produced by the KTP waveguides. In future works, one of the main tasks is to adopt different engineering strategies in order to forge properly the source, optimising the emission wavelengths for available photon detectors and customising the joint spectral amplitude to eliminate the need for filtering.

3

QUANTUM METROLOGY

"Accuracy of observation is the
Equivalent of accuracy of thinking."
— Opus Posthumous: Poems, Plays, Prose, W. Stevens

3.1 INTRODUCTION

Spectral correlations constitute non-negligible artifacts while discussing on photonics platforms simulating quantum systems, as we observed. The absolute control and understanding of such tools and their evolution due to the interaction with the environment open the way for new frontiers exploiting the unique nature of quantum mechanics [73], along with the capability of performing the best experimental devices possible for quantum computation and quantum information purposes. We focus now on the capability of taking advantages from this quantum uniqueness, going beyond the classical physical bounds concerning the measurement process, providing also a tool capable to face the manifold issues caused by the non-ideal photon-pair generation abovementioned. Such quantum enhancement of estimating measurable quantities leads to the scientific branch bearing the name of *quantum metrology*.

When considering a measurement on a system, extrapolating the information under the form of *parameters*, we need to know how to manipulate properly a state used as probe, highlighting the sensivity on the parameters under investigation. In the same way, the determination of the detection settings is crucial for the improvement of a proper measurement device enhancing the accuracy on the parameter-estimation. The concept behind "*information is physical*" asserting by Landauer [74] aids us to insert the information recovery in a physical context and to quantify its efficiency while

using classical or quantum probes. This leads to the definition of the relevant quantities [75–81] *Fisher Information* (FI) and *Quantum Fisher Information* (QFI).

3.2 CLASSICAL METROLOGY VS QUANTUM METROLOGY

The *International Bureau of Weights and Measures* (BIPM), serving since 1875 as one of the primary guards ensuring uniformity of weights and measures around the world, defines the term *metrology* as:

> "(...) the science of measurement, embracing both experimental and theoretical determinations at any level of uncertainty in any field of science and technology. (...)"

Nowadays, the presence of metrology assures the daily-life importance of precise measurements from *technological* point of view, allowing the emergence of increasingly advanced devices. Accurate GPS calibration systems, innovative auto-focusing automation or improvement in the quality of the healthcare for medical purposes are only few examples of the usefulness of a rigorous measurement approach monitored by metrology. The metrological authority is also evident in the *legal* field, necessary for the economy standardisation ensuring legal requirements vital to existence of modern society imposed by the national and international laws. The fundamental task concerning the *scientific* prospective of metrology is the constant improvement of the measurement efficiency providing the best achievable devices for the estimation of standard quantities like mass, length and time.
For this purpose, one should acknowledge the major branch of statistics, the *estimation theory*. This constitutes a markable development to establish the most efficient techniques achieving the most accurately estimation of the quantity of interest, identified by *parameters*, from any randomly distributed data collected experimentally. Generally, there are two possible approaches on such estimation problems, depending whether one assumes the parameter estimated to be a fixed variable, affecting deterministically

the ideal model that predicts the statistics of the outcome, or considering the stochastic character of the parameter itself, affecting the random fluctuations on the chosen techniques used for the measurement process.

Frequentist approach relies on the deterministic-parameter scheme, so that the statistical inference concerns only for the probabilistic nature of the measurement procedure, supposing that the variable that parametrised the system could in principle be stated up to any precision. In this case, it is possible to utilise a good measurement technique that allow to bound the effective *mean square error* of the estimation process. Otherwise, the *Bayesian* approach assumes the parameter of interest to also be randomly distributed. This method of inference exploits the *a priori* knowledge of the parameter statistical distribution, allowing to the propose of efficient adaptive measurement schemes due to its suitability for data-updating routine. As we will observe later, such approach results to be one of the closest to the maximum estimation resolution achievable, established by the Cramer Rao bound (CRB).

3.2.1 *Interferometric measurement and shot-noise limit*

In the limit of infinite number of resources probing the system, allowing to perform infinite experimental trials in order to provide the estimated parameter with indirect measurements, the distinction of the abovementioned statistical inferences aims to be approximately vanished, so that it is often the case that both methods may be directly interrelated. However, the unlimited resources hypothesis represents a hard obstacle to beat, so that one of the main tasks in metrology is to find a way in order to well optimise the finite number of resources available. The substantial improvement provided by quantum mechanical settings must be sought on the capability of many-particle quantum systems to benefit from their "non-classical" inter-particle correlations. Due to this quantum peculiarity, even when limiting to single-particle measurements, the corresponding outcomes are affected by their correlation nature and generally they are not independently distributed. This leads

to the possibility of enhancing the measurement process managing the quantum resources at the disposal differently from the classical case [82, 83].

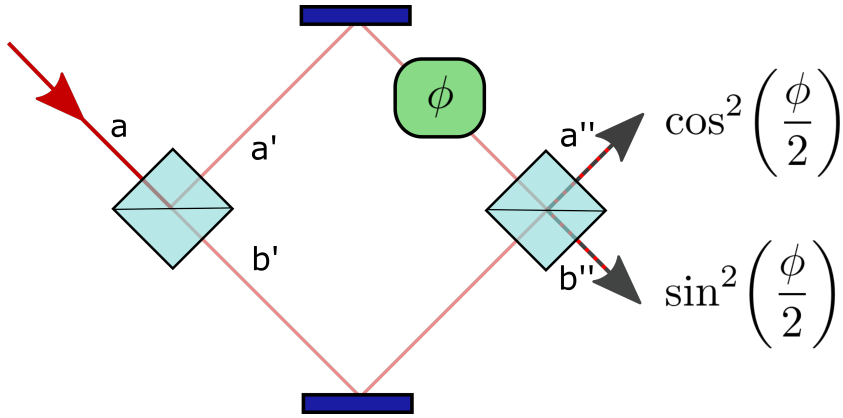

Figure 11: Mach-Zehnder interferometric scheme with the outcome probabilities for classical light.

In order to better understand this *quantum enhancement*, we focus on ultra-precise estimation via interferometric measurements. The chosen experimental apparatus is the widely used *Mach-Zehnder interferometer*, see Fig.11. In this scheme, the input light is divided in a reflected and a transmitted part by a beam splitter (BS) crystal; travelling with two different spatial paths, then they are recombined onto a second BS component. An indirect measure can be performed on the phase difference ϕ between these two paths of the interferometer by the detection of light intensity, *i.e.* the average photon number, on the two output beams.
Supposing that a coherent classical light with N on average photons enters in the interferometer on one of two possible inputs. If we consider the action of a 50:50 BS

$$\begin{pmatrix} a \\ b \end{pmatrix} = \frac{1}{\sqrt{2}} \begin{pmatrix} 1 & i \\ i & 1 \end{pmatrix} \begin{pmatrix} a' \\ b' \end{pmatrix} \tag{39}$$

transforming the input arms a and b into the reflected a' and transmitted b' paths, the output arms $a'' = 1/\sqrt{2}(a' + ie^{i\phi}b')$ and $b'' = 1/\sqrt{2}(ia' + e^{i\phi}b')$ depends on the phase difference ϕ; so that,

for one input classical beam, we can detect a fraction $\cos^2(\phi/2)$ of photons on the a'' outcome and the other fraction $\sin^2(\phi/2)$ on the b'' one. This permits to estimate the phase between the two paths on the interferometer by an intensity detection on the two output ports.
The estimation is done, but how *accurate* is the measurement? The answer relies on the intrinsic nature of the probe in use. Experimentally, the intensity detection on the abovementioned interferometer in one of the two outputs can be obtained as the statistical average $\sum_{j=1}^{N} x_j/N$ where x_j is 0 or 1 dependently on the presence of the jth photon. The classical nature of the light suggests that the x_js measurements are independent stochastic variables and they follow the *Poissonian statistics*, that represents a clue of the non-correlation between photons. So that, the relative error on that detection is given by

$$\Delta\left(\sum_{j=1}^{N}\frac{x_j}{N}\right)=\frac{\Delta x}{\sqrt{N}}. \tag{40}$$

As a bound of the measurement accuracy, $1/\sqrt{N}$ establishes the *shot-noise* limit, the ultimate precision of a phase estimation whose intensity corresponds to N photons. Such result is strongly connected to the intrinsic fluctuation of the number of photons while using coherent states measured on a Mach-Zehnder interferometer, pointing out again that the accuracy of a measurement comes from the statistical model of the employed probe.

3.2.2 *Heisemberg limit*

The occurring of even more sophisticated experiments, acting at the investigation of quantum peculiarities for large particles ensembles, as the *entanglement* property, it has been explicitly demonstrated that a quantum enhancement for the estimation problem is possible in atomic spectroscopy [84, 85] and optical interferometry [86–88]. A general framework is then established [82, 83] in order to demonstrate qualitatively the convenience of quantum strategies capable to conduct a super-resolutive estimation, beating the bounds imposed by classical systems and enhancing the accuracy

of parameter inference. Reminding the Mach-Zehnder scheme in Fig.11, one can now revisit the interferometric apparatus exploiting quantum correlation with quantum systems, see Fig.12.

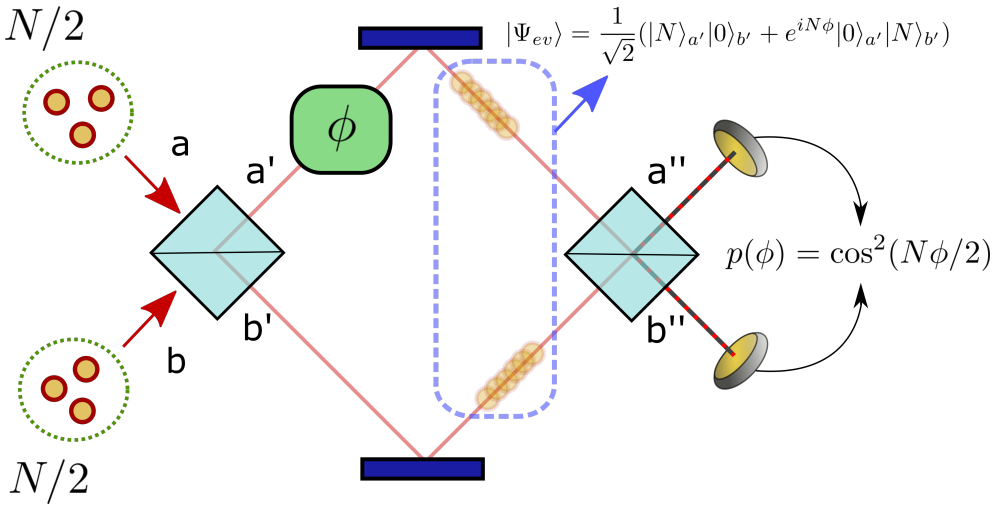

Figure 12: Interferometric scheme for phase estimation using N00N states.

In both input arms, before the first BS crystal, we inject N/2 single photons (N = 2), that create the highly entangled state, known as N00N *state*,

$$|\Psi\rangle = \frac{1}{\sqrt{2}}(|N\rangle_{a'}|0\rangle_{b'} + |0\rangle_{a'}|N\rangle_{b'}), \tag{41}$$

which describe the superposition of distinct Fock states $|n_{a'} = N\rangle|n_{b'} = 0\rangle$ and $|n_{a'} = 0\rangle|n_{b'} = N\rangle$ referring on the two paths a' and b'. Observing the Mach-Zehnder scheme, the unique nature of such state leads to the evolution of the state,

$$|\Psi_{ev}\rangle = \frac{1}{\sqrt{2}}(|N\rangle_{a'}|0\rangle_{b'} + e^{-iN\phi}|0\rangle_{a'}|N\rangle_{b'}). \tag{42}$$

In Eq.42 one notice the improvement of the phase affecting all the N photons at the same time, even maintaining the other path which can be considered as a reference. This quantum peculiarity is more evident while calculating the probability $p(\phi)$ that the output state $|\Psi_{ev}\rangle$ is equal to the initial state $|\Psi\rangle$,

$$p(\phi) = |\langle \Psi | \Psi_{ev} \rangle|^2 = \cos^2(N\phi/2), \tag{43}$$

whose variance is $\Delta^2 p(\phi) = p(\phi) - p^2(\phi)$. The error of the phase difference can finally be obtained from the error propagation $\Delta\phi = \Delta p(\phi) / \left| \frac{\partial p(\phi)}{\partial \phi} \right|$ that results to be equal to $1/N$, that represent the so-called *Heisenberg limit*, constituting a bound for the measurement precision.

The enhancement of $\sqrt{N}$ over the accuracy of the measurement using N photons with classical approach can be achieved within the joint strategy of using quantum correlation between the probe-particles and the proper collective nonlocal measurements, allowing us to exploit the most from the entanglement.

3.3 QUANTUM ESTIMATION THEORY

The mentioned estimation approaches with coherent light and N00N states constitute two markable examples of different stochastic management of the amount of resources within reach highlighting the differences between classical and quantum metrology scheme. The aim of this section is to extend such paradigm on generic states and investigate the conditions achieving an optimal measurement system.

We observed that a super-resolution indirect measurement on a parameter, identified by the phase difference in optical interferometry, is reached with a smart optimisation of the N resources used as a probe, thanks to the quantum properties of single-photon beams. In particular, such improvement can be performed due to the different statistical model of quantum systems compared to the classical ones. This capability of accurate measurements beyond the limits of classical schemes is addressed in the *quantum estimation theory* (QET) scenario, which provides analytical tools finding the optimal measurement for a certain quantum system [79–81]. Two main stances of QET can be identified: *Global* QET looks for the optimisation of measurements that does not depend on the value of the parameter under investigation, averaging on

all the possible values assumed by such parameter. Such global QET strategy is often used on that estimation problems, evaluating the lower bounds on accuracy for the estimation of parameters imposed by unitary transformations. Some of this theory approach can be observed for single-mode phase [89], squeezing [90] and two-mode transformation [91]. The other paradigm, *local* QET, refers on the minimisation of the variance on the measurement procedure at a fixed value of the parameter. This kind of strategy has been applied for quantum phase estimation and to estimation problems with non-unitary processes. Some examples are the noise estimation of amplitude damping [92] and depolarising quantum channels [93]. In this section we present some metrological tools in the local QET context, exploring the explicit formulas for FI and QFI, looking at the possibility of saturate the ultimate bounds imposing by the Cramer Rao and quantum Cramer Rao inequalities.

3.3.1 *Metrological scheme*

We consider a generic metrological scenario for the estimation process, depicted in Fig.13, highlighting the three-steps approach for the indirect measurement of a ϕ parameter. Firstly, one must create the optimal input state defined by a density matrix ρ acting as a probe for the parameter estimation; that procedure aims at finding the suitable quantum setting in order to improve the parameter sensivity on the quantum state itself.

This prepared quantum state then senses the action of the parameter we want to estimate, permitting us to illustrate the evolved state as a ϕ-dependent density matrix ρ_ϕ. After the interaction, one must extrapolate the highest amount of information of the parameter unknown value from the ρ_ϕ state; for doing so, a suitable *quantum measurement* must be performed on such system.
A quantum measurement corresponds to an hermitian operator $\hat{O}$ acting on the Hilbert space. In particular, we look at the group of measurements specifically efficient for our purposes, called *positive operator valued measure* elements (POVMs). A POVM is generally represented by any set of quantum measurement operators,

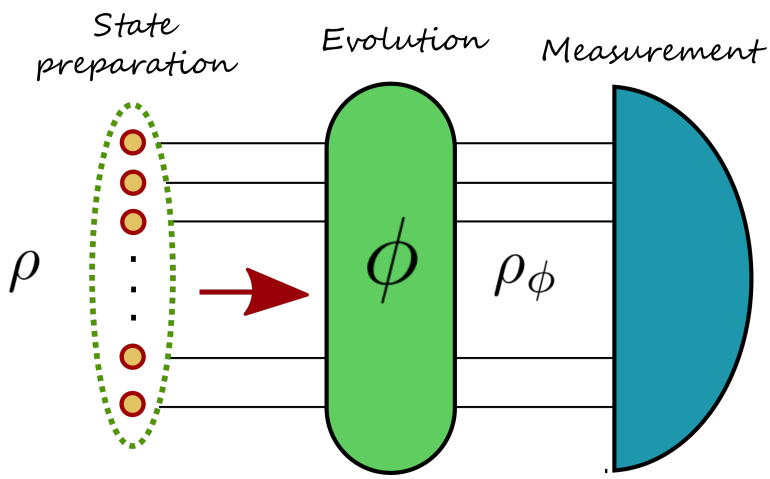

Figure 13: Metrological scheme of quantum estimation process.

$\{\Pi_i\}$, defined as non-negative $\Pi_i \geqslant 0$ and satisfying the completeness condition $\sum_i \Pi_i = \mathbb{I}$; each outcome i of the measurement is then obtained with probability $\eta_i = \mathrm{Tr}[\rho\Pi_i]$.
From metrological point of view, in such scheme we are interested on evaluating the ultimate bounds on sensivity occurring for a general ρ quantum state preparation choice and its evolution ρ_ϕ and determining the optimal measurements able to reach these bounds.

3.4 SINGLE PARAMETER ESTIMATION

Before starting to study the estimation limits taken into account previously, we need to review the fundamental tools behind the problem of *parameter estimation theory* [94] and in particular we need to investigate the measurement processes, *i.e.* the data collection acquired, while testing a system.

3.4.1 *Parameter estimators*

The mathematical approach, that is valid either for quantum or classical systems, is following described: from the experimental device one gives N-point data set $\mathbf{x} = \{x_1, x_2, \ldots, x_N\}$ which rep-

resents a N-independent random variables with identical distribution according to a common *Probability Density Function* (PDF), $p_\varphi(X)$, that depends on the unknown parameter φ we aim to determine. With the measurement procedure, one wish to constructs an estimator $\tilde{\varphi}_N(\mathbf{x})$ that can be interpreted as a function that supply the most precise estimate of the parameter φ, considering the given data set $\mathbf{x}$. It is important to remark that as the random data collection has statistical properties, the estimator $\tilde{\varphi}_N(\mathbf{x})$ is afflicted also by the data statistics leading to a collective PDF that can be factorised as $p_\varphi(\mathbf{x}) = \prod_{i=1}^{N} p_\varphi(x_i)$. So that, for the local theory approach, *i.e.* assuming that φ is deterministic with a fixed value, within a frequentist approach it is possible to define a *mean value* of the estimator $\tilde{\varphi}_N(\mathbf{x})$,

$$E[\tilde{\varphi}_N(\mathbf{x})] = \langle \tilde{\varphi}_N(\mathbf{x}) \rangle = \int d^N x p_\varphi(\mathbf{x}) \tilde{\varphi}_N(\mathbf{x}), \tag{44}$$

and, the *variance*,

$$\begin{aligned} \mathrm{Var}[\tilde{\varphi}_N(\mathbf{x})] =& \left\langle \left(\tilde{\varphi}_N(\mathbf{x}) - \langle \tilde{\varphi}_N(\mathbf{x}) \rangle_\varphi \right)^2 \right\rangle \\ =& \int d^N x p_\varphi(\mathbf{x}) \left(\tilde{\varphi}_N(\mathbf{x}) - \langle \tilde{\varphi}_N(\mathbf{x}) \rangle \right)^2. \end{aligned} \tag{45}$$

We now restrict to the case of *unbiased* estimators, allowing us to always output on average the true parameter, $\langle \tilde{\varphi}_N(\mathbf{x}) \rangle_\varphi = \varphi$, and to match the variance in Eq.45 with the *mean square error* (MSE),

$$\Delta^2 \tilde{\varphi}_N(\mathbf{x}) = \int d^N x p_\varphi(\mathbf{x}) \left(\tilde{\varphi}_N(\mathbf{x}) - \varphi \right)^2. \tag{46}$$

For sake of simplicity, all the quantities analysed below are defined assuming a single-outcome PDF, $p_\varphi(x)$.

3.4.2 *Cramér-Rao Bound*

The solution at the estimation problem can be found looking at the *optimal estimators*, which are those saturating the *Cramér-Rao inequality* [95],

$$\Delta^2\tilde{\varphi}_N(x) \geqslant \frac{1}{NF_\varphi(x)} \tag{47}$$

which establishes a lower bound, *i.e. Cramér-Rao Bound* (CRB), on the mean square error $\Delta^2\tilde{\varphi}_N(x)$ of any estimator of the parameter φ, with N trials of measurement. It is important to stress that, due to the unbiasedness hypothesis, the defined bound on Eq.132 dictates a lower limit also for the variance of the estimator $\mathrm{Var}[\tilde{\varphi}_N(x)]$, which is the more experimentally important entity that could be determined for an unknown φ based only on the measured data set.
The relevant quantity that limits the mean square error in Eq.132 is the so-called classical *Fisher Information* (FI),

$$F_\varphi(x) = \int dx p_\varphi(x)\left(\frac{\partial \ln p_\varphi(x)}{\partial\varphi}\right)^2 = \int dx \frac{1}{p_\varphi(x)}\left(\frac{\partial\, p_\varphi(x)}{\partial\varphi}\right)^2. \tag{48}$$

In terms of information extrapolation, the FI can be read as the amount of knowledge of φ achievable with a measurement, undergoing with a statistical distribution $p_\varphi(x)$. Indeed, looking at the CRB in Eq.132, for a given parameter φ_0, if $F_\varphi(x)\big|_{\varphi_0} = 0$ the extraction of any information from the system is not possible, while for $F_\varphi(x)\big|_{\varphi_0} = \infty$ it is in principle possible to determine with absolute certainty the true value of φ. For completeness, a discrete version of FI information can be exposed as,

$$F_\varphi(x) = \sum_x p_\varphi(x)\left(\frac{\partial \ln p_\varphi(x)}{\partial\varphi}\right)^2. \tag{49}$$

The quantities analysed above results to be valid both for classical and quantum entities; for quantum systems we remark that the estimation problem relies on the evolution of a density matrix ρ into ρ_φ. So that, the quantum parameter estimation aims at finding a optimal quantum estimator, that is a selfadjoint operator $\hat{O}_\varphi$, for φ which describe a quantum measurement obtained from any classical data processing. In quantum mechanics, the probabilities $p_\varphi(x)$ characterising the FI are distributed following the *Born's rule*,

$$p_\varphi(x) = \mathrm{Tr}[\Pi_x \rho_\varphi], \tag{50}$$

where $\{\Pi_x\}$ constitutes a POVM set, introduced in Sec. 3.3.1.

It is important to mention the properties of *non-negativity* and *additivity* of FI; in particular, the second property allows us to include the main differences between quantum and classical approach on the estimation problem. Indeed, proceeding with M repetitions of the same measurement, if their statistics are *independently* distributed, the global FI can be defined as the sum of the singular measurement FI, $F_\varphi[p_\varphi^M(x)] = MF_\varphi[p_\varphi(x)]$, for factorable probability $p_\varphi^M(x) = \otimes_{l=1}^M p_\varphi^{(l)}(x)$, leading to the already mentioned *shot-noise* scaling $1/M$ for the MSE. Concerning quantum probes, this classical limit on precision also happens for independentely quantum distributed samples, for example N00N states with $N = 1$ particle, taking the name of *Standard Quantum Limit* (SQL). Furthermore, it is important to point out the difference between the measurement repetition rate M and the number of photons used on the system N; actually, in the classic case the statistically independence of the probes causes the equivalence between N and M.

3.4.3 *Quantum Cramér-Rao Bound*

Accordingly to such quantum description, one can assert that the FI is strongly correlated to the chosen measurement we utilise for the extraction of the unknown parameter, determined by the POVM set; this means that in principle an optimal estimator can be found through the proper settings of measurement apparatus. However, an ultimate bound holding for any POVM set $\{\Pi_x\}$ can be derived [79, 80, 96]. Introducing the Hermitian operator L_φ called *Symmetric Logarithmic Derivative* (SLD), defined for any state ρ_φ via the relation,

$$\frac{\partial \rho_\varphi}{\partial \varphi} = \frac{1}{2}[L_\varphi \rho_\varphi + \rho_\varphi L_\varphi], \tag{51}$$

we have that [97, 98],

$$\frac{\partial p_\varphi(x)}{\partial \varphi} = \mathrm{Tr}\left[\frac{\partial \rho_\varphi}{\partial \varphi}\Pi_x\right] = \mathrm{Re}\{\mathrm{Tr}[\rho_\varphi \Pi_x L_\varphi]\}. \tag{52}$$

With this relation, it is possible to rewrite the FI in Eq.48 as,

$$F_\varphi(x) = \int dx \frac{(\mathrm{Re}\{\mathrm{Tr}[\rho_\varphi \Pi_x L_\varphi]\})^2}{\mathrm{Tr}[\rho_\varphi \Pi_x]}. \tag{53}$$

With the help of Cauchy-Schwartz inequality and the completeness property of the set $\{\Pi_x\}$, we can find the ultimate bound on precision, maximising the FI over the quantum measurements,

$$\begin{aligned} F_\varphi(x) \leqslant & \int dx \left| \frac{(\mathrm{Re}\{\mathrm{Tr}[\rho_\varphi \Pi_x L_\varphi]\})^2}{\mathrm{Tr}[\rho_\varphi \Pi_x]} \right|^2 \\ \leqslant & \int dx \mathrm{Tr}[\Pi_x L_\varphi \rho_\varphi L_\varphi] \\ = & \mathrm{Tr}[L_\varphi \rho_\varphi L_\varphi] = \mathrm{Tr}[\rho_\varphi L_\varphi^2]. \end{aligned} \tag{54}$$

The last entity on the above inequality chain is defined as *Quantum Fisher Information* (QFI), $H_\varphi = \mathrm{Tr}[\rho_\varphi L_\varphi^2]$, leading to the quantum version of the inequality in Eq.47,

$$\Delta^2 \tilde{\varphi}_M(x) \geqslant \frac{1}{M H_\varphi} \tag{55}$$

constituting the *Quantum Cramér-Rao Bound* (QCRB) on the estimator $\tilde{\varphi}_M(x)$; in this description we identify the number of the experimental repetitions as M in order to highlight that the sample size *does not* corresponds to the N number of particles using for the estimation.
Usually, an alternative depiction of QFI can be adopted by writing the parameter dependent density operator ρ_φ on its eigenbasis $\rho_\varphi = \sum_n \rho_n |\psi_n\rangle\langle\psi_n|$; this allows us to redefine the SLD operators as,

$$L_\varphi = 2 \sum_{nm} \frac{\langle\psi_m|\partial\rho_\varphi/\partial\varphi|\psi_n\rangle}{\rho_n + \rho_m} |\psi_m\rangle\langle\psi_n|, \tag{56}$$

where the sums include only terms with $\rho_n + \rho_m \neq 0$. The QFI so reads,

$$H_\varphi = \sum_{nm} \frac{|\langle\psi_m|\partial\rho_\varphi/\partial\varphi|\psi_n\rangle|^2}{\rho_n + \rho_m}. \tag{57}$$

The QCRB suggests a fundamental aspect for the QET: as we observed from the QFI $H_\varphi(x)$, it depends only on the geometrical structure of the quantum statistical model, while there is no connections with the type of measurement approach, differently from the FI. So that, one could supposed to define the QFI as a measure of the maximal information extraction for a certain φ-dependent quantum state described by the density operator ρ_φ.

Some *additivity* considerations can be made similarly to the classical case; most importantly, the QFI generalises the notion of additivity of FI, from the probability to density matrices what may be verified by considering *separable* states, *i.e.* $\rho_\varphi^N = \otimes_{n=1}^N \rho_\varphi^{(n)}$, leading to the global QFI, $H_\varphi[\rho_\varphi^N] = NH_\varphi[\rho_\varphi]$. This formulation allows us to assume that each particle $\rho_\varphi^{(n)}$ can be treated as a separate copy, and consequently observing a linear precision improvement of the QCRB leading to the SQL-like scaling. For certain maximal N-particle entangled states, we observe the *quantum enhancement* achieving the Heisenberg-scaling $1/N^2$. This QFI peculiarity allows us to discriminate separability from multipartite entanglement in a N qubit states makes it an useful entanglement criteria which has been proved to be sufficient for arbitrary quantum states and also necessary for pure states [99–101].

3.5 SATURABILITY CONDITIONS

The search of optimal quantum measurements via the above bounds on the estimator variance in Eqs.47 and 55 has been a challenging subject of study [102–104]. Such optimisation corresponds to the POVMs such that the FI equal the QFI, *i.e.* saturating both Cramér-Rao inequalities. Looking at the inequality chain in Eq.54, the saturation occurs when $\mathrm{Tr}[\rho_\varphi \Pi_x L_\varphi]$ is a real number $\forall\varphi$, and when

$$\frac{\sqrt{\rho_\varphi}\sqrt{\Pi_x}}{\mathrm{Tr}[\rho_\varphi \Pi_x]} = \frac{\sqrt{\rho_\varphi} L_\varphi \sqrt{\Pi_x}}{\mathrm{Tr}[\rho_\varphi \Pi_x L_\varphi]} \tag{58}$$

$\forall \varphi$. This condition is sadisfied *if and only if* the POVM set $\{\Pi_x\}$ is made by the set of projectors over the eigenstates of L_φ, which, in turn, represents the optimal POVM to estimate the parameter φ, permitting us to equal the FI with the QFI.

3.5.1 *Multiparameter case*

The considerations mentioned above requires a more tricky approach while dealing with systems dependent reliant on more than one parameter [105–113]. In this situations we consider a family of quantum states $\rho_{\boldsymbol{\varphi}}$ that depends on a set of K parameters identified by the parameter vector $\boldsymbol{\varphi} = \{\varphi_\mu\}$ with $\mu = 1, \ldots, K$. So that, the accuracy on the unbiased estimator $\tilde{\boldsymbol{\varphi}}(x)$ we want to optimise relies on its *covariance matrix* $\boldsymbol{\Sigma}[\boldsymbol{\varphi}]$, whose elements are defined as

$$\Sigma[\boldsymbol{\varphi}]_{ij} = \langle (\tilde{\varphi})_i - \varphi_i)(\tilde{\varphi})_j - \varphi_j) \rangle. \tag{59}$$

Consequently, in the multiparameter scenario the classical CRB reads,

$$\boldsymbol{\Sigma}[\boldsymbol{\varphi}_M] \geqslant \frac{1}{M} \mathbf{F}_{\boldsymbol{\varphi}}^{-1}(x), \tag{60}$$

where now, the FI $\mathbf{F}_{\boldsymbol{\varphi}}(x)$ is defined as a $K \times K$ matrix, and its elements are

$$\{\mathbf{F}_{\boldsymbol{\varphi}}(x)\}_{ij} = \int dx p_\varphi(x) \left(\frac{\partial \ln p_\varphi(x)}{\partial \varphi_i} \right) \left(\frac{\partial \ln p_\varphi(x)}{\partial \varphi_j} \right). \tag{61}$$

The quantum counterpart of multiparameter estimation problem, the relevant object is identified by the QFI matrix; considering that L_i are the SLD operator referred to the parameter φ_i, the QFI matrix elements are defined as

$$\begin{aligned}\{\mathbf{H}_{\boldsymbol{\varphi}}\}_{ij} =& \mathrm{Tr}\left[\rho_{\boldsymbol{\varphi}}\frac{L_i L_j + L_j L_i}{2}\right] = \mathrm{Tr}\left[\frac{\partial\rho_{\boldsymbol{\varphi}}}{\partial\varphi_i}L_j\right] = \mathrm{Tr}\left[\frac{\partial\rho_{\boldsymbol{\varphi}}}{\partial\varphi_j}L_i\right] \\ =& \sum_n \frac{(\partial\rho_n/\partial\varphi_i)(\partial\rho_n/\partial\varphi_j)}{\rho_n} + \sum_{n\neq m}\frac{(\rho_n-\rho_m)^2}{\rho_n+\rho_m} \\ & \times [\langle\psi_n|\partial\psi_m/\partial\varphi_i\rangle\langle\partial\psi_m/\partial\varphi_j|\psi_n\rangle + \langle\psi_n|\partial\psi_m/\partial\varphi_j\rangle\langle\partial\psi_m/\partial\varphi_i|\psi_n\rangle].\end{aligned} \tag{62}$$

where we use the matrix decomposition abovementioned.
As observed before, in the single parameter scenario the ultimate achievement precision of estimating involves while choosing the projective measurement on the eigenbasis of the SLD that define the QFI, which is always possible. However, with the multiparameter approach, this possibility is not ensured; in general, it is not obvious that the optimal measurement is compatible for all the parameters characterising the system. So that, if the SLD operators commute, $[L_i, L_j] = 0$, one can reach the optimality by performing a projection set of measurements on the single eigenbasis for both SLDs, allowing to extract information on the parameter φ_i as well as φ_j. This condition results to be sufficient but not necessary; indeed, for no-commuting SLD L_i, a *weaker condition* has been proved to be necessary for pure states [103, 114] that can be achieved providing

$$\mathrm{Tr}[\rho_{\boldsymbol{\varphi}}[L_i, L_j]] = 0, \tag{63}$$

where we focus on the vanishing of the expectation value on the probe state of the commutator, instead of the simple commutation condition. Such condition reminds the better known *observable incompatibility* condition that leads to the *Heisenberg uncertainty*, but averaging on the probe state $\rho_{\boldsymbol{\varphi}}$ suggests that the state preparation plays a key role for the achievability of optimal measurement, in quantum metrological protocol. In fact, this puts stringent constraints on the preparation strategies we adopt, in order to provide any chances for reaching the maximal informative measurement approach; so that, in this circumstance, no measurement strategy may help enhancing the simultaneous estimation on a multiparameter system, since the QFI is the ultimate limit on the accuracy,

and the FI, backing to the statistical independent case. The assessment of the weak condition has been verified for some unitary evolutions, as spin rotation on two orthogonal directions [103, 115], *only* for specific input probe states while the non-commutativity of the SLD operators associated to the rotation parameter prevents the possibility of optimal joint-estimation process.

While dealing with multiparameter metrology an important task to consider is the dependency of the parameters we want to estimate, thus the study of statistical correlations between the chosen estimators. Indeed, even concerning classical probes and measurements, this leads to the possibility of saturating the CRB while the FI matrix is *diagonal*, *i.e* off-diagonal elements vanish $\{\mathbf{F}_{\boldsymbol{\varphi}}(x)\}_{ij} = 0$ for $i \neq j$. In some sense, the amount of correlation between estimators oppose to the possibility of joint-estimate optimally all the parameters affecting the system $\rho_{\boldsymbol{\varphi}}$. The same conjecture is valid also for the maximum information extraction on a probe state described by the QFI matrix. The parameter-independence holds while the off-diagonal of such matrix are zero. Combining this uncorrelation condition with the weak condition on Eq.63, a necessary requirement for a multiparameter compatibility is [103]

$$\mathrm{Tr}[L_i L_j \rho_{\boldsymbol{\varphi}}] = 0, \tag{64}$$

while $i \neq j$; such requirement can be rewritten considering the explicit form of the SLD L_i in Eq.56 as

$$\sum_{nm} \frac{\rho_m}{(\rho_n + \rho_m)^2} \langle \psi_m | \partial \rho_{\boldsymbol{\varphi}} / \partial \varphi_i | \psi_n \rangle \langle \psi_n | \partial \rho_{\boldsymbol{\varphi}} / \partial \varphi_j | \psi_m \rangle = 0. \tag{65}$$

This independence condition remark a fundamental aspect of quantum metrology: the ultimate bound on precision for the estimation of a set of one or more parameters $\boldsymbol{\varphi}$ corresponding to the QCRB in Eq.47 *does not* depend on the chosen measurement implemented on our system $\rho_{\boldsymbol{\varphi}}$. However, it relies *exclusively* on the sensivity of the prepared quantum system respect on the parameters which aims to provide the maximum QFI for all the parameters.

One the final goal in quantum metrology is the saturation of the inequality $\mathbf{F}_{\boldsymbol{\varphi}}(x) \leqslant \mathbf{H}_{\boldsymbol{\varphi}}$ that requires the existence of compatible measurements ensuring the achievability of extracting the maximal amount of information of $\boldsymbol{\varphi}$.

3.6 BAYESIAN ESTIMATION

The estimation problem has been addressed previously on its key references, investigating the limits on information extraction from a system within a chosen set of measurements. We observed that these bounds establish the ultimate measure precision using a certain estimator, able to provide the true value of unknown parameter set. We focus now on the *Bayesian estimator* and its asymptotical properties capable to saturate the CRB to its variance.

The Bayesian approach represents one example of global estimation of stochastic parameter; indeed, in contrast to the local strategy, that holds the hypothesis that the unknown parameter φ has a fixed value φ^*, in the global estimation the estimated parameter is assumed to be a random variable, distributed according to *a priori* PDF, $p(\varphi)$, which is the knowledge about φ before the measurement procedure. In this instance, we now must consider two statistical inferences while performing the estimation, the prior parameter distribution $p(\varphi)$ and the overall probability $p(x)$ from the random variable x obtained from the set of data measured; in turn, also some consideration on conditional probabilities $p(\varphi|x)$ and $p(x|\varphi)$ need to be conducted. The relation of all this quantities has been described by Bayes [116],

$$p(x|\varphi)p(\varphi) = p(\varphi|x)p(x). \tag{66}$$

After M independent measurements the a posteriori probability to obtain φ from a given data set $x = \{x_1, x_2, \ldots, x_M\}$ is,

$$p_M(\varphi|x) = \frac{1}{\mathcal{N}} \prod_{k=1}^{M} p(x_k|\varphi), \tag{67}$$

assuming that the a priori distribution $p(\varphi)$ is uniform, and where $\mathcal{N} = \int_\Phi d\varphi p_M(\varphi|x)$ is a normalisation factor over the pa-

rameter space Φ.
The Bayesian estimator are thus obtained as,

$$\begin{aligned}\varphi_B &= \int_\Phi d\varphi\, \varphi p_M(\varphi|x),\\ \Delta^2\varphi_B &= \int_\Phi d\varphi\, (\varphi-\varphi_B)^2 p_M(\varphi|x).\end{aligned} \tag{68}$$

It has been shown that such estimator is asymptotically optimal, ensuring the saturability of CRB for a large size of data sample [116, 117].
In fact, for $M \gg 1$, we can use the law of large numbers, and Eq.134 can be written as,

$$p_M(\varphi|x) \simeq^{M\gg 1} \frac{1}{\mathcal{N}} \prod_x p(x|\varphi)^{Mp(x|\varphi^*)} \equiv p(\varphi|M), \tag{69}$$

where φ^* is the true and unknown value of the parameter.
In this limit, the a posteriori probability can be explicitly calculated as,

$$p(\varphi|M) = \frac{1}{\mathcal{N}} \exp\left[M \int dx p(x|\varphi^*) \log p(x|\varphi)\right], \tag{70}$$

where we used $\log \prod_x \to \int dx$.
The Eq.70 can be interpreted as the relative entropy between the two distributions $p(x|\varphi^*)$ and $p(x|\varphi)$. It has been demonstrated that, for homodyne detection, the maximum of this distribution occurs for a suitable estimator capable to provide the true value φ^* [117].
Furthermore, the Eq.70 can be approximated by a Gaussian distribution, with mean φ^* and variance Δ^2_G,

$$\begin{aligned}\Delta^2_G &= -\left[\frac{1}{p(\varphi^*|M)} \frac{d^2 p(\varphi|M)}{d\varphi^2}\bigg|_{\varphi=\varphi^*}\right]^{-1}\\ &= \frac{1}{M}\left[\sum_x \frac{1}{p(x|\varphi^*)} \frac{d^2 p(x|\varphi)}{d\varphi^2}\bigg|_{\varphi=\varphi^*}\right]^{-1} = \frac{1}{MF(\varphi^*)}\end{aligned} \tag{71}$$

where $F(\varphi^*)$ is the FI associated to the distribution $p(x|\varphi^*)$, proving the saturability of Bayesian inference asymptotically.

4

ENTANGLING MEASUREMENTS FOR MULTIPARAMETER ESTIMATION

"The only real life is the collective
Life of the race; individual life has no
Existence except as an abstraction."
— A General View of Positivism, A. Comte

4.1 INTRODUCTION

Photonic devices play a fundamental role for the new quantum technology era, as discussed before; in particular the sensing and imaging fields are one of the most representative examples of progress using optical systems. Schematising the operating principle of *optical sensors* as a difference of reference unperturbed beam and the one that interact with the environment under investigation, the problem of performing an efficient sensor is reduced to an estimation of relative *phase* between these two beams. This kind of technology is widely used on modern devices, *i.e.* laptop, smartphones etc., but results a very important tool also for many novel researches. One example is the recent observation of gravitational waves, measuring very small phase fluctuations detected by the Michelson interferometers of Laser Interferometer Gravitational-Wave Observatory (LIGO) located in Livingstone (US) and Virgo in Pisa (Italy).

Considering the large use of such optical sensors, the optimisation of the required number of resources for a very accurate phase-estimation experiments is needed. Indeed, this improvement represents a fundamental requirement for the detection of very small perturbations, like gravitational-wave, as well as the highly-damage sample characterisation, like biological materials. Following this concept, quantum metrology aims to be a suitable tool for the

achievement of this optimisation task, as described in the previous chapter. However, even the transformation occurring on phase-shifts are frequently unitary transformations, we consider a dissipative behavior in order to define our experimental scenario. Such approach occurs if we consider optical devices where the probes, *i.e.* single-photon states, are not monochromatic. A large spectral band in dispersive medium induces a different response on the phase-shift, causing a broadening of the phase-shift distribution. As discussed in the previous Chapter, the joint-estimation strategy offers a suitable approach, making the most of the resources exploited for the estimation procedure combined with the proper measurement set. In this work I present a particular choice of measurement approach, *i.e.* the *entangling measurement*, in a multiparameter scheme, where the action of our device is investigated either for the estimation of phase and dissipation and for the estimation of two phases on two different basis, showing two different experimental examples of measurement compatibility.

4.2 MULTIPARAMETER ESTIMATION ON DISPERSIVE MEDIUM

In Chapt.3 we observed that the performance of a measurement is strictly linked to the quantum state used as the probe and the measurement apparatus, *i.e.* the positive operator-valued measurements (POVMs). The probe state and measurement device choices define the Fisher Information (FI) and Quantum Fisher Information (QFI) matrices, and consequently the ultimate precision for the multi-parameter estimation process established by the the Cramér-Rao bound (CRB).
We observed before that pure states constitutes a relevant case on the achievability of optimal measurements; for this reason we focus now on pure qubit states that represents an effective description of coherent states and N00N states in optical interferometry as well as in Ramsey instance [105, 118]. A general density matrix modelling a single qubit state, can be described in a two-level picture,

$$\rho_0 = \begin{pmatrix} \cos^2\left(\frac{\theta}{2}\right) & \cos\left(\frac{\theta}{2}\right)\sin\left(\frac{\theta}{2}\right) \\ \cos\left(\frac{\theta}{2}\right)\sin\left(\frac{\theta}{2}\right) & \sin^2\left(\frac{\theta}{2}\right) \end{pmatrix}, \tag{72}$$

where θ represent the probe value associated to the degree that span the x-z plane on the Bloch sphere.
Parametrising the phase-shift evolution of the system as ϕ and the phase diffusion as δ, the single-qubit state reads,

$$\rho_{\phi,\delta} = \begin{pmatrix} \cos^2\left(\frac{\theta}{2}\right) & \cos\left(\frac{\theta}{2}\right)\sin\left(\frac{\theta}{2}\right)e^{-i\phi-\delta^2} \\ \cos\left(\frac{\theta}{2}\right)\sin\left(\frac{\theta}{2}\right)e^{i\phi-\delta^2} & \sin^2\left(\frac{\theta}{2}\right) \end{pmatrix}. \tag{73}$$

The associated QFI matrix $H_{ij} = \mathrm{Tr}[\rho_{\phi,\delta}\{L_i, L_j\}]$, with $\{A, B\}$ denoting the anti-commutator, can be calculated using the SLD operators $\{L_i\}$ as showed in the previous chapter, and it reads [105]

$$\overline{H} = \sin^2\theta \begin{pmatrix} e^{-2\delta^2} & 0 \\ 0 & \frac{4\delta^2}{e^{2\delta^2}-1} \end{pmatrix}, \tag{74}$$

while the FI matrix $\overline{F}$ is defined by the probabilities

$$p_i(\phi, \delta) = \mathrm{Tr}[\overline{\Pi}_i \rho_{\phi,\delta}] \tag{75}$$

for the estimation parameters $\{\phi, \delta\}$ associated to the chosen measurement $\overline{\Pi}_i$. It is worth to pointing out that the QFI matrix described in Eq.74 is in diagonal form, which means that the parameters ϕ and δ are statistically independents ensuring one of the important task for the attainment of optimal measurements.

It is now crucial to remark a fundamental concept behind the optimisation of a measurement in such scenario. While the QFI matrix determines the ultimate achievable precision of estimating the parameter on density matrices $\rho_{\vec{\varphi}}$ dependent on a set of parameters $\vec{\varphi} = \{\varphi_1, \varphi_2, \ldots\}$, the FI matrix defines the amount of the extrapolated information by the use of a chosen measurements described by the matrices $\overline{\Pi}_i$. This lead to the already mentioned Quantum CRB (QCRB) $\overline{H} \geqslant \overline{F}$ that imposes a limit on the maximal precision measurement with a given quantum state $\rho_{\vec{\varphi}}$. In order to establish

the goodness of a measurement for the two-parameter estimation, it is useful to introduce the trade-off quantity,

$$\Upsilon = \mathrm{Tr}[\overline{F}^{\mathrm{eff}}\overline{H}^{-1}] = \frac{F^{\mathrm{eff}}_{\phi\phi}}{H_{\phi\phi}} + \frac{F^{\mathrm{eff}}_{\delta\delta}}{H_{\delta\delta}}, \tag{76}$$

where $\overline{F^{\mathrm{eff}}} = 1/\overline{F}$ is the *effective* FI that consider all the possible correlations between the parameters ϕ and δ. In fact, the diagonal elements of the effective FI can be calculated as,

$$F^{\mathrm{eff}}_{11} = F_{11} - \frac{F^2_{12}}{F_{22}}, \tag{77a}$$

$$F^{\mathrm{eff}}_{22} = F_{22} - \frac{F^2_{12}}{F_{11}}, \tag{77b}$$

that are explicitly dependent on the correlation elements of the FI matrix $F_{12} = F_{21}$.
The quantity defined in Eq.76 represents a figure of merit for the performance of a measurement strategy in the multi-parameter estimation scenario on a fixed quantum state $\rho_{\phi,\delta}$. We remark that the necessary and sufficient condition for the saturation of the QCRB, and consequently for the maximal achievable performance of the measurement choice relies on the weak condition,

$$\mathrm{Tr}[\rho_{\phi,\delta}[L_i, L_j]] = 0. \tag{78}$$

We have already studied the impact of such condition for the possibility of find optimal measurements in the estimation problem; for this work in particular, we will see that such compatibility condition is valid for the dispersive joint-estimation case, while is not always addressed for two phase-shifts along different orthogonal directions. We now explore the main differences between two possible measurements approaches: the *separable measurements* and the *collective measurements* [105].

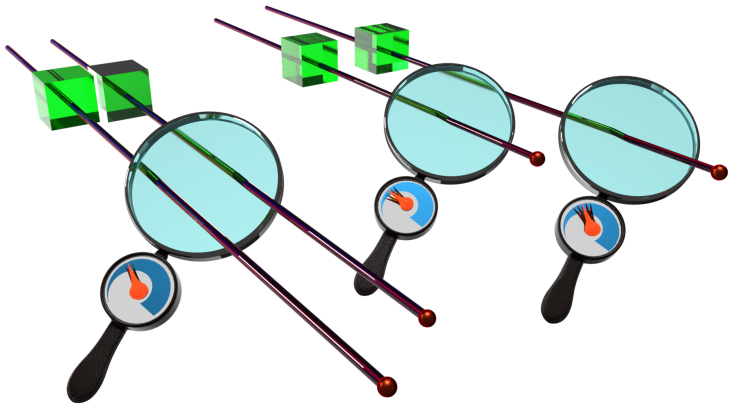

Figure 14: Conceptual figure of collective measurements and separable measurements.

4.2.1 *Separable measurements*

Individual or separable measurements consist on a set of POVMs that its elements $\overline{\Pi}_i$ can be decomposed into a sum of terms proportional to projectors onto separable states of N particles [102],

$$\overline{\Pi}_i = \sum_k a_{ik} |\psi_{i_k}\rangle\langle\psi_{i_k}|, \tag{79}$$

where $|\psi_{n_i}\rangle = |\psi^1_{n_i}\rangle \otimes \ldots \otimes |\psi^N_{n_i}\rangle$ and $\sum_i \sum_k |a_{ik}|^2 = 1$. Thus means that this kind of measurement can be carried out sequentially on separate particles individually; for this reason, that measurement can be referred as *classical* or *non-entangled*.
So that, let's consider the quantum state in Eq.73 and general POVMs consisting on 2D rank-1 measurement operators (higher rank of measurement operators can always be obtained by mixing rank-1 operators) that can be parametrised as [105]

$$\overline{\Pi}_i = n_i \begin{pmatrix} \cos^2\left(\frac{\theta_i}{2}\right) & \cos\left(\frac{\theta_i}{2}\right)\sin\left(\frac{\theta_i}{2}\right)e^{-i\chi_i} \\ \cos\left(\frac{\theta_i}{2}\right)\sin\left(\frac{\theta_i}{2}\right)e^{i\chi_i} & \sin^2\left(\frac{\theta_i}{2}\right) \end{pmatrix} \tag{80}$$

with $0 < n_i < 1$, $0 < \theta_i < \pi$ and $0 < \chi_i < 2\pi$.
In terms of such parameters, considering the completeness condition $\sum_i \overline{\Pi}_i = \mathbf{I}$ it is possible to define the equations

$$\begin{aligned}
&\sum_i n_i = 2,\\
&\sum_i n_i \cos(\theta_i) = 0,\\
&\sum_i n_i \sin(\theta_i)\sin(\chi_i) = 0,\\
&\sum_i n_i \sin(\theta_i)\cos(\chi_i) = 0.
\end{aligned} \tag{81}$$

Recalling the equation form of the elements of FI matrix,

$$F^i_{11} = \frac{1}{\mathrm{Tr}[\rho_{\phi,\delta}\overline{\Pi}_i]}\left(\frac{\partial}{\partial\phi}\mathrm{Tr}[\rho_{\phi,\delta}\overline{\Pi}_i]\right)^2, \tag{82a}$$

$$F^i_{22} = \frac{1}{\mathrm{Tr}[\rho_{\phi,\delta}\overline{\Pi}_i]}\left(\frac{\partial}{\partial\delta}\mathrm{Tr}[\rho_{\phi,\delta}\overline{\Pi}_i]\right)^2, \tag{82b}$$

$$F^i_{12} = \frac{1}{\mathrm{Tr}[\rho_{\phi,\delta}\overline{\Pi}_i]}\left(\frac{\partial}{\partial\phi}\frac{\partial}{\partial\delta}\mathrm{Tr}[\rho_{\phi,\delta}\overline{\Pi}_i]\right), \tag{82c}$$

and considering the system state in Eq.73 and the POVMs in Eq.80, the diagonal elements of the FI matrix reads,

$$F^i_{11} = \frac{n_i}{2}\sin^2(\theta)\sin^2(\theta_i)e^{-2\delta^2}\frac{\sin^2(\chi_i-\phi)}{1+\cos(\theta)\cos(\theta_i)+e^{-\delta^2}\sin(\theta)\sin(\theta_i)}, \tag{83a}$$

$$F^i_{22} = 2n_i\sin^2(\theta)\sin^2(\theta_i)e^{-2\delta^2}\frac{\delta^2\cos^2(\chi_i-\phi)}{1+\cos(\theta)\cos(\theta_i)+e^{-\delta^2}\sin(\theta)\sin(\theta_i)}. \tag{83b}$$

So that, with the use of the diagonal elements of the QFI matrix $\overline{H}$ in Eq.74 and assuming that the FI matrix has neglegible off-diagonal elements, the trade-off figure of merit Υ_i become,

$$\Upsilon_i = \frac{F^i_{11}}{H_{11}} + \frac{F^i_{22}}{H_{22}} = \frac{n_i}{2}\frac{\sin^2(\theta)\sin^2(\theta_i) - e^{-2\delta^2}\cos^2(\chi_i-\phi)\sin(\theta)\sin(\theta_i)}{1+\cos(\theta)\cos(\theta_i)+e^{-\delta^2}\cos(\chi_i-\phi)\sin(\theta)\sin(\theta_i)}. \tag{84}$$

Using the trigonometric inequality

$$\begin{aligned}&[1+\cos(\theta)\cos(\theta_i)]^2-\sin^2(\theta)\sin^2(\theta_i)\\&=[1+\cos(\theta)\cos(\theta_i)]^2-[1-\cos^2(\theta)][1-\cos^2(\theta_i)]\\&=[\cos(\theta)+\cos(\theta_i)]^2\geqslant 0\end{aligned}\tag{85}$$

we can find a bound to the Υ_i figure of merit

$$\begin{aligned}\Upsilon_i&\leqslant\frac{n_i}{2}\frac{[1+\cos(\theta)\cos(\theta_i)]^2-e^{-2\delta^2}\cos^2(\chi_i-\phi)\sin^2(\theta)\sin^2(\theta_i)}{1+\cos(\theta)\cos(\theta_i)+e^{-\delta^2}\cos(\chi_i-\phi)\sin(\theta)\sin(\theta_i)}=\\&=\frac{n_i}{2}[1+\cos(\theta)\cos(\theta_i)]-e^{-\delta^2}\cos(\chi_i-\phi)\sin(\theta)\sin(\theta_i).\end{aligned}\tag{86}$$

Summing over the i and using the completeness conditions from Eq.81 gives

$$\Upsilon=\frac{F_{11}}{H_{11}}+\frac{F_{22}}{H_{22}}\leqslant 1.\tag{87}$$

This represents the ultimate bound of trade-off quantify by extrapolating the information on the quantum system $\rho_{\phi,\delta}$ using individual measurements described by 2D rank-1 set of POVMs in Eq.80. If we consider the CRB and the variance matrix $\overline{\Sigma}$ associated to the estimators in use, it is possible to define the trade-off bound for such estimators

$$\Upsilon_{est}=\frac{H_{11}^{-1}}{\Sigma_{11}}+\frac{H_{22}^{-1}}{\Sigma_{22}}\leqslant M,\tag{88}$$

where M is the number of experimental runs and $\Sigma_{11}=\Sigma_{\phi,\phi}$, $\Sigma_{22}=\Sigma_{\delta,\delta}$ are the diagonal elements of the variance matrix.
It can be noticed that for $\theta=\pi/2$ and $\theta_i=\pi/2$, $\forall i$, the inequalities used above are all saturated. This means that, we can always saturate the bound imposed by the Eq.87 when the probe state and all the measurement operators are in the equatorial plane of the Bloch sphere. Furthermore, some important considerations can be made by focus the attention on the off-diagonal elements of the FI matrix. The inequality in the Eq.87 refers only the diagonal elements of the FI matrix while in the Eq.76 we consider the $\overline{F}^{eff}$.

Not negligible off-diagonal elements of FI matrix affects the $\overline{F}^{eff}$ by reducing its diagonal elements; that prevents the saturation of the trade-off figure of merit, because the parameter-independence criterion is not more valid.

4.2.2 *Collective measurements*

Differing from the separable scheme, the collective or entangled measurements read as the ones constituted by a set of POVMs that have not all separable projectors. In this collective case it is possible to investigate the entangled properties of the quantum state under estimation, leading to a more complete understanding of the system.

Since the individual measurements are studied by focusing only on the single probe state in Eq.73 and assuming that the estimation acts even for a larger states of $N > 1$ qubits just performing the overmentioned estimation N times for each qubit, for the collective measurements we must consider the expanded quantum state. We look at the tensor product of two identically prepared single qubit equatorial states,

$$\rho^{(2)}_{\phi,\delta} = \frac{1}{4}\begin{pmatrix} 1 & e^{-\delta^2-i\phi} & e^{-\delta^2-i\phi} & e^{-2\delta^2-2i\phi} \\ e^{-\delta^2+i\phi} & 1 & e^{-2\delta^2} & e^{-\delta^2-i\phi} \\ e^{-\delta^2+i\phi} & e^{-2\delta^2} & 1 & e^{-\delta^2-i\phi} \\ e^{-2\delta^2+2i\phi} & e^{-\delta^2+i\phi} & e^{-\delta^2+i\phi} & 1 \end{pmatrix}. \tag{89}$$

A remarkable example of entangled measurement is the *Bell measurement*; for a dichotomic logical quantum basis $\{|0\rangle, |1\rangle\}$ the Bell measurement rely on the POVM set $\overline{\Pi}_i = |\psi_i\rangle\langle\psi_i|$, where $\{|\psi_1\rangle, |\psi_2\rangle, |\psi_3\rangle, |\psi_4\rangle\}$ constitutes the four Bell basis defined by the states,

$$
\begin{aligned}
|\psi_1\rangle &= \frac{1}{\sqrt{2}}\big(|0\rangle|0\rangle + |1\rangle|1\rangle\big),\\
|\psi_2\rangle &= \frac{1}{\sqrt{2}}\big(|0\rangle|0\rangle - |1\rangle|1\rangle\big),\\
|\psi_3\rangle &= \frac{1}{\sqrt{2}}\big(|0\rangle|1\rangle + |1\rangle|0\rangle\big),\\
|\psi_4\rangle &= \frac{1}{\sqrt{2}}\big(|0\rangle|1\rangle - |1\rangle|0\rangle\big).
\end{aligned}
\tag{90}
$$

For $\phi = \pi/4$ one can calculate the ratios between FI matrix and QFI matrix diagonal elements,

$$\frac{F_{\text{Bell}}(\phi)}{2H_{11}} = e^{-2\delta^2} \tag{91a}$$

$$\frac{F_{\text{Bell}}(\delta)}{2H_{22}} = \frac{1}{1+e^{2\delta^2}} \tag{91b}$$

The sum of these ratios, which correspondes to the trade-off figure of merit Υ, is equal to $3/2$ for $\delta = 0$ and it decrease monotonically with δ. Recently [105], it has been demonstrated that for a large range of phase diffusion δ the maximum value of the trade-off is

$$\Upsilon_{\text{Bell}} = \frac{F_{\text{Bell}}(\phi)}{2H_{11}} + \frac{F_{\text{Bell}}(\delta)}{2H_{22}} \leqslant \frac{3}{2}, \tag{92}$$

and consequentially the statistical variance estimation obey

$$\Upsilon = \frac{H_{11}^{-1}}{\Sigma_{\text{Bell}}(\phi)} + \frac{H_{22}^{-1}}{\Sigma_{\text{Bell}}(\delta)} \leqslant \frac{3}{2}M. \tag{93}$$

4.3 ENTANGLING MEASUREMENTS

In this section the experimental implementation of such Bell measurement, called from now *entangling measurement*, is shown. The method used for the implementation of the entangling measurements is tha linear-optical Control-Sign (CS) gate acting on two polarisation qubits [119, 120], each of the form $\alpha|H\rangle + \beta|V\rangle$; thus,

we are assuming that the horizontal ($|H\rangle$) and the vertical ($|V\rangle$) polarisations of light form the quantum logical basis states $|0\rangle$ and $|1\rangle$ respectively.
The CS gate imparts a π-phase shift to the $|V\rangle_1|V\rangle_2$ with respect to the other three states $|H\rangle_1|H\rangle_2$, $|H\rangle_1|V\rangle_2$ and $|V\rangle_1|H\rangle_2$, and its matrix representation reads

$$\mathrm{CS} = \begin{pmatrix} 1 & 0 & 0 & 0 \\ 0 & 1 & 0 & 0 \\ 0 & 0 & 1 & 0 \\ 0 & 0 & 0 & -1 \end{pmatrix}. \tag{94}$$

In this experiment we consider the action of the CS gate in the rotated basis $|D\rangle = 1/\sqrt{2}(|H\rangle + |V\rangle)$, $|A\rangle = 1/\sqrt{2}(|H\rangle - |V\rangle)$ on one of the two qubits; so that, the Bell states

$$\begin{aligned} |\phi^+\rangle &= \frac{1}{2}(|H\rangle_1|D\rangle_2 + |V\rangle_1|A\rangle_2) \\ |\psi^+\rangle &= \frac{1}{2}(|H\rangle_1|A\rangle_2 + |V\rangle_1|D\rangle_2) \\ |\phi^-\rangle &= \frac{1}{2}(|H\rangle_1|D\rangle_2 - |V\rangle_1|A\rangle_2) \\ |\psi^-\rangle &= \frac{1}{2}(|H\rangle_1|A\rangle_2 - |V\rangle_1|D\rangle_2) \end{aligned} \tag{95}$$

are mapped onto separable states $\{|D\rangle_1|D\rangle_2, |D\rangle_1|A\rangle_2, |A\rangle_1|D\rangle_2, |A\rangle_1|A\rangle_2\}$ respectively, forming an orthogonal set of POVMs Π_k. For example, if we consider as a input the overmentioned $|\phi^+\rangle$ Bell state the CS gate acts as

$$\begin{aligned} |\phi^+\rangle &= \frac{1}{2}(|H\rangle_1|H\rangle_2 + |H\rangle_1|V\rangle_2 + |V\rangle_1|H\rangle_2 - |V\rangle_1|V\rangle_2) \\ &\overset{\mathrm{CS}}{\Longrightarrow} \frac{1}{2}(|H\rangle_1|H\rangle_2 + |H\rangle_1|V\rangle_2 + |V\rangle_1|H\rangle_2 + |V\rangle_1|V\rangle_2) = \\ &= \frac{1}{2}(|H\rangle + |V\rangle)_1 \otimes (|H\rangle + |V\rangle)_2 = |D\rangle_1|D\rangle_2. \end{aligned} \tag{96}$$

As said previously, the best estimation performance can be delivered with equatorial states in yx-plane on the Bloch sphere,

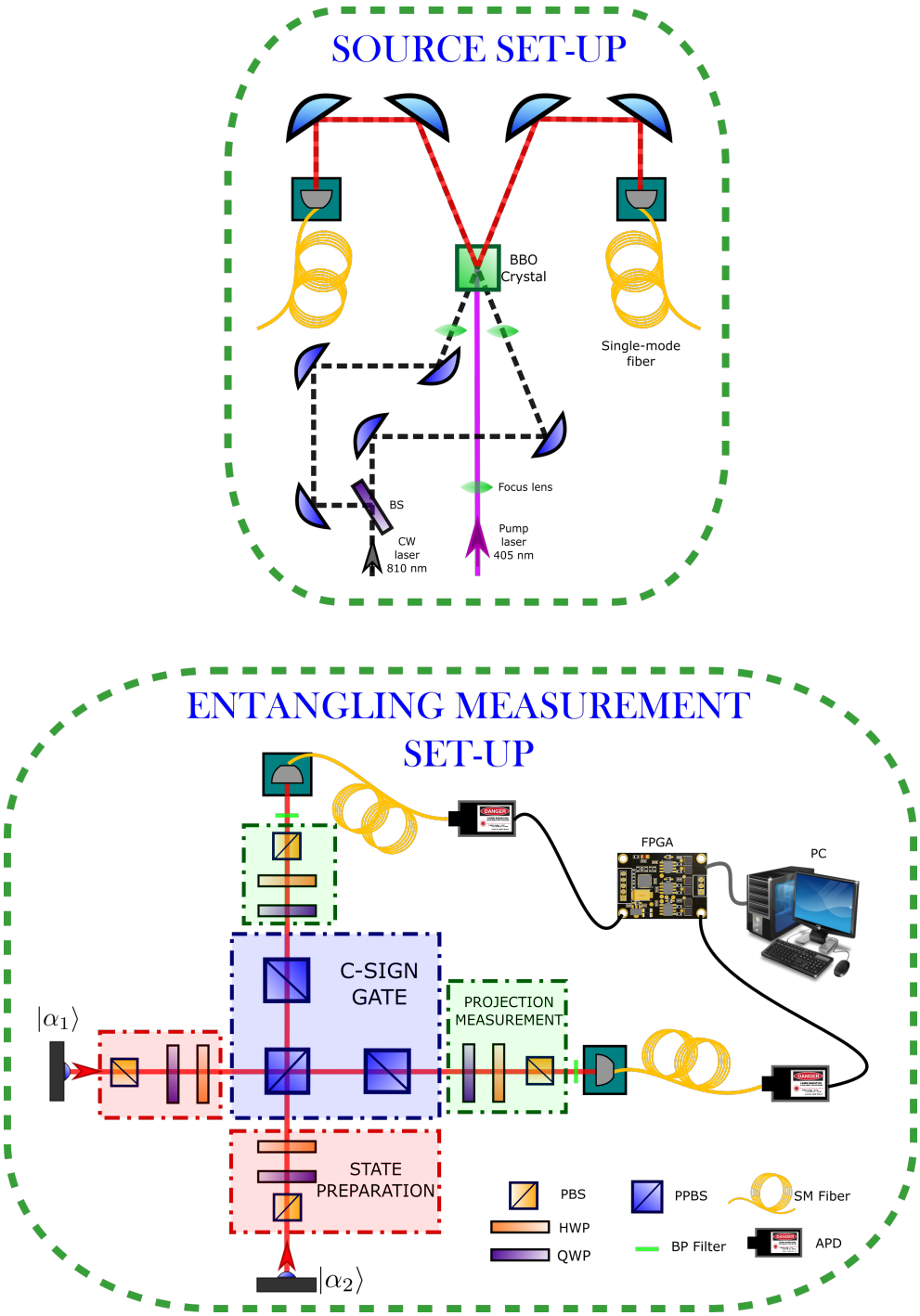

Figure 15: Scheme of the experimental apparatus. All the acronyms in the figure are: beamsplitter (BS), half-wave plate (HWP), quarter-wave plate (QWP), partially-polarised beam splitter(PPBS), polarised beam splitter (PBS), band-pass (BS) filter, avalanche photo-diode (APD), single-mode (SM) fiber.

i.e. $|\psi_0\rangle = 1/\sqrt{2}(|H\rangle + e^{i\xi}|V\rangle)$; for these states, we consider single phase rotations along z-axis in the form $R(\phi) = e^{i\phi\hat{\sigma}_3}$, where $\{\hat{\sigma}_i\}_{i=1,2,3}$ denote the three Pauli matrices, applied on the initial state $|\psi_0\rangle$. Since the second photon state is rotated from the $\{|H\rangle, |V\rangle\}$ basis to the $\{|D\rangle, |A\rangle\}$, the state we investigate in this work is

$$\rho^{(2)} = \rho_1^{(1)} \otimes M\rho_2^{(1)}M^\dagger \tag{97}$$

where $\rho_i^{(1)}$ denotes the single qubit density matrix, and introducing the rotation matrix $M = 1/\sqrt{2}(\hat{\sigma}_1 + \hat{\sigma}_3)$.

4.3.1 *Experimental apparatus*

The experimental implementation of such entangling measurement is described on Fig. 15. For the preparation of the state, we use a photon pair source based on parametric down-conversion (PDC) consisting of a 2-mm barium borate crystal (BBO), pumped with a 405 nm laser diode. The photons converted are nearby frequency-degenerate at 810 nm, and they are emitted with an angle of 6 degrees; they are also coupled into single-mode fibers and then delivered to the entangling measurement set-up. For sake of simplicity on coupling procedures, we exploit a brighter CW laser at 808 nm ($\sim 1.5mW$), splitted with a beam-splitter (BS) crystal and matched on the same spatial-modes of the PDC-generated photons. The entangling measurement is performed by a system of partially polarised beam-splitters (PPBSs) interferometric system. Differently from other interferometric schemes, which are based on the path interaction between the two-photon system, this approach ensures a better stability, since this proposal relies on single-polarisation interference at a PPBS, making the gates more compact and robust against vibrations.
In order to understand the role of such beam-splitter having different reflection coefficients depends on the polarisation direction of the input photons, we consider the four-input modes annihilation operators on the PPBS $\{\hat{a}_H, \hat{a}_V, \hat{b}_H, \hat{b}_V\}$ that correspond to the two input spatial modes $\{a, b\}$ considering the polarisation degree of freedom, and the four-output modes $\{\hat{a}'_H, \hat{a}'_V, \hat{b}'_H, \hat{b}'_V\}$ associated to the two output spatial modes (a', b'), see Fig. 16 [121].

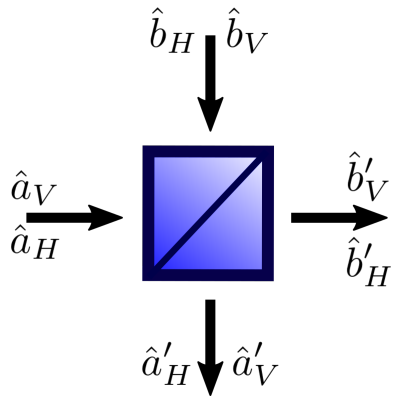

Figure 16: Scheme of the input and output modes on the PPBS.

The relation between the input and the output modes is expressed as,

$$\begin{pmatrix} a'_H \\ b'_H \\ a'_V \\ b'_V \end{pmatrix} = \mathbf{U}_{PPBS} \begin{pmatrix} a_H \\ b_H \\ a_V \\ b_V \end{pmatrix}, \tag{98}$$

where $\mathbf{U}_{PPBS}$ constitutes the action of the associated unitary operator of the PPBS defined as

$$\mathbf{U}_{PPBS} = \begin{pmatrix} t_H & ir_H & 0 & 0 \\ ir_H & t_H & 0 & 0 \\ 0 & 0 & e^{i\varphi}t_V & ie^{i\varphi}r_V \\ 0 & 0 & ie^{i\varphi}r_V & e^{i\varphi}t_V \end{pmatrix}, \tag{99}$$

where φ is the phase difference between the horizontal and vertical polarisation of light and $t_H = 1 - r_H$ and $t_V = 1 - r_V$ are the trasmittivity coefficients of horizontally and vertically polarized light, respectively.
In our experiment, the PPBS parameters reads $t_H = 1$ and $t_v = 1/\sqrt{3}$, and $\varphi = 0$, so that the matrix in Eq.99 is,

$$\mathbf{U}_{\mathrm{PPBS}} = \begin{pmatrix} 1 & 0 & 0 & 0 \\ 0 & 1 & 0 & 0 \\ 0 & 0 & 1/\sqrt{3} & i\sqrt{2/3} \\ 0 & 0 & i\sqrt{2/3} & 1/\sqrt{3} \end{pmatrix}. \tag{100}$$

When the input state of PPBS is $|V\rangle_a|V\rangle_b = \hat{a}_V^\dagger \hat{b}_V^\dagger|0\rangle$ the output state can be derived using the transformation defined by equations Eq.98 and Eq.100 as follows:

$$\begin{aligned} \mathbf{U}_{\mathrm{PPBS}}\hat{a}_V^\dagger \hat{b}_V^\dagger|0\rangle =& \left(\frac{1}{\sqrt{3}}\hat{a}'_V + i\sqrt{\frac{2}{3}}\hat{b}'_V\right)^\dagger \otimes \left(i\sqrt{\frac{2}{3}}\hat{a}'_V + i\frac{1}{\sqrt{3}}\hat{b}'_V\right)^\dagger |0\rangle = \\ =& \left(-\frac{1}{3}\hat{a}'_V\hat{b}'_V + i\frac{\sqrt{2}}{3}\hat{a}'^2_V + i\frac{\sqrt{2}}{3}\hat{b}'^2_V\right)^\dagger |0\rangle = \\ =& -\frac{1}{3}|H\rangle_{a'}|H\rangle_{b'} - i\frac{\sqrt{2}}{3}|2H\rangle_{a'}|0\rangle_{b'} - i\frac{\sqrt{2}}{3}|0\rangle_{a'}|2H\rangle_{b'}. \end{aligned} \tag{101}$$

Within the calculation on the other three possible input modes, it is possible to notice that the output state results having a π-phase only on the $|V\rangle|V\rangle$, conditioned on post-selecting a coincidence detection, *i.e.* neglecting the detection of multiple qubit state on the same mode.
Then, the first PPBS ensures us to perform effectively the CS gate with two single-photon state; however, the absolute values of the amplitudes need to be equal for any input, so that we still need to attenuate the contributions that include horizontal polarization. In order to achieve this task, we inserted one more PPBS on each arm rotated by 90 degrees, so that the role of horizontal and vertical polarisations are exchanged: the output probability then becomes polarisation insensitive.

4.4 DETECTOR TOMOGRAPHY

In order to quantify the efficiency of our device we need to perform a *detector tomography*, [122]; this characterisation consists of

determining the POVM set corresponding to the action of our apparatus. As mentioned before, the CS gate maps the POVM set $\overline{\Pi}_i^{th} = |\psi_i\rangle\langle\psi_i|$ constituted by the Bell basis in Eq.90 onto separable states in the diagonal logical basis; so that, if at the output arms of the CS gate we project the system in the four possible combination of $\{|D\rangle, |A\rangle$ basis, we are able to reconstruct the associated $\overline{\Pi}_i^{exp}$ matrices, with $i = DD, DA, AD, AA$, by observing the respectively probability outcome associated to the input state $\rho^{(2)}$,

$$p(i) = \mathrm{Tr}[\rho^{(2)}\overline{\Pi}_i^{exp}]. \tag{102}$$

In state tomography, an unknown $\rho^{(2)}$ is characterized by carrying out a set of known measurements, each on many identical copies of the state to estimate $p(i)$. From this kind of estimate, one can invert Eq.102 to find $\rho^{(2)}$. The interchangeability of $\rho^{(2)}$ and $\overline{\Pi}_i^{exp}$ in Eq.102 shows that detector tomography has a dual role to state tomography. In this case, measuring a set of known probe states $\{\rho^{(2)}\}$ enables us to characterize an unknown detector, and thus find $\overline{\Pi}_i^{exp}$. From the definition of a POVM set, we remark that constraints on the measured detector matrices $\overline{\Pi}_i^{exp}$ are needed: these matrices must be non-negative $\overline{\Pi}_i^{exp} \geqslant 0$ and they must sum to the identity operator $\sum_i \overline{\Pi}_i^{exp} = \mathbf{I}$.

In order to reconstruct the experimental probabilities, we use as input the product of single-qubit reference states $|\alpha_1\rangle, |\alpha_2\rangle$ by choosing among all the six possible polarisation states of light $\{|H\rangle, |V\rangle, |D\rangle, |A\rangle, |R\rangle, |L\rangle$ where $|R\rangle = 1/\sqrt{2}(|H\rangle - i|V\rangle)$ and $|L\rangle 1/\sqrt{2}(|H\rangle + i|V\rangle)$ are the two circular polarisation of light. Experimentally, for all output projections on the diagonal basis, consisting on a Quarter-Wave Plate (QWP), Half-Wave Plate (HWP) and Polarised Beam-Splitter (PBS), see Fig. 15, we prepare the state by projecting the input photons on all the 36 possible combinations of polarisation inputs. Such preparation can be achieved by projecting the input states in the horizontal polarisation by the use of a PBS, not shown in figure, a QWP and a HWP on either input arms. Data acquisition is performed by collecting coincidences using avalanche photo-diodes and a Field Programmable Gate Array (FPGA) board.

$\|\alpha_1\rangle\backslash\|\alpha_2\rangle$	$\|H\rangle$	$\|V\rangle$	$\|D\rangle$	$\|A\rangle$	$\|R\rangle$	$\|L\rangle$
$\|H\rangle$	1704	1382	3074	16	1531	1513
$\|V\rangle$	1387	880	136	2121	1233	1016
$\|D\rangle$	2734	133	1681	1191	1511	1369
$\|A\rangle$	21	2301	1247	1074	1229	986
$\|R\rangle$	1590	1085	1724	1018	2644	111
$\|L\rangle$	1339	1207	1420	1043	100	2477

Table 2: Data acquisition of coincidence rate by setting the projection on the two output arms at $|D\rangle|D\rangle\langle D|\langle D|$. All the coincidences are collected within 1 second of acquisition time.

The tomography algorithm proceeds to find the closest set $\{\overline{\Pi}_i^{exp}\}$ that fits the collected data (in Table 2 there is an example for the POVM $\{\overline{\Pi}_{DD}^{exp}\}$ associated to the $|D\rangle|D\rangle\langle D|\langle D|$ projection on the two output arms) to the expected values

$$n_i^{ideal} = \mathrm{Tr}[|\alpha_1\rangle\langle\alpha_1| \otimes |\alpha_2\rangle\langle\alpha_2|\overline{\Pi}_i^{exp}] \tag{103}$$

exploiting the maximum likelihood approach. Considering the i-data set of 36 measurements $\{n_{ij}\}_{j=1,\dots,36}$ associated to the matrix $\overline{\Pi}_i^{exp}$, the aim is to find the minimum of the "likelihood function"

$$\mathcal{L}_i = \sum_{j=1}^{36} \left(\mathrm{Tr}[(|\alpha_1\rangle\langle\alpha_1| \otimes |\alpha_2\rangle\langle\alpha_2|)_j\overline{\Pi}_i^{exp}] - n'_{ij}\right)^2 \frac{N_j}{n'_{ij}} \tag{104}$$

where $N_j = \sum_{i=1}^{4} n_{ij}$ is the normalisation over all the four $\overline{\Pi}_i^{exp}$ matrices and $n'_{ij} = n_{ij}/N_j$.
In order to consider the uncertainties on the data set, instead of increasing the amount of coincidence rate collections we choose to simulate multiple runs of the reconstruction experiment by means of *Monte Carlo* routine; such *propagation procedure* results an useful approach, since permits to prevent loss of information about the parameter correlations.

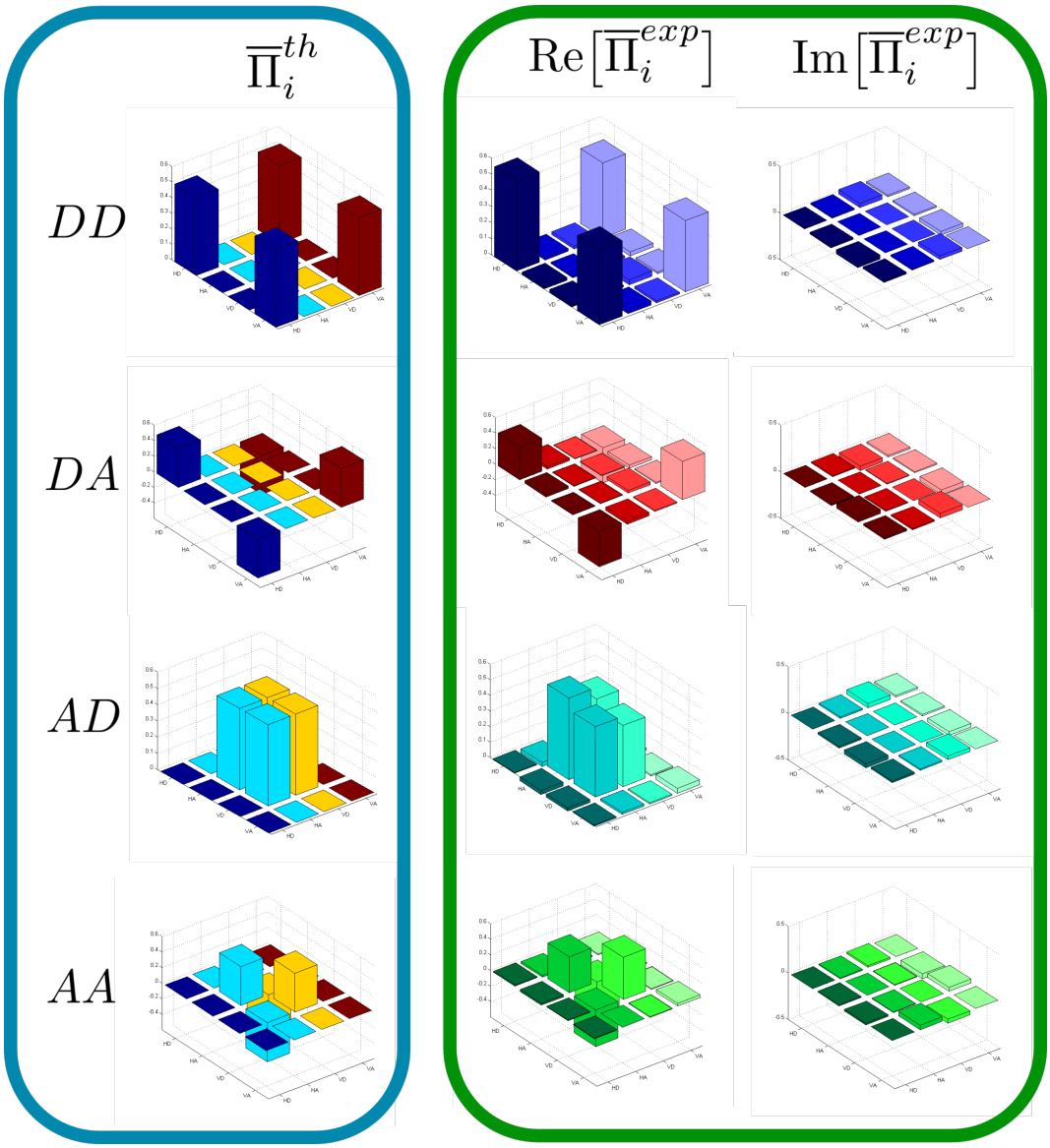

Figure 17: Histograms representation of the four ideal entangling measurement POVM-set $\overline{\Pi}_i^{th}$ and of the four reconstructed real part $\mathrm{Re}\left[\overline{\Pi}_i^{exp}\right]$ and imaginary part $\mathrm{Im}\left[\overline{\Pi}_i^{exp}\right]$ matrices.

At each run the detected coincidence counts varying within uncertainty extrapolated by a normal distribution; to do so, we generate two single uniformly distributed random numbers r_1 and r_2

chosen in the interval $(0,1)$. The normal distribution number is then calculated by using the formula

$$z = \sqrt{-2\mathrm{Log}(r_1)}\cos(2\pi r_2), \tag{105}$$

and the relative data at each routine results $n_{ij}^{MC} = n_{ij} + z\sqrt{n_{ij}}$, coherently to the Poissonian statistic of the photons used in the experiment. Following it is reported the mean values of the four entangling POVM-set calculated with 100 iterations,

$$\Pi_{DD} = \begin{pmatrix} 0.559 & 0.017 + i0.016 & 0.019 + i0.045 & 0.466 + i0.017 \\ 0.0165 - i0.016 & 0.008 & 0.012 - i0.001 & 0.024 - i0.015 \\ 0.0188 - i0.045 & 0.012 + i0.001 & 0.032 & 0.012 - i0.040 \\ 0.466 - i0.017 & 0.024 + i0.015 & 0.012 + i0.040 & 0.441 \end{pmatrix} \tag{106a}$$

$$\Pi_{DA} = \begin{pmatrix} 0.004 & -0.025 - i0.017 & -0.020 - i0.015 & -0.006 - i0.001 \\ -0.025 + i0.017 & 0.525 & 0.453 + i0.014 & 0.014 + i0.053 \\ -0.020 + i0.015 & 0.453 - i0.014 & 0.393 & 0.008 + i0.048 \\ -0.006 + i0.001 & 0.014 - i0.053 & 0.008 - i0.048 & 0.032 \end{pmatrix} \tag{106b}$$

$$\Pi_{AD} = \begin{pmatrix} 0.425 & 0.032 + i0.010 & -0.006 - i0.046 & -0.450 - i0.017 \\ 0.032 - i0.010 & 0.005 & 0.007 - i0.007 & -0.040 + i0.012 \\ -0.006 + i0.046 & 0.007 + i0.007 & 0.036 & -0.013 - i0.050 \\ -0.450 + i0.017 & -0.040 - i0.012 & -0.013 + i0.050 & 0.492 \end{pmatrix} \tag{106c}$$

$$\Pi_{AA} = \begin{pmatrix} 0.013 & -0.023 - i0.009 & 0.007 + i0.017 & -0.010 + i0.001 \\ -0.023 + i0.009 & 0.462 & -0.471 - i0.007 & 0.002 - i0.050 \\ 0.007 - i0.017 & -0.471 + i0.007 & 0.540 & -0.007 + i0.042 \\ -0.010 - i0.001 & 0.002 + i0.050 & -0.007 - i0.042 & 0.035 \end{pmatrix} \tag{106d}$$

in the basis $\{|HD\rangle, |HA\rangle, |VD\rangle, |VA\rangle\}$.
For each reconstructed matrices, we calculate the proper *fidelity*

$$F_i(|\psi_i\rangle, \overline{\Pi}_i^{exp}) = \sqrt{\langle\psi_i|\overline{\Pi}_i^{exp}|\psi_i\rangle} \tag{107}$$

compared to the ideal set $|\psi_i\rangle$ defined in Eq.90. In our experiment the fidelities result to be

$$\begin{aligned} F_{\phi^+} &= (96.60 \pm 0.23)\% \\ F_{\phi^-} &= (90.84 \pm 0.37)\% \\ F_{\psi^+} &= (91.13 \pm 0.34)\% \\ F_{\psi^-} &= (97.23 \pm 0.15)\% \end{aligned} \tag{108}$$

4.5 RESULTS

The value of the Υ factor using reconstructed matrices $\overline{\Pi}_i^{exp}$ in Eq.106 is reported in Fig. 18.

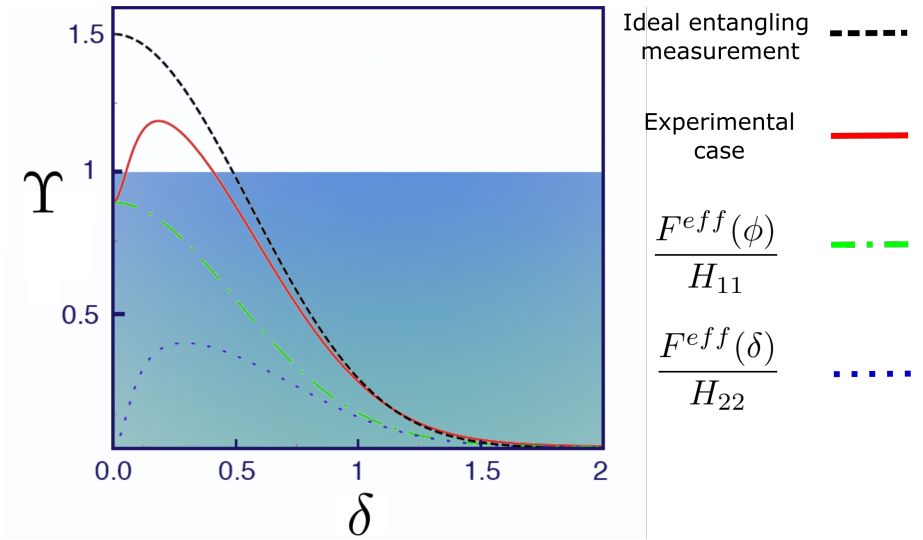

Figure 18: Trade-off figure of merit from experimentally reconstructed detector matrices in Eq.106 for the phase-dephasing estimation. The blue shadowed area $\Upsilon \leqslant 1$ constituted the accessible area from separable measurement. The lines represent: prediction for the ideal case of entangling measurement (black dashed line), the experimental Υ value (red solid line), the contribution of the effective FI of the phase (dash-dotted green line) and for the dephasing (dotted blue line).

Fixing the ϕ parameter on its best performance value $\simeq 0.89$, it is shown the behavior of trade-off figure of merit as a function of the dephasing parameter δ, along the prediction of the ideal case. In the figure we highlight also the contributions of the Υ function for both parameters (blue and green dashed lines) and the blue area achievable by the individual probe strategy. In such results, the input states are chosen individually on two qubits establishing numerically $\xi = 0$ for the first qubit, and $\xi = 0.10$ for the second; in real condition there are not bound to be equatorial in order to accommodate for imperfections.

From the figure, we notice that there exists a range of δ for which an improvement over the separable strategy ($\Upsilon \leqslant 1$) is assessed; the optimal value is $\Upsilon^* = 1.18 \pm 0.02$, nine standard deviations above the limit. Looking at the ideal case, we expect that the larger amelioration can be achieved for low values of dephasing. However, the experimental line suggests that for $\delta \simeq 0$ there is a drop of information due to experimental imperfections. Indeed, for low dispersion instance the capability of the apparatus of estimating δ is strongly linked to the repartition of counts among the four possible outcomes. This asymmetric behavior prelude the possibility to achieve the best performance measurement in the low δ regime, even trying to reduce the non-idealities by biasing the input states.
Another observation is the evolution of the entanglement measurement against the single probe measurement. The last one, results to be insensitive on the value of δ due to the lack of coherence of the estimation while the collective one, which is the maximum expression of quantum coherence, seems to be strictly δ-dependent. This highlights the fact that the amelioration on the joint-estimation occurs for a limited range of dephasing values and if the measurement becomes less entangled, the Υ factor becomes consequently flatter, see Fig. 19.

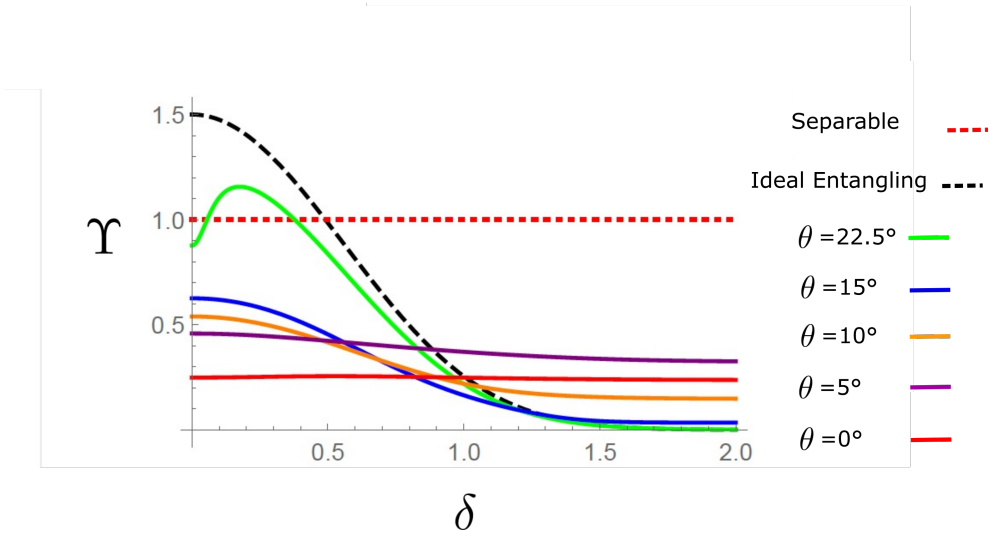

Figure 19: Trade-off figure of merit with different correlation strengths.

In this graph we use different correlation strengths by maintaining the projection of one output arm into the diagonal basis while the other is projected into the basis $\{|\alpha(\theta)\rangle, |\alpha(\theta + 45^o)\rangle\}$ where the equatorial state is defined $|\alpha(\theta)\rangle = 1/\sqrt{2}(\cos(\theta)|H\rangle + \sin(\theta)|V\rangle)$; we check for different settings of the entanglement strength $\theta = \{22.5^o, 15^o, 10^o, 5^o, 0^o\}$, spanning from the maximum entangled measurement (projecting in $\{|D\rangle, |A\rangle\}$) to the separable one (projecting in $\{|H\rangle, |V\rangle\}$).
At the end, it is possible to remark the effectiveness of collective measurement approach, that improves the information extrapolation from the system, breaking the separable bound. However, the entangling strategy are affected considerably to the presence of dispersion, because of the fragile nature of quantum correlation, leading to an ameliorated narrow range of δ for information extraction.

4.6 PHASE-PHASE ESTIMATION

In the multi-parameter scenario the achievement of the ultimate bound impose by the QCR inequality is strongly connected to the maximum information extrapolation imposed by the QFI matrix;

in particular, as mentioned in the previous chapter, the optimal FI can be attained following the weaker condition

$$\mathrm{Tr}[\rho_{\phi,\delta}[L_i, L_j]] = 0, \tag{109}$$

that it has been proved to be necessary and sufficient.
Despite this is proved for the phase-dephasing parameter estimation, we consider now the case of the unitary transformation $R(\phi_y, \phi_z) = \exp\{i(\phi_y\sigma_2 + \phi_z\sigma_3)\}$, a rotation along the y and z-axis on the Bloch sphere representation applied to the state $|\psi_0\rangle$. The two SLD operators corresponding to the parameters ϕ_y and ϕ_z can be easily calculated and one obtains that the condition in Eq.109 is never satisfied, unless for a specific initial equatorial states [103]. The impossibility of reaching the weaker condition implies that the saturation of the two-parameter QCR bound can not be assessed, no matter how many copies of the qubit probe state are accessed with entangling measurements, differing to the case of the joint ϕ-δ estimation that always satisfied the condition 109 with a non-singular QFI matrix.

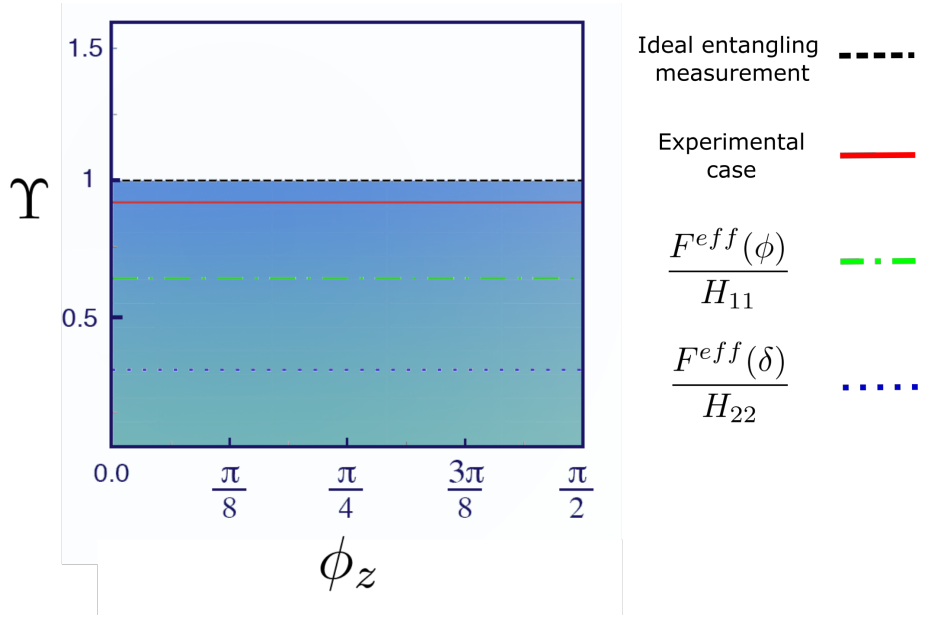

Figure 20: Trade-off figure of merit from experimentally reconstructed detector matrices in Eq.106 for the ϕ_y-ϕ_z estimation.

In Fig. 20 we report the Υ figure of merit of two-phase estimation with the same numerical investigation performed for the previous joint estimation of phase and dephasing; one finds that the separable bound $\Upsilon \leqslant 1$ is always satisfied regardless of how much entangling the measurements we consider are on two copies of quantum state. So that, for this case the enhancement of collective approach results pointless because of the no-zero expectation value of the commutator of the ϕ_y-ϕ_z SLD operators on the probe state $\rho_{\phi,\delta}$.

4.7 CONCLUSIONS

We have evaluated the usefulness of a particular collective measurements, the entangling measurements, for the multi-parameter estimation scenario using two-qubit probes. The impact of this collective strategy to the phase and phase diffusion estimation results significant. There is a range of dephasing values where the extractable information from the quantum probe system goes beyond the limit imposed by the individual approach. The results are in accordance with the ideal case under opportune conditions, even within some features due to experimental imperfections of our apparatus. In order to focus on the importance of the necessary and sufficient weaker condition 109, we perform the same analysis on the two-phase estimation that not satisfied such condition. In this case the trade-off figure of merit results to have the same bound compared to the separable case, so that no enhancement of using entangling measurement is observed.

At the end, even observing experimentally the advantage of the collective measurement strategy, this results to be hard to implement efficiently with the apparatus above discussed. Indeed, as the obtained fidelities of the chosen POVM set could result to be good enough, the sensivity of the performed measurement within experimental imperfection has proved to be a not negligible aspect. This has been noted on the very different behavior of the experimental trade-off figure of merit compared to the ideal one,

caused by a not perfect symmetry of the redistribution counts on all possible outcomes, which constitutes a difficult task to control.

5

MULTIPARAMETER QUANTUM ESTIMATION OF NOISY PHASE SHIFTS

"It's conical. So what you do is, you see, you fill it
With fine white sand, alright? Or sugar. Fine white sand,
And/or sugar. Anything. Doesn't matter. Sugar's fine.
And when it's full, you pull the plug out... are you listening?"
— The Hitchhiker's Guide to the Galaxy, D. Adams

5.1 INTRODUCTION

The characterisation of biological systems plays a fundamental role in pharmaceutical industry. This because non-intrusive probes represents one of the exciting challenges in medical research. Quantum metrology helps us to solve this task exploiting the resources of quantum light states with minimal risk of sample damaging. For this reason, researchers of biology and chemistry focus the attention on the strong coherence properties of quantum systems, which are capable of enhancing the measurement sensivity and resolution even with a few amount resources. One of the most important parameter example for the characterisation of biological samples is the optical activity of aqueous solutions, *i.e.* the phase-difference between the two circular polarisations.

In this chapter I discuss the results for the chirality estimation of aqueous samples using multi-parameter estimation approach. The novelty of this work is figured by the joint characterisation of the focused parameter, *i.e.* the phase-shift on the circular polarisation of light, and the quality of the probe used for the investigation on the material. In this particular case, the probe efficiency is identified by the amount of indistinguishability of two input Fock states into the interferometric system generating a two-photon N00N state. The effect of post-selection on the Fisher information and

the generalisation to 2N-photon Holland-Burnett states are also discussed.

5.2 QUANTUM INTERFEROMETRY

As described in the previous chapter, quantum metrology breaks the classical shot-noise bound for parameter estimation accuracy. In optics, the most remarkable example of this resolution improvement beyond the Heisenberg limit consists in multiphoton entangled states, known as N00N states. These states are commonly associated to the *Schrödinger cat* ones, as they consist of a superposition of two highly distinct states corresponding to the "dead and alive" cat. The high sensivity to decoherence effects on multiparticle states makes N00N states a valuable tool for many quantum technology fields, including quantum metrology. The idea behind these states is that there are a fixed number of particles N, *i.e.* photons for our purposes, that are either all in the mode a or in the mode b producing the superposition state,

$$|\Psi\rangle_{N00N} = \frac{1}{\sqrt{2}}\left(|N\rangle_a|0\rangle_b + |0\rangle_a|N\rangle_b\right). \tag{110}$$

The physics behind this quantum system takes its foundations from the famous work of photon indistinguishability performed by the group of Mandel in 1987. Become known as one of the most influent works demonstrating the fundaments of quantum mechanics, the Hong-Ou-Mandel (HOM) effect showed the intrinsic boson nature of two indistinguishable single photons interacting on a beam splitter (BS), see Fig.21.

Describing the input quantum state before the BS as

$$|\Psi_{in}\rangle_{12} = \int dt \int dt' \beta(t,t') \hat{a}_1^\dagger(t) \hat{a}_2^\dagger(t')|0\rangle_{12}, \tag{111}$$

where $\hat{a}_1^\dagger$ and $\hat{a}_2^\dagger$ are the creation operations on the 1 and 2 respective input modes, the times t and t' are associated with the same input arms, and $\beta(t,t')$ corresponds to the joint two-photons wavepacket amplitude.
By defining as 3 and 4 the output modes of the beam splitter, the relation between input and output creation operators reads

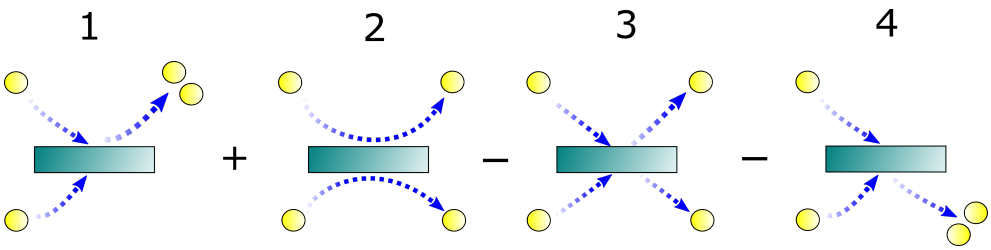

Figure 21: Scheme of the four possibilities outputs for two-photon interaction in to a 50:50 beam splitter. The indistinguishability of both single photons ensures the erasure of the configuration 2 and 3; the remaining possibilities describe the intrinsic bosonic nature of the photons that follow the same output mode.

$$\begin{aligned}\hat{a}_1^\dagger(t) &= \mathcal{R}\hat{a}_3^\dagger(t) + \mathcal{T}\hat{a}_4^\dagger(t),\\ \hat{a}_2^\dagger(t) &= \mathcal{T}\hat{a}_3^\dagger(t) + \mathcal{R}\hat{a}_4^\dagger(t),\end{aligned} \tag{112}$$

where $\mathcal{R}$ and $\mathcal{T}$ are the reflection and transmission coefficients, respectively.
The substitution of the input operators by the output operators in Eq.111 gives

$$\begin{aligned}|\Psi_{in}\rangle_{12} = \int dt \int dt' \beta(t,t') \Big[&\mathcal{R}\mathcal{T}\hat{a}_3^\dagger(t)\hat{a}_3^\dagger(t') + \mathcal{R}^2\hat{a}_3^\dagger(t)\hat{a}_4^\dagger(t')\\ &+ \mathcal{T}^2\hat{a}_4^\dagger(t)\hat{a}_3^\dagger(t') + \mathcal{T}\mathcal{R}\hat{a}_4^\dagger(t)\hat{a}_4^\dagger(t') \Big] |0\rangle_{12}.\end{aligned} \tag{113}$$

For this state at the output of the BS we consider the probabilities for both photons to emerge in the same output arm as

$$P(2_3, 0_4) = P(0_3, 2_4) = \frac{1}{2}|\mathcal{R}|^2|\mathcal{T}|^2 \int dt \int dt' |\beta(t,t') + \beta(t',t)|^2, \tag{114}$$

and the probability for one photon to emerge in each output arm as

$$P(1_3, 1_4) = \frac{1}{2}\int dt \int dt' |\mathcal{R}^2 \beta(t, t') + \mathcal{T}^2 \beta(t', t)|^2. \qquad (115)$$

The abovementioned probabilities suggest us that the state at the output of the BS strictly depends on the form of the pair-state wavepacket $\beta(t, t')$ and the transmitency and reflectancy coefficients $|\mathcal{R}|^2$ and $|\mathcal{T}|^2$. Indeed, considering a factorable joint wavepacket amplitude $\beta(t, t') = \xi_1(t)\xi_2(t')$ for non-entangled input states and a completely balanced beam splitter ($|\mathcal{R}|^2 = |\mathcal{T}|^2 = 1/2$), these probabilities reduced to

$$\begin{aligned} P(2_3, 0_4) = P(0_3, 2_4) &= \frac{1}{4}\left(1 + |J|^2\right) \\ P(1_3, 1_4) &= \frac{1}{2}\left(1 - |J|^2\right) \end{aligned} \qquad (116)$$

where $|J|^2 = |\int dt \xi_1^*(t)\xi_2(t)|^2$ is the overlap integral taking into account the normalisation and the invariance under interchange of the integration variables t and t' of the wavefunction $\beta(t, t')$.

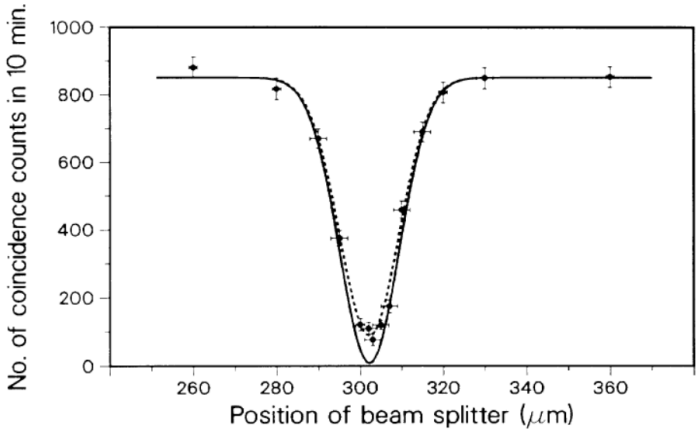

Figure 22: Results of the coincidence measurement for different delay times τ performed by Mandel in 1987, taken from [8]. The lack of coincidences at delay time $\tau = 0$ confirms the bosonic nature of of the system after the interaction.

This overlap integral has a simple form for individual wavepacket amplitudes $\xi_1(t)$ and $\xi_2(t)$ of Gaussian shape

$$\xi(t) = \left(2\Delta^2/\pi\right)^{1/4} \exp\left[-i\omega_0 - \Delta^2(t_0 - t)^2 \right]; \tag{117}$$

considering two different arrival times of the photons at the BS, denoted respectively t_{01} and t_{02}, the overlap function reads,

$$J = \exp\left[-\frac{1}{2}\Delta^2(t_{01} - t_{02})^2 \right]. \tag{118}$$

As observed in Fig. 22, for a simultaneous arrival of the peaks of the two input-photons at the BS ($t_{01} = t_{02}$) the output coincidence rate is erased due to the impossibility to distinguish the photons during the interaction on the BS. It is very important to mark that this totally destructive interference is a quantum-mechanical effect that does not occur for any classical counterpart of the experiment.

5.3 N00N STATE PROBING CHIRAL SOLUTIONS

The preparation of N00N-like quantum state via interferometric apparatus allows us to exploit a very reliable tool in order to detect, measuring the photon coincidences, even the smallest difference between two probes under examination. For this reason this technique aims at playing a central role in metrology experiments. In this experiment we want to characterise some solutions preparing properly a N00N state in order to perform a phase-shift estimation issued by the chirality nature of the samples. We consider the action of a chiral material, typical examples are sugar aqueous solutions, on a circular superposition quantum light state $|\Phi_{in}\rangle = 1/\sqrt{2}(|R\rangle + |L\rangle)$; the interaction of the light with this sample can be described with a phase-shift imparted by the solution to the left-circular polarisation of the state that evolves in

$$|\Phi_{out}\rangle = \frac{1}{\sqrt{2}}(|R\rangle + e^{i\varphi}|L\rangle). \tag{119}$$

In order to implement an interfometric apparatus enhancing the sensivity to such evolution, we choose to prepare optically a N00N state encoded on circular polarisation of light,

$$|\Phi_{\text{prep}}\rangle = \frac{1}{\sqrt{2}}(|2_R\rangle|0_L\rangle - |0_R\rangle|2_L\rangle). \tag{120}$$

The scheme we use for the implementation and preparation of N00N state on circular polarisation is described in Fig. 23.

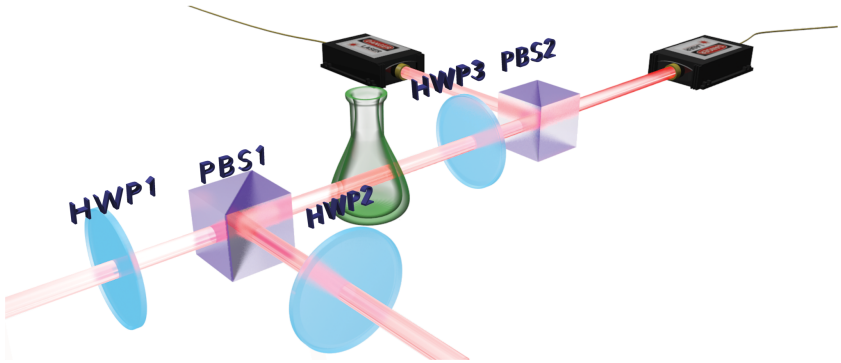

Figure 23: Experimental scheme of N00N state preparation.

The approach we use for this chirality-estimation experiment is the joint characterisation of phase-shift imparted by the material under investigation and the efficiency of the interferometric apparatus. As we will see later, this choice permits us to access on a more informative estimation compared to the single phase-estimation approach. Considering the two input modes, labeled with 1 and 2, we have the input state at the horizontal polarisation of light $|\Phi_{\text{in}}\rangle = (\hat{a}_H^\dagger)_1(\hat{a}_H^\dagger)_2|0\rangle$. Before the interaction on the polarised-beam splitter (PBS1) one of the two states preserves the horizontal polarisation and passes through an half-wave plate (HWP1) at 0 degree respect to its fast optical axis while the other one changes in to the vertical polarisation passing in to an HWP at 45 degrees. After the interaction on the PBS1 the state become

$$|\Phi_{\text{int}}\rangle = \hat{a}_H^\dagger \hat{a}_V^\dagger|0\rangle = \frac{1}{2}((\hat{a}_R^\dagger)^2 - (\hat{a}_L^\dagger)^2)|0\rangle = \frac{1}{\sqrt{2}}(|2_R\rangle|0_L\rangle - |0_R\rangle|2_L\rangle), \tag{121}$$

which is the N00N state defined in the (120).
Parametrizing the action of the aqueous solution on this state as

a phase-shift ϕ on the R-mode, such phase induces a polarisation rotation described by the transformations

$$\begin{aligned} \hat{a}_H^\dagger &\to \cos(\phi/2)\hat{a}_H^\dagger + \sin(\phi/2)\hat{a}_V^\dagger, \\ \hat{a}_V^\dagger &\to \cos(\phi/2)\hat{a}_V^\dagger - \sin(\phi/2)\hat{a}_H^\dagger. \end{aligned} \tag{122}$$

So that, the evolution of the state in Eq.121, due to the interaction of the sample, is

$$|\Phi_{ev}\rangle = \cos\phi\,\hat{a}_H^\dagger\hat{a}_V^\dagger|0\rangle - \sin\phi\,\frac{(\hat{a}_H^\dagger)^2 - (\hat{a}_V^\dagger)^2}{2}|0\rangle. \tag{123}$$

The detection scheme consists of an half-wave plate (HWP3) and a second PBS, in order to select an arbitrary linear polarisation of the state by the angular position θ of the half waveplate. At the end, we perform the photon counting by the use of avalanche photodiodes (APDs) place at the end of each output arms of the interferometer.

5.4 N00N STATE PREPARATION

The approach we use in this experiment aims at exploring the consequences due to the probe state interaction with the sample under investigation. Indeed, such evolution of the system can provoke a change on the experimental apparatus exploited for the phase estimation process. As stated previously, preparing an optimal quantum state ensures us an estimation of the phase-shift is nearby to the effective value imparted by the solution under investigation. Experimentally, the optimability of quantum state preparation relies at on good interferometric set-up with indistinguishable photons. However, the alteration affects the metrological process abovementioned, inducing to a different estimation of the phase; this can be described as a loss of efficiency of the experimental device, that in our case reflects on the photon distinguishability in the interferometric system. Considering that this decreasing efficiency is strictly associated to the evolution of the probe itself, every pre-estimation of the experimental interferometer performance, *i.e.* the visibility of the output fringes, results

pointless. This scenario leads to a multi-parameter approach that characterise phase-shift and the efficiency of the experimental device at the same time.
Considering the evolved state in Eq. (123) and introducing the rotation degree θ and the visibility ν, see the Appendix A, the relevant detection probabilities are:

$$\begin{aligned} p(1|\theta;\phi,\nu) &= \frac{1}{1+\nu}\left(1+\nu\cos(8\theta-2\phi)\right) \\ p(2|\theta;\phi,\nu) &= \frac{\nu}{1+\nu}\sin^2(4\theta-\phi) \end{aligned} \tag{124}$$

where $p(1|\theta;\phi,\nu)$ describe the probability of a coincidence count between two arms, associated to the state $|1_H\rangle|1_V\rangle$, and $p(2|\theta;\phi,\nu)$ is the probability to find both photons in one arm, associated to the state $(|2_H\rangle|0_V\rangle - |0_H\rangle|2_V\rangle)\sqrt{2}$. These probabilities are used for the multi-parameter estimation with the Bayesian method (see Chapter 3). However, in this experiment the available measurement apparatus does not allow to achieve the full set of outcome probabilities in Eq. (124). For this reason we choose to approach this problem with a *post-selection* strategy, see Sec.5.5.

5.4.1 *Alignment system*

Due to the low probability of photon pair emission in the PDC process a brighter laser beam is necessary for the alignment of the interferometric apparatus. In Fig. 24 a sample scheme of optical simulation setup is described. In this scheme we use a continuous wave (CW) diode laser at 808 nm of wavelength, horizontally polarised; this choice is dictated by the need of being as close as possible to the spectrum and the polarisation of the PDC photon-pair.

For both of simulation apparatus and experiment setup we use broadband dielectric mirrors with transmission range $750-1100$ nm. Simulating the two single-photon beams path we split the laser with a plate beamsplitter (BS); we measure the input power of the laser (12.8 mW) and the output power of the reflection path (3.5 mW) and the transmission path (9.1 mW). The reason of this

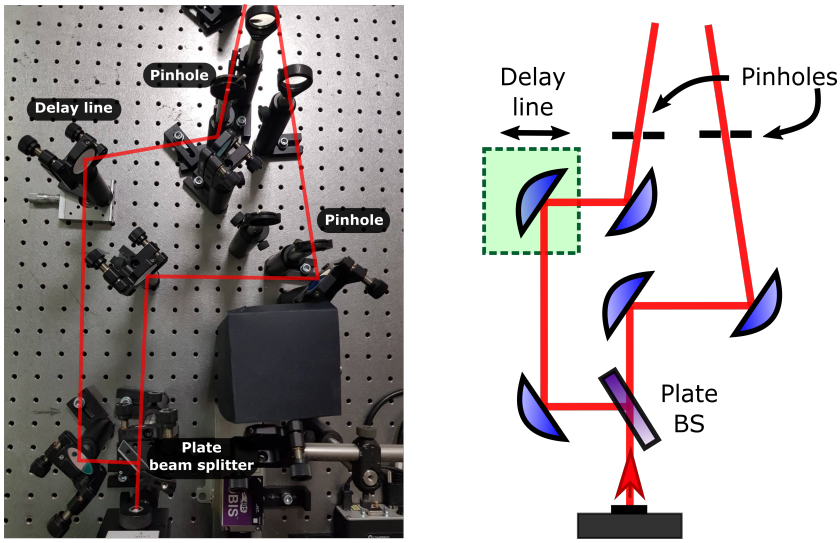

Figure 24: Experimental set-up of the optical simulation for the alignment.

high unbalance is due by the impossibility of controlling the polarisation of the input laser and so the response of the BS; however, this displacement does not represent a crucial problem. A delay line is assembled on one of the two paths. This permits us to synchronise the arrival time of the two classical beams into the BBO crystal. Then we purify the spatial mode with the use of two pinholes in order to facilitate the following coupling.

The collinearity of this simulation beams compared to the single-photon paths is performed by crossing the classical beams into the focus of photon-pair generation, spreaded at 6 degrees referring to the axis of propagation (see Fig. 25).

5.4.2 N00N *apparatus*

The apparatus used for the N00N state preparation with classical light is described in Fig. 25.

We choose to implement a compact geometry of the set up due to the high spatial mode divergence of beams, both classical and

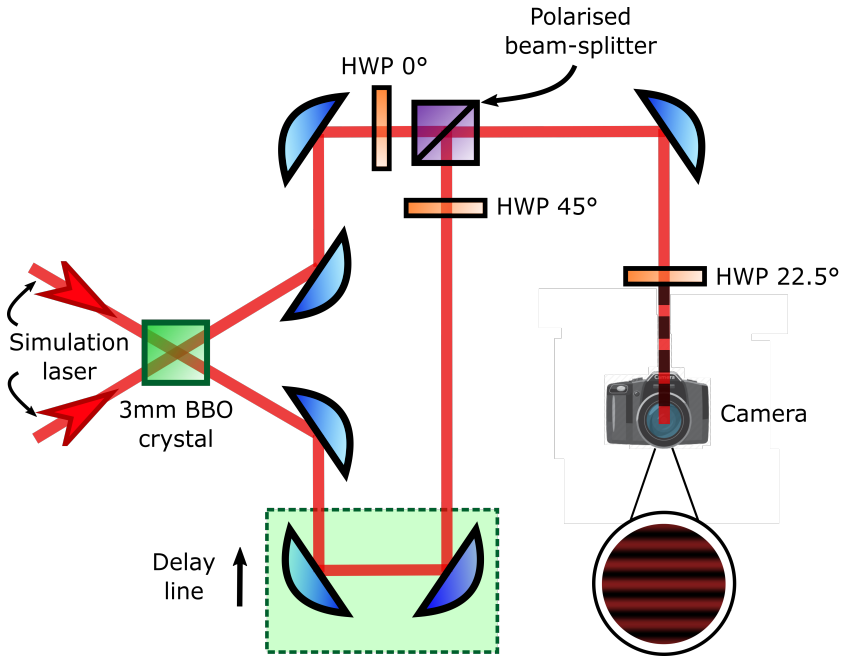

Figure 25: Experimental apparatus of N00N state in circular polarisation.

quantum. One of the two beams is directed toward the interaction PBS, preserving the horizontal polarisation while the other one passes in a delay line system and goes to the PBS after a polarisation rotation from the horizontal to the vertical polarisation. In order to optimise the interferometer, *i.e.* creating the indistinguishability conditions, we rotate the projection half waveplate at 22.5 degrees and we match the spatial mode of the beams, tuning the path lengths with the delay line system; the goodness of this procedure is controlled by the observation of the interferometric fringes image, recorded by a CCD camera. This represent a first order of optimisation which is integrated by the finest one using the single photons status.

5.5 THE EFFECT OF POST-SELECTION

Recalling the probabilities described in Eq. (195), we remark that $p(1|\theta;\phi,\nu)$ and $p(2|\theta;\phi,\nu)$ represent the outcome states with one

photon in each output arms of the interferometer and both of two photons for either output arms respectively. However, the measurement system, which consists on two APDs and a correlator, does not consent to resolve the photon number of the state; for this reason, it is not possible to determine the two states associated to the probability $p_2(\theta|\phi,\nu)$. Furthermore, we need at least four settings of θ in order to resolve the two parameters, $\theta = \{0, \pi/16, \pi/8, 3\pi/16\}$. This leads to define the post selected probabilities

$$p(\theta;\phi,\nu)_{PS} = \frac{1}{4}(1 + \nu\cos(8\theta - 2\phi)) \tag{125}$$

associated only to the coincidence counts; the derivation of these probabilities are performed by

$$p(\theta;\phi,\nu)_{PS} = \frac{p(1|\theta;\phi,\nu)}{\sum_\theta p(1|\theta;\phi,\nu)}. \tag{126}$$

Some considerations must be made regarding the main differences between the ultimate accuracy limit of estimation, described by the Fisher information matrix, considering the complete set of probabilities in Eq. (195) and the post-selected probabilities in Eq. (125). For a flat distribution of the settings $p(\theta) = 1/4$ the complete Fisher information matrix reads

$$F_{ij} = \frac{1}{4}\sum_\theta \left(\frac{\partial_i p(1|\theta;\phi,\nu)\partial_j p(1|\theta;\phi,\nu)}{p(1|\theta;\phi,\nu)} + 2\frac{\partial_i p(2|\theta;\phi,\nu)\partial_j p(2|\theta;\phi,\nu)}{p(2|\theta;\phi,\nu)} \right), \tag{127}$$

where in the second half of the sum we consider the double occurence of $p(2|\theta;\phi,\nu)$. The post-selected Fisher information matrix is given by:

$$F_{ij}^{PS} = \frac{1}{4}\sum_\theta \left(\frac{\partial_i p(\theta;\phi,\nu)\partial_j p(\theta;\phi,\nu)}{p(\theta;\phi,\nu)} \right), \tag{128}$$

which is the one used in the experiment. The explicit forms are:

$$\mathcal{F}_{\phi,\phi} = 4 - \frac{16(\nu^4 - 3\nu^2 + 2)}{(1 - \cos(8\phi))\nu^4 - 8\nu^2 + 8} \tag{129}$$

$$\mathcal{F}_{\phi,\nu} = -\frac{2\nu^3 \sin(8\phi)}{(1 - \cos(8\phi))\nu^4 - 8\nu^2 + 8} \tag{130}$$

$$\mathcal{F}_{\nu,\nu} = \frac{4 - (1 - \cos(8\phi))\nu^2}{(1 - \cos(8\phi))\nu^4 - 8\nu^2 + 8}. \tag{131}$$

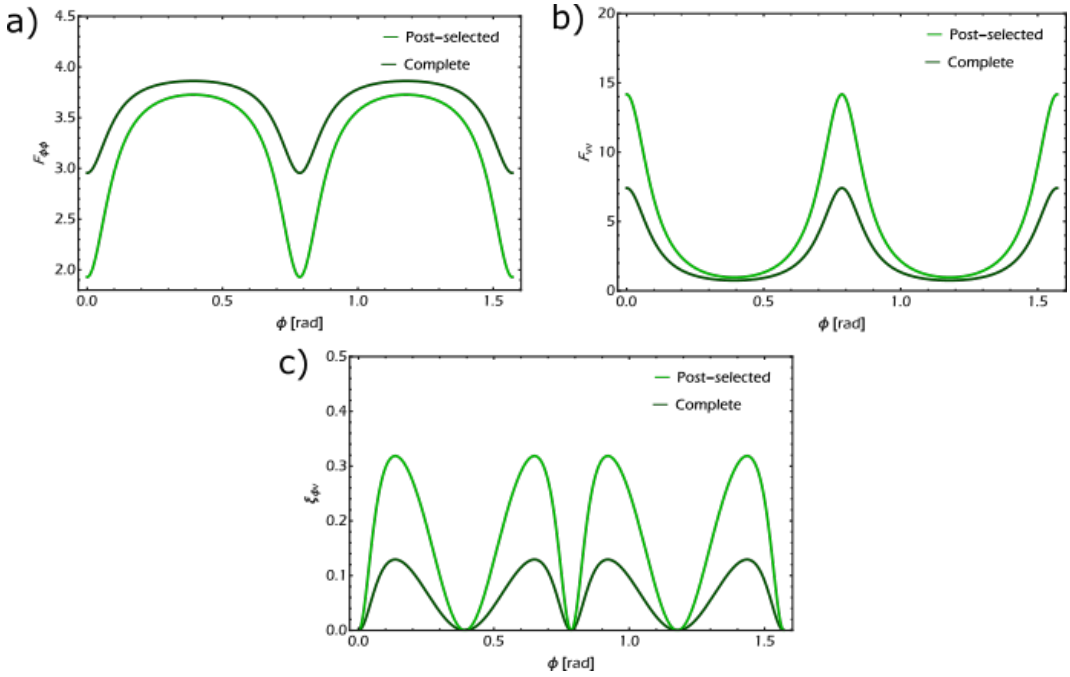

Figure 26: The post selected (bright green line) and complete (dark green line) Fisher information matrix elements, $F_{\phi,\phi}$ (a), $F_{\nu,\nu}$ (b) and $\xi_{\phi,\nu}$ (c).

Quantitative comparison of the two Fisher matrices can be appreciated in Fig. 26; the effect of post-selection leads to a reduction of the available information of the phase $F_{\phi\phi}$, while inducing an amelioration for the amount of information concerning the visibility parameter $F_{\nu\nu}$. However, taking into account the probability of the favorable events that are post-selected, the weighted post-selected Fisher information matrix elements are in general always

lower than the complete Fisher information due to the compensation of the loss of resource erased by the post-selection process.

Another important mark of the post-selection effect is the enhancement of the oscillations on the off-diagonal term $\xi_{\phi,\nu} = F_{\phi,\nu}/(F_{\phi,\phi}F_{\nu,\nu})^{1/2}$. This enhancement represent a clue of the critical increasing amount of correlation properties phase and visibility. The effect of post-selection acts on the information extraction with a decreasing number of resources used for the estimation; for this reason, the achievable information devided among the two parameters is lower, leading to an improving of the correlation between phase and visibility.

5.6 ESTIMATION PROCEDURE

The metrological test we want to perform is the goodness of accuracy achievable with the N00N apparatus described above, *i.e.* the saturation of the Cramér-Rao bound (CRB) introduced previously in Chapter 3 which imposes a limit to the covariance matrix Σ,

$$\overline{\Sigma} \geqslant \overline{F}^{-1}/M, \tag{132}$$

where M is the given number of trials and

$$\overline{F} = \begin{pmatrix} F_{\phi\phi} & \xi_{\phi\nu} \\ \xi_{\phi\nu} & F_{\nu\nu} \end{pmatrix} \tag{133}$$

is the Fisher information matrix associated to the probabilities in Eq. (125), see Fig. 27.

The joint distribution, experimentally measured for the values of ϕ and ν, is obtained by Bayesian estimation. With the use of Bayes's theorem we update the *a priori* joint probability $P_A(\phi,\nu)$ considering the number of measured copies n_θ, that is the number of coincidences associated to each set of θ. This procedure leads to the Bayesian joint probability distribution

$$P_B(\phi,\nu|\overline{n}) = NP_A(\phi,\nu)\Pi_\theta p(\theta|\phi,\nu)^{n_\theta}, \tag{134}$$

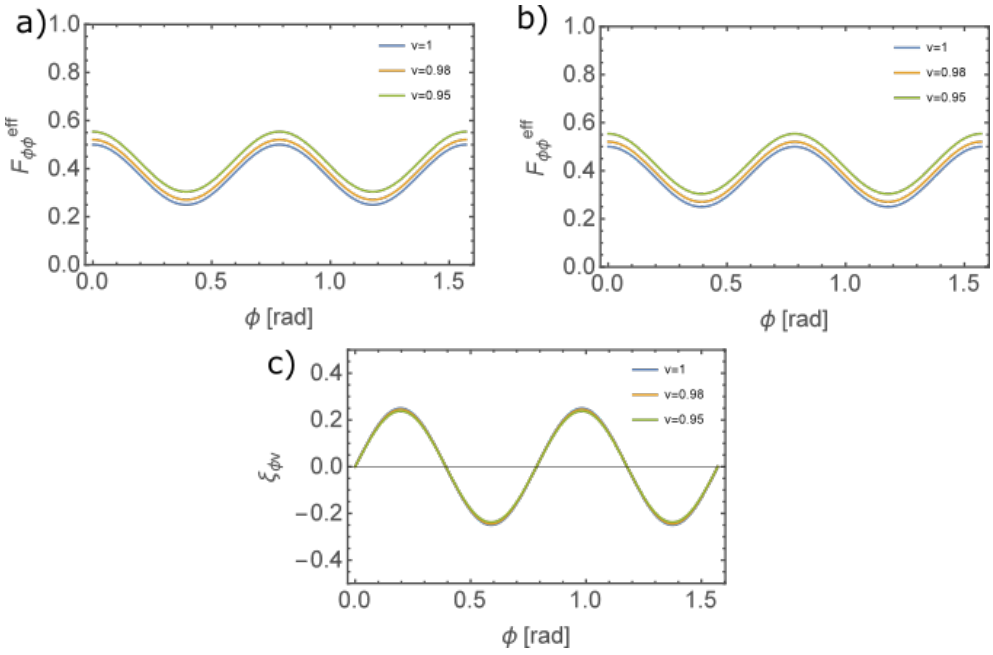

Figure 27: CRB per number of trial unit associated to the variance of ϕ (a), the variance ν (b) and the covariance of both parameter (c) as a function of the phase parameter ϕ for different values of visibility. For sake of simplicity we introduce the effective Fisher information matrix elements $F^{eff}_{ij} = (1/\overline{F}^{-1})_{ij}$.

where N is a normalisation constant and $\overline{n}$ is the vector formed by the four coincidence count rates n_θ. All the estimation results in this experiment are performed by quantifying the first moments of the marginal distributions from $P_B(\phi, \nu|\overline{n})$,

$$\phi_B = \int \phi P_B(\phi, \nu|\overline{n}) d\phi d\nu, \tag{135a}$$

$$\nu_B = \int \nu P_B(\phi, \nu|\overline{n}) d\phi d\nu, \tag{135b}$$

which are the main values of the estimated phase and visibility respectively. Furthermore the experimental covariance matrix elements are defined as the second moments of $P_B(\phi, \nu|\overline{n})$:

$$\Sigma_{\phi\phi} = \Delta^2\phi = \int (\phi - \phi_B)^2 P_B(\phi, \nu|\overline{n}) d\phi d\nu, \tag{136a}$$

$$\Sigma_{\nu\nu} = \Delta^2\nu = \int (\nu - \nu_B)^2 P_B(\phi, \nu|\overline{n})\, d\phi\, d\nu, \tag{136b}$$

$$\Sigma_{\phi\nu} = \Sigma_{\nu\phi} = \int (\phi - \phi_B)(\nu - \nu_B) P_B(\phi, \nu|\overline{n})\, d\phi\, d\nu. \tag{136c}$$

5.7 CHARACTERISATION OF THE EXPERIMENTAL APPARATUS

After the preliminary check with classical light we start the experiment using single photons as quantum probes for the multi-parameter estimation. Firstly, we have tested the performance of the interferometric device with a calibration step, by inserting an additional HWP_ϕ, see Fig. 28; the suitability of this system allow us to control properly the apparatus thanks to the knowledge of the set phases ϕ imparted by the HWP depending on its angle setting.

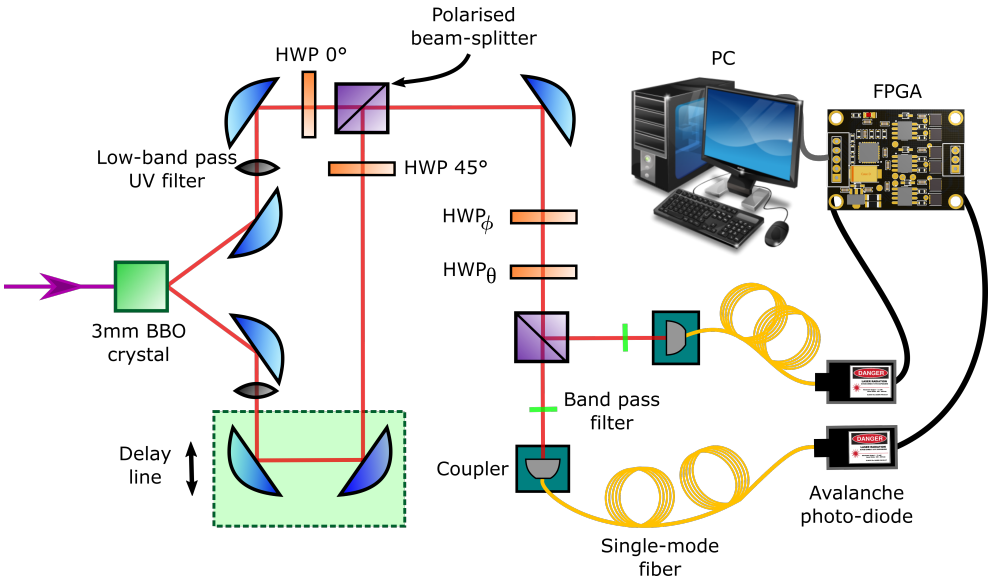

Figure 28: Experimental set-up for the calibration step.

Two single photons are generated via Type-I spontaneous PDC from a BBO non-linear crystal of 3 mm length excited with a continuous wave pump laser of 80 mW of average power and 405 nm wavelength. The photon pair generated, at 810nm wavelength,

follow the same path of classical light described above. In this configuration we use low-band pass UV filter (721 nm longpass) in order to cut the spectrum of the pump laser which has several orders of power magnitude compared to the single-photon pairs. At the two-output arms of the interferometer we perform the measurement of the amount of coincidences by the use of two Gaussian bandpass filters, centered at 810 nm and with a full width half maximum of 7.3 nm, two coupling systems and two APDs using single mode fibers. The electric signals converted by the APDs are then carried to the Field Programmable Gate Array (FPGA) board which transfer the information to the PC.
In a similar way of the classical light case, we assure the goodness of interferometry by tuning the distances with the delay line, both arms are 77 cm length, and by rotating the HWP_θ at 22.5 degrees leaving the HWP_φ at 0 degree; with this procedure and without any phase-shifts we can firstly establish the visibility of the system

$$\nu_{cal} = \frac{C_{out} - C_{in}}{C_{out}}, \tag{137}$$

where C_{out} and C_{in} are the coincidences in distinguishability condition, without matching the spatial patterns of the single photon beams, and indistinguishability condition respectively. In this scheme the pre-calibrated visibility is $\nu = 0.98$; as previously mentioned, we will see that this efficiency pre-calibration is inconvenient when the conditions change.

5.7.1 *Calibration results*

The estimation of 11 phases imparted by the HWP_ϕ is reported in Fig. 29. The goodness of phase estimation ϕ is showed in Fig. 29(a); as the blue dashed graph represents the expected value of ϕ, with a slope coefficient equal to 1, the experimental estimation (blue triangles) shows similar linear regression as its slope is $s_\nu = 1.011 \pm 0.004$. A very interesting behavior conditioning the visibility estimation; indeed, it appears to be affected by fluctuations around a constant mean value, as confirmed by the slope of the linear fit, $s_\nu = -0.001 \pm 0.003$.

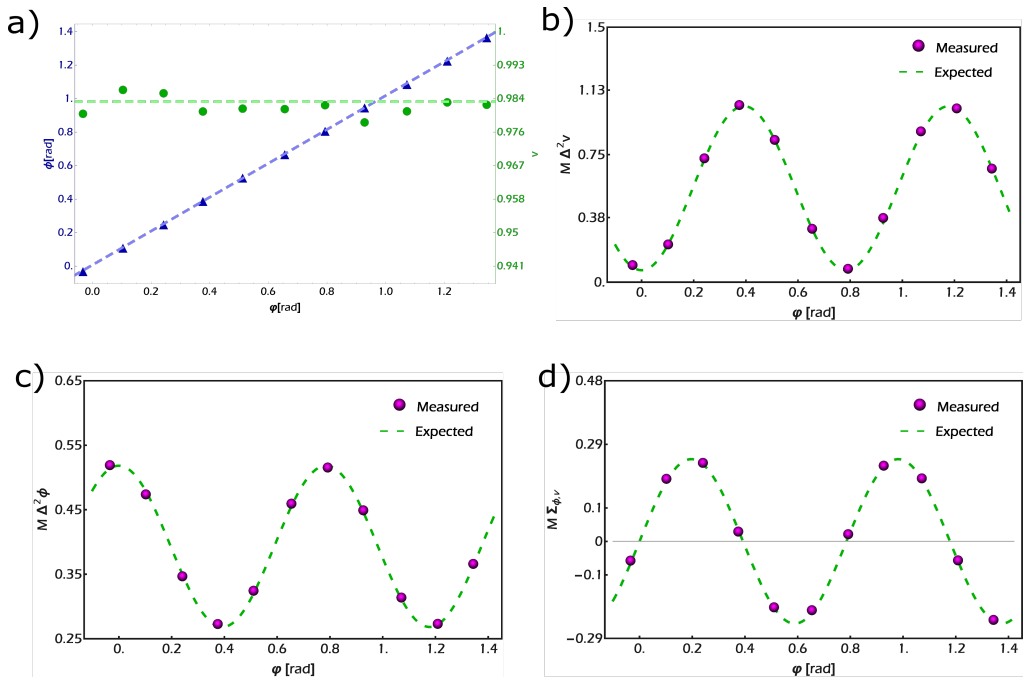

Figure 29: Bayesian multi-parameter estimation for the apparatus calibration.

We address this fluctuation as the manifestation of different coupling effects on the experimental apparatus. Considering the case in which the photon initially in the H polarisation is transmitted by the beamsplitter, while the V photon is reflected (this corresponds to $\phi = 0$). Labelling the two detection efficiency as η_{1H} and η_{1V}, respectively, the rate of coincidences is $\eta_{1H}\eta_{1V}N$, where N is the number of pairs produced. By swapping the photons on their orthogonal states using HWP_ϕ, setting the phase to $\phi = \pi/4$, the coincidence count rate amounts to $\eta_{2H}\eta_{2V}N$ and generally it is slightly different from the previous rate. This happens because of the difficulty on the coupling procedure, the single mode fiber core has a $\sim 5\mu m$ diameter, and even for a good coupling rate η for classical beams on the couplers, both around $\eta \sim 40\%$, while the phase changing even little mismatches cause the coupling unbalance on the output arms of the interferometer.
The estimation accuracy check is showed in Fig. 29(b)-(c)-(d) with

the comparison of covariance elements weighted by the number of resources $M = \sum_\theta n_\theta =\simeq 70000$ (purple dots), with the corresponding CRBs (dashed green line). As mentioned during the post-selection discussion, we notice that the available information is distributed between the two parameters, ϕ and ν, depending on the value of the phase observing the oscillations of $\Delta\phi^2$ (Fig. 29(b)) and $\Delta\nu^2$ (Fig. 29(c)). This fluctuation is observed in the covariances as well (Fig. 29(d)) allowing us to appreciate that the best estimation for either individual parameter occurs when the correlation is minimal.

So, the closeness of the experimental variances to the ultimate accuracy limit imposed by the CRB is an index of the good quality of our method for phase estimations. Furthermore, the multiparameter estimation approach enhances the difficulty to establish *a priori* the efficiency ν of the interferometric apparatus because of unknown effects, like unbalanced couplings, generated by the phase shift impact.

5.8 APPLICATION ON SUGAR AQUEOUS SOLUTIONS

After the calibration step, we test our apparatus with two different aqueous solutions of fructose and sucrose, which are two remarkable examples of chiral molecules. As introduced before, the benefit of performing circular phase-shift, and the relative rotation on the linear polarisation, via light-matter coupling, represents a valuable approach for the characterisation of this aqueous solution interacting with the surroundings. Furthermore, the handling of the number of resources using quantum light ensure a good phase information extraction combined with a low damage probability of the sample, a fundamental request for biological experiments. Using the same apparatus in Fig. 28, replacing the HWP_ϕ with the aqueous sample, we achieve to the multi-parameter estimation of phase and visibility with fructose and sucrose solutions, see Fig. 30-31. The technical difficulties due to the interaction of the light with the aqueous solution, beam deviation and absorption, cause further fine coupling of the system; this induces to a differ-

ent visibility of the interferometer compared to the pre-calibration procedure.

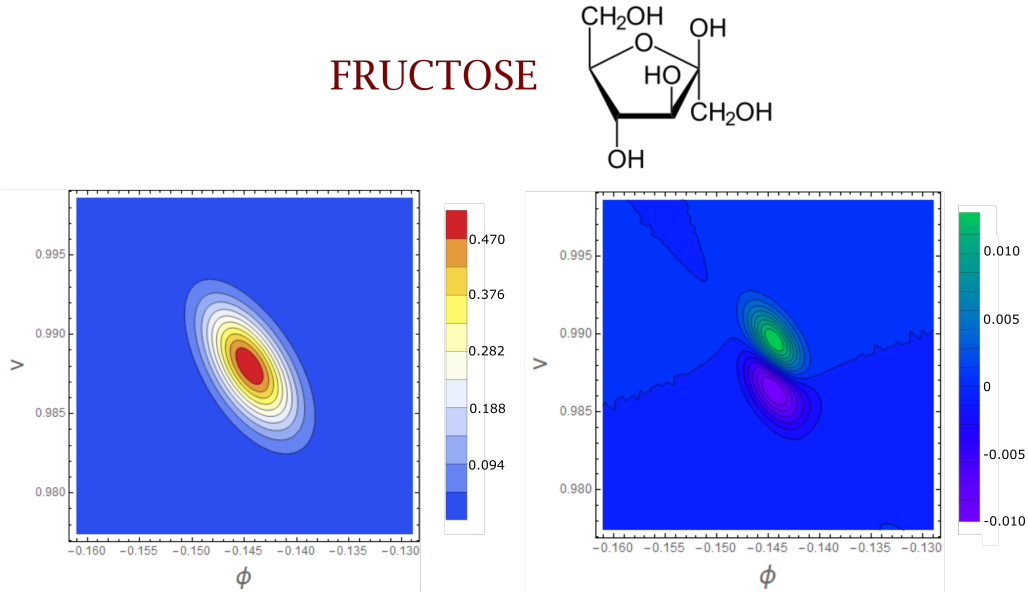

Figure 30: Bayesian joint probability for visibility (ν) and phase (ϕ) (left panel) and its difference with respect the one at the CRB (right panel) for fructose in aqueous solution.

In these figures are reported the 2-dimensional Bayesian joint probability distribution for the overmentioned sugar solutions at the same nominal concentration $c = 0.3$ g/ml, normalised to unit; on the left panel there is the reconstructed distribution $P_B(\phi, \nu|\overline{n})$ described in Eq. 134, which give back the average values of phase-shifts, $\phi_F = -0.145$ rad for the fructose (visibility $\nu_F = 0.988$) and $\phi_S = 0.089$ rad for the sucrose (visibility $\nu_S = 0.955$). In order to confirm the consistency of these estimated values we made a test using classical light of a close wavelength (808 nm) in the same apparatus obtaining the same results.
The contour plots in the right panel on both figures show the difference between $P_B(\phi, \nu|\overline{n})$ and the expected Gaussian saturating the CRB,

$$P_{exp}(\phi, \nu) = \frac{1}{C} Exp\Big[-\frac{1}{2}(\mathbf{x} - \mathbf{x}_B)^T \overline{\Sigma}^{-1}_{\nu_B, \phi_B}(\mathbf{x} - \mathbf{x}_B)\Big], \tag{138}$$

where C is a normalisation constant $C = \int P_{exp}(\phi, \nu) d\phi d\nu$, $\mathbf{x}$ and $\mathbf{x}_B$ are real 2-dimension vectors of the variables $\{\phi, \nu\}$ and of the expectation values obtained by the Bayesian method $\{\phi_B, \nu_B\}$ respectively and $\overline{\Sigma}_{\nu_B,\phi_B} = \overline{F}^{-1}_{\nu_B,\phi_B}/M$ is the covariance matrix saturating the CRB calculated at $\{\phi_B, \nu_B\}$.

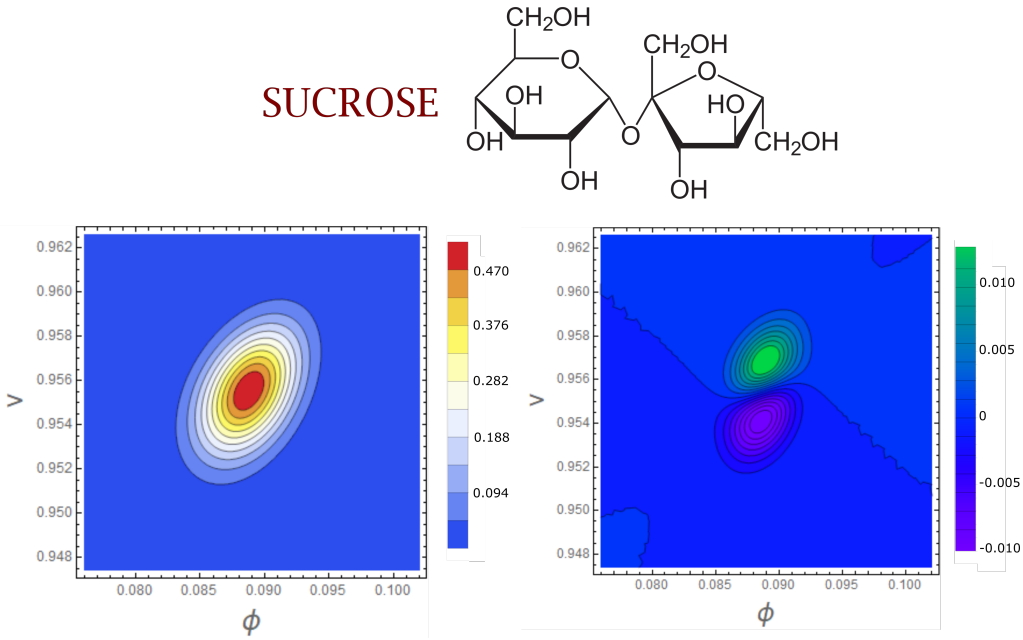

Figure 31: Bayesian joint probability for visibility (ν) and phase (ϕ) (left panel) and its difference with respect the one at the CRB (right panel) for sucrose in aqueous solution.

From the figures it is possible to see the excellence of our method observing that the deviation of the reconstructed distribution from the expectation remain of the order of 1% for both concentrations.

5.8.1 *Statistical hypothesis test*

During the pre-calibration check we compared the elements of the experimental covariance matrix with the ultimate precision limit defined by the CRB. In order to perform a more stringent statistical test comparing the estimated covariance matrix $\overline{\Sigma}_{exp}$ with the

one saturating the CRB $\overline{\Sigma}_{\nu_B,\phi_B} = (M\overline{F}_{\nu_B,\phi_B})^{-1}$, we choose to perform a *statistical hypothesis* test.

The hypothesis test constituted a method in order to compare two statistical data sets or a data set obtained by sampling compared against a synthetic data set from an idealized model. In order to quantify the statistical relationship between the two data sets, it is commonly proposed the *null hypothesis*; in our case it represents a likelihood ratio test assessing quantitatively the closeness of the estimated covariance matrix $\overline{\Sigma}_{exp}$ to the one saturating the CRB, and it reads

$$H_0 : \overline{\Sigma}_{exp} = (M\overline{F}_{\nu_B,\phi_B})^{-1}, \tag{139}$$

where $\overline{\Sigma}_{exp}$ saturates the Eq.132.

This comparison is defined statistically significant if the relationship between the data sets would be an unlikely realization of the null hypothesis according to a threshold probability, that represents the significance level of such comparison. In order to determine how much the two data sets are statistically significant, a parameter l-value must be calculated which is the probability of observing an effect of the same magnitude or more extreme given that the null hypothesis is true. With fixed dimensions of the covariance matrix under investigation and with a large number of resources used for the statistics (we exploit a very high number of resources, $M \simeq 50000$ for the fructose and $M \simeq 70000$ for the sucrose), the likelihood ratio test predicts that the variable

$$l = M^2 \mathrm{Tr}(\overline{F}_{\nu_B,\phi_B} \cdot \overline{\Sigma}_{exp}) - M(\ln \det(\overline{\Sigma}_{exp}) + \ln \det(M\overline{F}_{\nu_B,\phi_B})) - 2 \tag{140}$$

is distributed as χ^2 variable with 3 degrees of freedom [123].

The measured values for the two solutions are $l_F = 2.63$, and $l_S = 0.10$, both compatible with the critical significant level value 7.81 for the 95% confidence interval.

5.9 THE SINGLE PARAMETER ESTIMATION APPROACH

In order to show the convenience of multi-parameter estimation approach described above we now explore the performance of single-parameter estimation of phase-shift with fixed pre-calibrated visibility ν_0. The post-selected probability in Eq.125 become

$$p(\theta;\phi) = \frac{1}{4}(1 + \nu_0 \cos(8\theta - 2\phi)), \tag{141}$$

where the error on ν_0 is considered negligible. Recalling the CRB

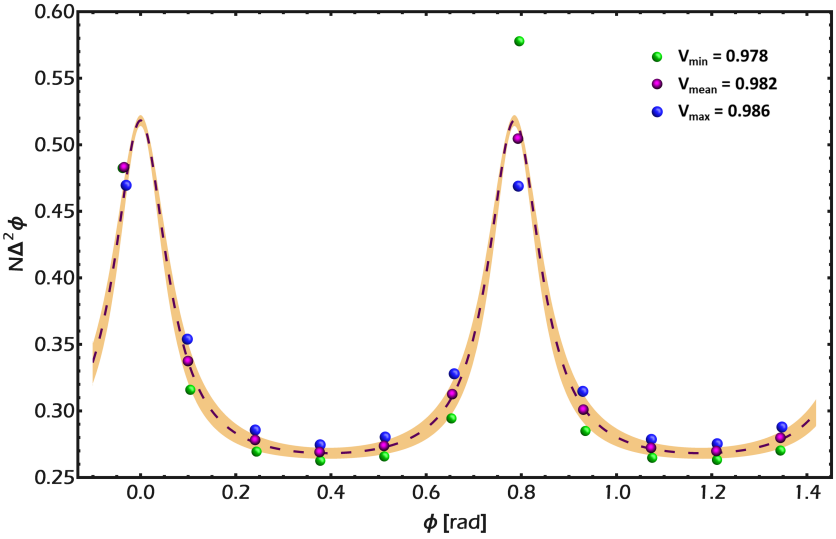

Figure 32: The estimated phase variance for three values of visibility, $\nu_{min} = 0.978$ (green dots), $\nu_{mean} = 0.982$ (purple dots), $\nu_{max} = 0.986$ (blue dots), compared with the expected CRB for pre-calibrated visibilities ranging from $\nu_0 = \nu_{min}$ to $\nu_0 = \nu_{max}$ (shaded area): $\nu_0 = \nu_{mean}$ is highlighted (purple dashed line).

in Eq.132, the ultimate bound of the phase accuracy is than given by $1/M\mathcal{F}_{\phi\phi}$; in Fig. 32 we compare the uncertainties on the phase to this limit, considering three instances for the visibility, namely the maximum (ν_{max}), the mean (ν_{mean}) and the minimum (ν_{min}) values obtained in the multiparameter pre-calibration analysis, see Fig. 29. As reported on the graph, the extreme values of visibility ν_{min} and ν_{max} lead to an estimation which is far from the corre-

sponding CRBs. Even though the estimation using the mean visibility ν_{mean} seems to achieve an ameliorated overlap with the expectation accuracy, the discrepancy with respect the relative CRB is three times larger than those achieved with the multi-parameter approach. Furthermore, some effect of the bias on the uncertainties can be examined even in such controlled conditions.

A single-parameter approach check for the characterisation of the sugar solutions is also performed. In Fig 33 we show what happens to the quality of the estimation approach when the visibility ν_0 is not properly considered; indeed, the real visibility of the apparatus could change due to the interaction with the sample as previously described, leading to an improper estimation if we consider ν_0 as a fixed parameter. As reported in this graph the effect of bias is limited only around the measured value of ν_0; we quantify this by the quantity $K_M = \sigma^2 \mathcal{F}_{\phi,\phi} M$. Comparing the variance of ϕ of the single-parameter approach (solid diamonds) to the multi-parameter one (open diamond), we notice that part of the resources needed for the estimation have to be shared to the visibility estimation; this does not fall on the single-parameter CRB despite being compatible with that of the multiparameter approach.

5.10 THE SCALING LAW FOR MULTI-PARAMETER ESTIMATION

In Chapter 3 we explored the usefulness of quantum metrology on the precision on given parameters by the proper arranging of the number of resources used for the estimation; we describe that the accuracy of a measurement scale with the number of the resources N, which are photons in our case, in the probe. In particular, we mark the enhancement of using quantum probes that permits to reach a scaling law of the Fisher information as N^2 instead of classical resources that are limited to N. In this section we generalise the N00N state previously studied from 2 photon input state to 2N photons: we consider Holland-Burnett states that are obtained by quantum interference of two N photon states arriving on input modes with creation operators $\hat{a}^\dagger_H$ and $\hat{b}^\dagger_V$.

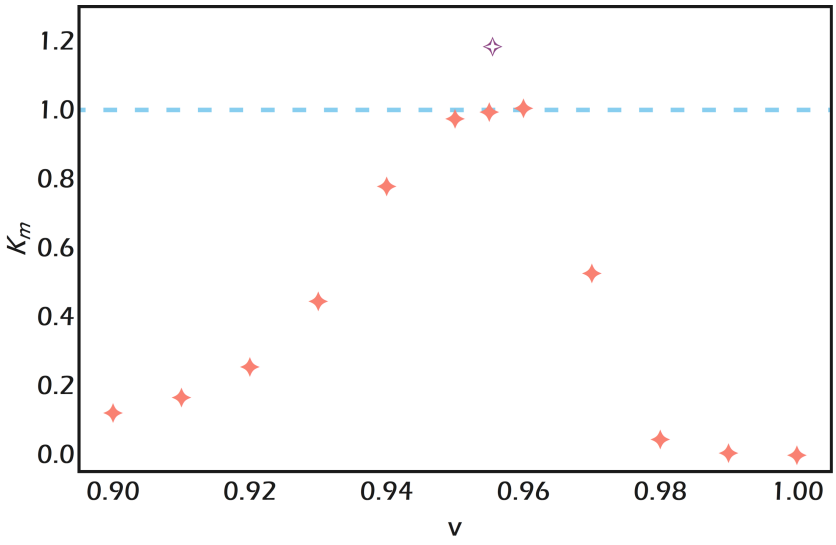

Figure 33: The estimated phase variance in units of $1/(M\mathcal{F}_{\phi,\phi})$ for the sucrose solution as a function of the pre-set visibility v.

If we insert a phase ϕ inside the interferometric scheme, these two modes could interfere even accounting the distinguishability of the photons; we consider the standard decomposition

$$\hat{b}_V^\dagger = \sqrt{1-\epsilon^2}\hat{a}_V^\dagger + \epsilon\hat{q}_V^\dagger, \tag{142}$$

where $\hat{a}_V^\dagger$ mode interferes perfectly with $\hat{a}_H^\dagger$, while $\hat{q}_V^\dagger$ does not. The parameter ϵ defines the amount of distinguishability of the two modes $\hat{a}_H^\dagger$ and $\hat{b}_V^\dagger$: from $\epsilon = 0$ to $\epsilon = 1$ for a complete indistinguishability or distinguishability respectively. Using this definitions, the initial state reads

$$\begin{aligned}|\Psi_0\rangle =& \frac{1}{N!}(a_H^\dagger)^N(b_V^\dagger)^N|0\rangle \\ =& \frac{1}{N!}(a_H^\dagger)^N(q_H^\dagger)^0\sum_{k=0}^{N}\binom{N}{k}(1-\epsilon^2)^{k/2}\epsilon^{(N-k)/2}(a_V^\dagger)^k(q_V^\dagger)^{N-k}|0\rangle.\end{aligned} \tag{143}$$

Similarly to the two-photon case, the evolved state $|\Psi_\phi\rangle$ can be calculated, also with the introduction of an additional control

phase θ for the measurement of the system with different settings. In order to investigate the scaling of the estimation accuracy with the number of photons N, we introduce as quantifiers the effective values of Fisher information associated to ϕ and ϵ, $\tilde{F}_{i,i} = 1/(F^{-1})_{i,i}$ for $i = \phi, \epsilon$, optimized over all possible phases. For the calculation of the probabilities we use POVM considering counts the total photon number on modes a_H and q_H, without resolving the individual populations; due to photon number correlations, adding a second counter on the modes a_V and q_V would provide no extra information. The operator associated to the outcome x is then written in the Fock basis as:

$$\Pi_x = \sum_{s=0}^{x} \Pi_x^{(s)} = \sum_{s=0}^{x} |s\rangle\langle s|_{aH} \otimes I_{aV} \otimes |x-s\rangle\langle x-s|_{qH} \otimes I_{qV}. \quad (144)$$

Each detection probability is then found as

$$\begin{aligned} p(x, \theta|\phi, \epsilon) &= \langle \Psi_{\phi+\theta}|\Pi_x|\Psi_{\phi+\theta}\rangle \\ &= \sum_{s=0}^{x} p^{(s)}(x, \theta|\phi, \epsilon) \end{aligned} \quad (145)$$

for all possible outcomes $x = 0, ..., 2N$. In our calculations we considered two possible settings $\theta = 0$ and $\theta = \pi/2$, alternated with equal probability.

In Fig. 34(a)-(b) we report the results of our numerical simulations: for moderate distinguishability, the effective Fisher information on ϕ on Fig. 34(b) decreases with respect to its value $2N(N+1)$ (black solid line) at $\epsilon = 0$, but it growth quicker than the classical scaling N (red solid line), obtained for complete indistinguishability. As we notice from the plot, the presence of correlation between the two parameters leads to a reduction of the effective Fisher information $\tilde{F}_{\phi\phi}$ but an asymptotic quadratic scaling is maintained also for distinguishability $0 < \epsilon < 1$. Regarding the distinguishability ϵ on Fig. 34(a) we observe a non-monotonic behavior: the information initially decreases with respect to the linear scaling, but a quadratic behavior $2N^2$ (black solid line) is eventually observed in the complete indistinguishability limit $\epsilon = 1$.

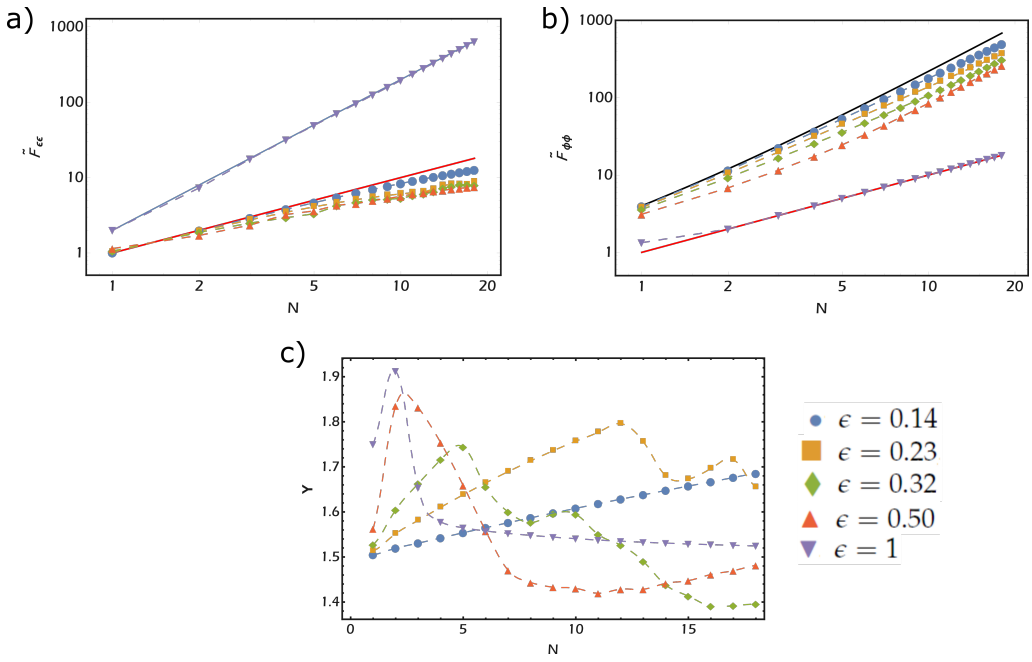

Figure 34: Scaling of the Fisher information: (a) effective Fisher information for the distinguishability parameter ϵ. The points correspond to numerical results. (b) effective Fisher information for the phase ϕ. (c) Trade-off in the optimality of individual estimations quantified by Υ.

In order to understand how the information is partitioned between ϕ and ϵ and how is possible to determine the optimality conditions, we introduce the parameter

$$\Upsilon = \max_{\gamma} \left(\frac{\tilde{F}_{\phi,\phi}(\gamma)}{\max_{\alpha} \tilde{F}_{\phi,\phi}(\alpha)} + \frac{\tilde{F}_{\epsilon,\epsilon}(\gamma)}{\max_{\beta} \tilde{F}_{\epsilon,\epsilon}(\beta)} \right). \tag{146}$$

This figure of merit quantifies how close one can get to the optimal estimation for both parameters simultaneously. In Fig. 34(c) we report the corresponding results by calculating the sum of the ratios between the effective Fisher information for respectively ϕ and ϵ, and their maximum values, optimized for a particular value of ϕ; we can determine that for each value of distinguishability ϵ there exist an optimal value of N that achieve the best joint estimation compromise. In the graph it is also possible to appreciate that

for large values of ϵ, *i.e.* highly amount of noise, this optimal value is achieved for small N, while for small values of ϵ, nearly-ideal probes, the optimality is reached for larger values of N, where the quantum enhancement for the phase estimation is more evident, as assert before.

5.11 CONCLUSIONS

In this work, we highlight the impact of the multi-parameter estimation in order to probe phase-shift material even considering the noise effect, an unavoidable challenge in realistic conditions. We have performed such approach that integrates phase estimation with a characterisation of the probe at the same time, by measuring the imparted phase-shift of the material and the efficiency of the devices, parametrised by the visibility of the fringes. After a pre-calibration test, with the use of an HWP that simulates the phase-shift on circular polarisations by a rotation on the linear polarisation, we use this scheme in order to investigate the optical activity of fructose and sucrose solutions. Expanding this concept to a larger number of photons, in Holland-Burnett states, we study with numerical simulations how the precisions of estimation scale with the photon number N. This study in particular, highlights the presence of trade-off conditions, as part of the information need being devoted to determine the quality of the probe while the information needed for the precision on the phase is lower. The trade-off seems to change for different scales of the number of photons of the system.

6

ASSESSING FREQUENCY CORRELATION THROUGH A DISTINGUISHABILITY MEASUREMENT

"An idea which can be used only once
Is a trick. If one can use it more
Than once it becomes a method."
— Problems and Theorems in Analysis I: Series. Integral Calculus. Theory of Functions, G. Polya

6.1 INTRODUCTION

Previously in this thesis, I have discussed the spectral correlation effect from a three-wave mixing occurrence, the parametric down-conversion. The implementation of a measurement apparatus, able to quantify the amount of frequency entanglement in such two-photon generation event, implies quite a few experimental difficulties. As observed before, JSA and auto-correlation function constitute some of these quantification methods, but suffer inevitably from the spectral resolution, especially when operating with PDC events pumped with continuous wave (CW) light beams; in fact, as we will see, in such cases the correlation strength is of the order of the narrow pump bandwidth (which is in general < 1 GHz), a very hard task to detect on the very broad photon-pair generated distribution (of the order of some nm). To deal with this issue, a less demanding approach would be desirable even accepting measurement results with reduced spectral resolution, but still confirming the presence of correlations and put a number on their strength.

Throughout this thesis we also noticed a useful implementation of quantum metrology for the estimation of chiral solution, with the multi parameter approach. In particular, we exploit the metro-

logical method with dispersive material, allowing to compose the phase-shift distribution by estimating the dispersion parameter, jointly with the main phase-shift one. Exploiting the strong relation between the dispersion properties of a material with the spectral nature of light, in this chapter we explore the possibility of utilise the multi parameter procedure, in order to estimate the correlation strength of a PDC-photon pair which encounters a highly dispersive material; such measurement aims at observe the visibility on a N00N-state interferometric scheme, similar to the one above mentioned for the fructose and sucrose chiral characterisation.

6.2 DISPERSION CANCELLATION

We already observed that probing dispersive samples with broad band photons leads to a Gaussian-like distribution of phase-shift response. In particular, using interferometry as a metrological tool for characterisation of such samples, the presence of dispersion unavoidably reduces the efficiency of interferometer apparatus, leading to a lower visibility on the coincidence rate detection. Thus, dispersion and visibility itself as such may constitute a useful tool for the quantification of non-classical spectral correlations of photon-pair emission event, mentioned at the beginning of this paper.

Moving in this direction, a phenomenon similar to that associated to non-local *dispersion cancellation* using spectral-entangled photons has been examined by Franson and Beak [124–126]. In this work, a two broad single-photon system traveling through a dispersive material is investigated. For uncorrelated photons, the presence of dispersion provokes an unavoidable visibility reduction of the coincidence rate in an interferometric scheme. However, they notice that for a pair of entangled photons, it is possible to observe an improvement on the visibility for the same configuration. The strong frequency correlation among the two light beams permits to cancels the dispersion experienced by one photon with the dispersion experienced by the other photon. In order to ex-

plored this phenomenon from the metrological point of view, one can consider firstly the action of dispersion for uncorrelated photons; assuming that the two light beams, *signal* and *idler*, have been sufficiently well collimated that they can be represented by plane waves, we can denote the field associated to these pulse beams as [124],

$$E_{s,i}(x_{s,i}, t_{s,i}) = \frac{E_0}{2\pi} \int_{-\infty}^{\infty} d\omega_{s,i} g(\omega_{s,i}) e^{-i\omega_{s,i} t_{s,i}}, \tag{147}$$

where $g(\omega_{s,i})$ is the *transmission function* due to the action of the filters, assuming to have a Gaussian shape,

$$g(\omega) = e^{-(\omega-\omega_F)^2/2\delta\omega^2}, \tag{148}$$

where ω_F is the center frequency of the filters and σ_F is their standard deviation.
The interaction with the dispersive media on the photons can be explored by writing the frequencies of the two photons in terms of the central filter frequency ω_F, shifted by a small amount identified by a single parameter ϵ:

$$\begin{aligned} \omega_s &= \omega_F + \epsilon, \\ \omega_i &= \omega_F - \epsilon. \end{aligned} \tag{149}$$

In this approximation, inside the sample, the photon wave vector $k(\omega)$ becomes a function of the frequency, and to second order, we can expand it as a Taylor series in the form,

$$\begin{aligned} k(\omega_s) &= k_F + \alpha_s \epsilon + \beta_s \epsilon^2, \\ k(\omega_i) &= k_F - \alpha_i \epsilon + \beta_i \epsilon^2, \end{aligned} \tag{150}$$

where the coefficients α_j and β_j are related to the group velocity and dispersion, respectively.
Within this scenario, the dispersion activity of the dispersive material can be examined by measuring the probe beams with single-photon detectors, able to resolve the light pulse events; assuming that the dispersion properties of the sample are equal for both photons, *i.e.* $\alpha_s = \alpha_i$ and $\beta_s = \beta_i$, for joint-detecting the two light

beams, one can consider to use semiclassical field theory in order to obtaining the probability of counting from either detector at times t_s and $t_i \equiv t_s + \tau$,

$$P(\tau) = \eta I_s(x_s, t_s) I_i(x_i, t_s + \tau), \tag{151}$$

where η is a constant related to the efficiency of detection, $I_j(x_j, t_j) = E_j(x_j, t_j) E_j^*(x_j, t_j)$ is the intensity of the fields and x_j are the distances between the detectors and the light source. By omitting all the calculations, it was demonstrated [124, 126] that, assuming for simplicity that $x_s = x_i = x$, the coincidence rate probability in Eq. 151 assumes a Gaussian-like form whose standard deviation reads,

$$\sigma_U^2 = \frac{2\sigma_0^4 + (\beta_s^2 + \beta_i^2)x^2}{\sigma_0^2}, \tag{152}$$

where $\sigma_0^2 = 1/\sigma_F^2$.

As expected, for uncorrelated case, the use of two photons that probe the dispersive media enhance the presence of dispersion, as one can notice from the sum of the squares of the individual coefficients β_j in Eq. 152; thus, for classical systems no cancellation of the classical dispersion coefficients is possible.

However, for a two-photon emission event that exhibits frequency correlation, like PDC, it is possible to demonstrate that the dispersion experienced by one photon may cancel the dispersion encountered by the other photon. By mentioning the PDC description introduced in Eq. 29, we can now consider the simple case where the JSA function is now replaced by the action of the same filtering system for both photons $f(\omega_s, \omega_i) = |g(\omega)|^2$, so that the PDC state can be written as

$$|\Psi_{PDC}\rangle = \int d\omega_s d\omega_i g^2(\omega) \hat{a}_H^\dagger(\omega_s) \hat{a}_V^\dagger(\omega_i) |0\rangle, \tag{153}$$

where for sake of simplicity we define the vacuum state as $|0\rangle \equiv |0\rangle_H |0\rangle_V$.

For the case of *anti-correlated* photons, that occurs due to the use of very narrow pump beam (or CW laser), the energy and mo-

mentum conservation laws can be summarised by the wavelength relation, see Chapters 1 and 2,

$$k_i = k_p - k_s, \tag{154}$$

and the interaction of both photons with a dispersive material causes, as in the uncorrelated scheme, a spectral shift by a small amount ϵ,

$$\begin{aligned} \omega_s &= \omega_p/2 + \epsilon, \\ \omega_i &= \omega_p/2 - \epsilon, \end{aligned} \tag{155}$$

where we assumed that the central frequency of the filters matches with the half of the pump.
Under these circumstances, we can determine the statistics of the coincidence rate, that reads,

$$P(\tau) = |\langle 0|E_i^+(t_s + \tau)E_s^+(t_s)|\Psi_{PDC}\rangle|^2, \tag{156}$$

and expanding the wavenumber of the photons accordingly to the Eq.150, we observe now that the broadness of such joint probability is established by the standard deviation,

$$\sigma_C^2 = \frac{2\sigma_0^4 + (\beta_s + \beta_i)^2 x^2}{\sigma_0^2}. \tag{157}$$

Looking at this result, one can assert that using such spectral-entangled states it is possible to erase any clue of dispersion on the media if the two photons encounter the same amount of β but with opposite signs observed in a specific entangled state [124]; thus, the only presence of phase-matching and energy conservation constraints, which establishes the correlation between momentum and frequencies of the photon-pair, leads to a completely different behavior while probing dispersive samples compared to the uncorrelated beams, permitting to ponder on the fact that the dispersion estimation on a system using spectral-entangled photons could be an helpful approach for determine the entanglement strength.

6.3 QUANTUM METROLOGY AS METRIC FOR FREQUENCY ENTANGLEMENT

The investigation of such method leads us to a very similar N00N apparatus exploited previously for the joint estimation of sugar solution chirality and the efficiency of the apparatus, see Fig. 35. The two single-photon state is generated via Type-I PDC source with a CW pump laser at central frequency $\Omega_p = 405\text{nm}$ with a linewidth of the order of 200MHz, producing degenerate photons at $\omega_{s,i} = 810\text{nm}$. The fundamentals of this experiment are the same of the above mentioned one: establishing the phase-shift and the visibility of the apparatus by the introduction of a very dispersive material, that in this case is a 3mm long beta barium borate (BBO) crystal, which have a very strong birefringence.

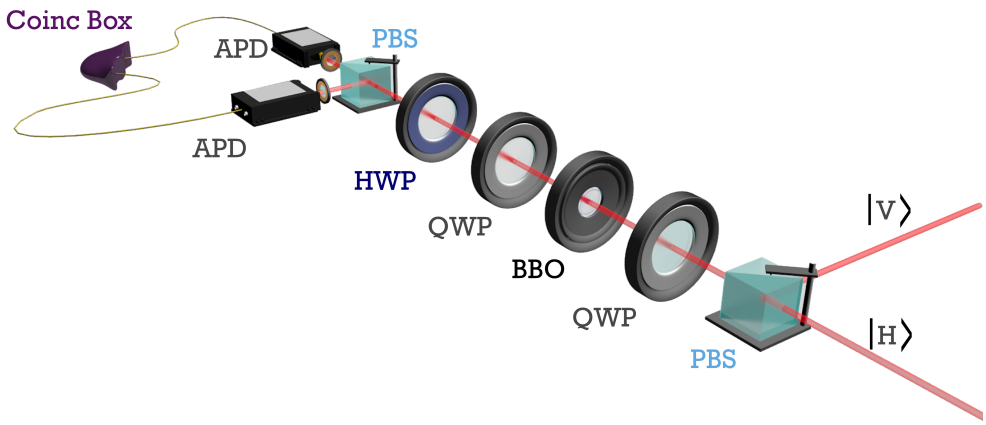

Figure 35: Experimental set-up of spectral degree of correlation estimation exploiting the high dispersion of BBO crystal.

The sensing of such birefringent phase with *R-L* N00N state described in Eq.121 can be performed by the insertion of two quarter-wave plates (QWPs) before and after the BBO, and by rotating of 45 degrees the optical axes of the plates and the dispersive crystal we ensure that the birefringent phase is imparted between the circular components. The detection of the evolved state is again analysed by means of a HWP, at different settings of its angle θ, and a PBS which transform the polarisation modes as,

$$\begin{aligned}\hat{a}_H^\dagger(\omega) \to & \cos(2\theta - \phi(\omega)/2)\hat{a}_H^\dagger(\omega) \\ & + \sin(2\theta - \phi(\omega)/2)\hat{a}_V^\dagger(\omega), \\ \hat{a}_V^\dagger(\omega) \to & \cos(2\theta - \phi(\omega)/2)\hat{a}_V^\dagger(\omega) \\ & - \sin(2\theta - \phi(\omega)/2)\hat{a}_H^\dagger(\omega),\end{aligned} \tag{158}$$

where $\phi(\omega)/2$ is the frequency-dependent polarisation rotation experienced by the photons while evolving under the action of the optically active material, due to the different refractive indexes between R and L polarisations. The projection measurement is then followed by a filtering system, having a spectral shape $g(\omega)$ described more accurately later, and by a couple of APDs on each output arm of the interferometer, in order to detect the coincidence rate. Using the rotation relations in Eq.158 and the PDC event state in Eq.29, it is possible to establish the coincidence detection amplitude at times t_s and t_i as

$$A(t_s, t_i) = \tilde{\varphi}_C(t_s, t_i) - \tilde{\varphi}_S(t_s, t_i), \tag{159}$$

with

$$\begin{aligned}\tilde{\varphi}_C(t_s, t_i) &= \int d\omega_s d\omega_i e^{i(\omega_s t_s + \omega_i t_i)} f(\omega_s, \omega_i) g(\omega_s) g(\omega_i) \cos(\theta_s)\cos(\theta_i), \\ \tilde{\varphi}_S(t_s, t_i) &= \int d\omega_s d\omega_i e^{i(\omega_i t_s + \omega_s t_i)} f(\omega_s, \omega_i) g(\omega_s) g(\omega_i) \sin(\theta_s)\sin(\theta_i),\end{aligned} \tag{160}$$

and $\theta_j = 2\theta - \phi(\omega_j)$, $j = s, i$.
From the coincidence amplitude one can obtain the actual detection probability by summing the contributions at all times,

$$P(\theta) = \int dt_s dt_i |A(t_s, t_i)|^2, \tag{161}$$

that depends on the oscillating terms $\theta_s - \theta_i$ and $\theta_s + \theta_i$, see Appendix B. A general expression of Eq.161, can be found utilising the *Parseval's theorem* that leads to a very useful simplification on the cases $f(\omega_s, \omega_i) = f(\omega_i, \omega_s) = f^*(\omega_s, \omega_i)$ where the spectral phase due to the dispersion of the source can be neglected,

combined with the symmetric properties of the phase-matching function. For this assumptions, one can determine the probability in Eq.161, which reads

$$P(\theta) = \int d\omega_s d\omega_i |f(\omega_s, \omega_i)|^2 |g(\omega_s)|^2 |g(\omega_i)|^2 \cos^2(\theta_s + \theta_i), \quad (162)$$

that is directly connected to the two-photon correlation. Assuming the dispersion of BBO crystal to be linear in the spectral domain ω for the frequency range used in this work, one can perform the approximation of the term $\theta_s + \theta_i \propto \omega_s + \omega_i$; so that, for sake of simplicity, we can easily calculate the above probability by switch in to the rotated coordinates $\omega_p = \omega_s + \omega_p$ and $\omega_- = \omega_s - \omega_p$. Furthermore, since the full width at half maximum (FWHM) of the spectral filters $\delta\omega = 7.3$nm are much narrower compared to the typical bandwidth of the phase-matching, it is possible to neglect the dependence of $f(\omega_s, \omega_i)$ on ω_- over the support of such filtering choice; thus permits us to identified the joint spectral function only ω_p dependent, that is taken as a Gaussian-like function,

$$f(\omega_p) = 2^{-2(\omega_p - \Omega_p)/\sigma^2}. \quad (163)$$

We choose to make σ coincide with the FWHM in order to consider the most generalised form possible.

6.3.1 *Filtering shape*

Observing the probability in Eq.162, some other consideration can be investigating concerning the role of the filters on the system. The filter shape of this set up has been measured by a *spectrophotometer*, and it well-fits with a super-Gaussian shape of order 4,

$$|g(\omega)|^2 = 2^{-\left(\frac{2(\omega - \Omega_0)}{\delta\omega}\right)^4}, \quad (164)$$

where $\Omega_0 = \Omega_p/2$, see the Fig. 36.

Following the assumptions on the joint spectral function mentioned before, the dependence on ω_- needs to be neglected on

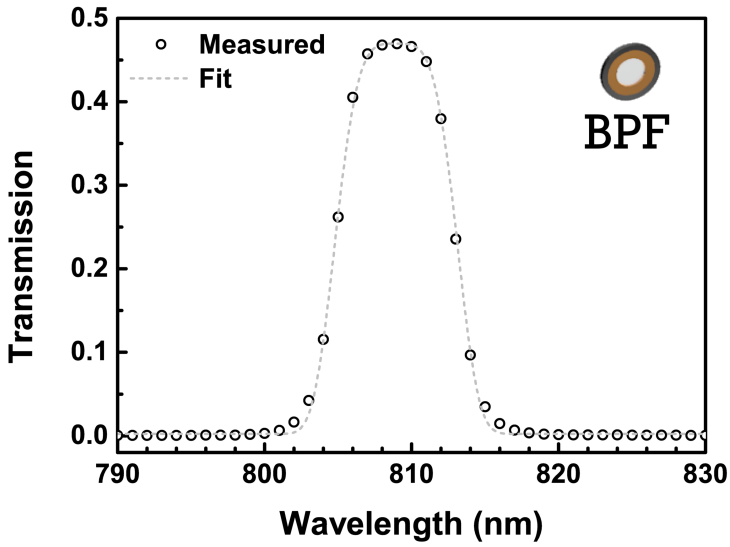

Figure 36: Measured spectral shape of the filters used in this work compared to the super-Gaussian of 4th order fit.

the spectral shape contribution as well, which can be achieved by performing the integration

$$G(\omega_p) = \int d\omega_- |g(\omega_s)|^2 |g(\omega_i)|^2 \\ \frac{1}{2}\int d\omega_- \left| g\left(\frac{\omega_p + \omega_-}{2}\right)\right|^2 \left| g\left(\frac{\omega_p - \omega_-}{2}\right)\right|^2, \tag{165}$$

The exact expression of $G(\omega_p)$ is then calculated, and it is found to be, up to an overall numerical factor,

$$G(\omega_p) = |\nu_p| e^{7\nu_p^4} K_{1/4}(9\nu_p^4), \tag{166}$$

with $\nu_p = (\omega_p - \Omega_p)/\delta\omega$ and $K_{1/4}(x)$ is a modified Bessel function of the second kind. Such function can be well approximated by a Gaussian shape having FWHM equal to that of the filters; this approximation is checked by calculating the Kullback–Leibler divergence [127] $D_{KL} = 0.0066$ that proves the closeness of the two functions.

Once consider that the spectral function $f(\omega_s, \omega_i) \sim f(\omega_p)$ has

a Gaussian profile in ω_p, its variance can be reconnected to the correlation degree of the two photons, κ, by taking $\sigma^2 = \kappa\delta\omega^2$; following this relation, states with no correlation exhibits a diverging value of κ, so that the spectral dependence of the probability $P(\theta)$ is only contained in the broadness of the filters; on the upside, a perfect frequency correlation occurs when $\kappa = 0$.

6.3.2 *Spectral degree estimation from visibility*

Following the approximation mentioned above, one can find the expression of the coincidence rate probability,

$$P(\theta) = \frac{1}{2}(1 + e^{-\sigma_\phi^2(\overline{\kappa})}\cos(8\theta + 2\phi(\Omega_p/2)), \tag{167}$$

where $\sigma_\phi(\kappa)$ is the variance of the phase distribution, which is expected to take a Gaussian form, and contains information on κ. As introduced at the beginning of this chapter, a measurement of the fringes *visibility* ν on the interferometric apparatus, leads to an estimation of the amount of correlation of the light beams probing the dispersive media. The coincidence rates, that oscillate according to the degree parameter θ, are reported in Fig. 37; in order to isolate the noise effects due to the not optimal efficiency of the set up, we measure the behavior first without the BBO crystal as a reference (red open diamonds) and then inserting it inside (green solid triangles). For the sake of clarity, the data acquisitions have been renormalized scaling their mean value to 1, thus highlighting a phase-shift ϕ_0, imparted by the birefringence of BBO, and a reduction in their visibility ν, cause by the dispersion of the medium.

From the measurement, collected with 4 second of acquisition time for all the experimental data, the phase imparted by the crystal results to be $\phi_0 = 0.244$rad modulus 2π, and the visibility is reduced to $\nu = 0.566 \pm 0.012$ due to its dispersion; with this estimation, the experimental value of $\overline{\kappa}$ is thus the one giving $\sigma_\phi(\overline{\kappa}) = -2\log(\nu)$, estimated in $\overline{\kappa} = 0.14 \pm 0.02$. This implies that respect to the broad uncorrelated case (occurring with $\sigma^2 = \delta\omega^2$), the bandwidth the correlation function $G(\omega_p)$ results strongly narrower, causing the relative compression of the FWHM by 8.5 ± 0.7

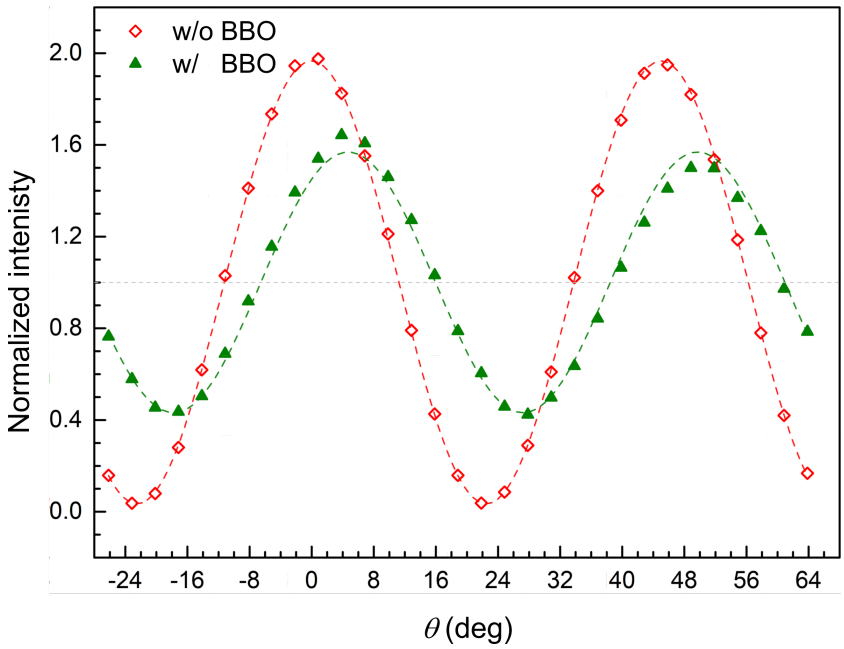

Figure 37: Coincidence rate as a function of the angle θ of the HWP with and without BBO compared to the relative fits with the probability $P(\theta)$ (dashed lines).

dB.

However, such a result does not constitute the actual value of κ, but instead it establishes its lower bound, while we are not able to determine an upper constraint which is taken to be the perfect limit $\kappa = 0$, *i.e.*, infinite compression, usually considered for CW-pumped SPDC; indeed, it is possible to explain such imperfect estimation to all the approximations hypothesized on the modeling as well as the experimental artifacts. The error bar associated to such estimation is performed by considering the uncertainty on the tilt of dispersive crystal respect the light beam path.

6.4 THE ROLE OF CORRELATION FOR PHASE-DEPHASING ESTIMATION

We already observed the quantification of spectral entanglement intensity can be accomplished by treating the system in a purely quantum metrological point of view. Since that such connection between spectral correlation strength and quantum metrology has been identified, one can reverse this relation, trying to establish the impact of frequency entanglement when performing experiments aiming at jointly estimating phase and dephasing in dispersive elements.
For such investigation we consider a two-photon state from PDC,

$$|\Psi_0\rangle = \int d\omega_s d\omega_i f(\omega_s, \omega_i) \hat{a}_D^\dagger(\omega_s) \hat{a}_D^\dagger(\omega_i) |0\rangle, \tag{168}$$

emitting photons at nearly-degenerate frequencies ω_s and ω_i, and with a diagonal polarisation; when this state interacts with a dispersive material which impart a relative phase-shift between horizontal and vertical polarisation $\phi(\omega_j) = h(\omega_j) - v(\omega_j)$, one can describe the evolved state as

$$|\Psi_\phi\rangle = \int d\omega_s d\omega_i f(\omega_s, \omega_i) |\Psi_s\rangle \otimes |\Psi_i\rangle, \tag{169}$$

where

$$|\Psi_j\rangle = \frac{\hat{a}_H^\dagger(\omega_j) + e^{i\phi(\omega_j)} \hat{a}_V^\dagger(\omega_j)}{\sqrt{2}} |0\rangle. \tag{170}$$

Since we choose to perform a detection which is insensitive respect to the frequency, one needs to trace out the spectral part, and only consider the polarisation subspace for the evolved density matrix:

$$\begin{aligned} \rho_\phi =& \mathrm{Tr}\left[|\Psi_\phi\rangle\langle\Psi_\phi|\right] \\ =& \int d\omega_s d\omega_i |f(\omega_s, \omega_i)|^2 \rho_s(\omega_s) \otimes \rho_i(\omega_i), \end{aligned} \tag{171}$$

where we defined,

$$\begin{aligned}\rho_j(\omega_j) =& \frac{|H_j\rangle\langle H_j| + |V_j\rangle\langle V_j| + e^{i\phi(\omega_j)}|H_j\rangle\langle V_j| + e^{-i\phi(\omega_j)}|V_j\rangle\langle H_j|}{2} \\ =& \frac{1}{2}(\mathbb{I} + \cos(\phi(\omega_j)\hat{\sigma}_1) + \sin(\phi(\omega_j)\hat{\sigma}_1)),\end{aligned} \tag{172}$$

introducing the shortcut notations $|H, V_j\rangle = \hat{a}^\dagger_{H,V}(\omega_j)|0\rangle$, and the Pauli operators $\sigma_{1,2}$.
In order to take into account the spectral correlations between the two-photon state, we restrict to spectral wavefunction in the most general expression for correlated photons,

$$|f(\omega_s, \omega_i)|^2 = \frac{1}{\pi\sigma_+\sigma_-} e^{-\omega_-^2/(2\sigma_-^2)} e^{-(\omega_p - \Omega_p)^2/(2\sigma_+^2)}, \tag{173}$$

where $\sigma_\pm = \sigma^2(1 \pm \epsilon)$, with ϵ as a spectral correlation degree such that $-1 \leqslant \epsilon \leqslant 1$. Differently from the previous case, now the correlation strength ϵ become negligible for uncorrelated states, while for $\epsilon = \pm 1$ the photons are perfectly correlated or anti-correlated.

From a Stokes operator projective measurements $\hat{X}_j = 2|D_j\rangle\langle D_j| - \mathbb{I}$ and $\hat{Y}_j = 2|R_j\rangle\langle R_j| - \mathbb{I}$, permitting to compose the relative POVM set Π_k and then to define the probability outcome over the density operator $\rho_{\bar{\phi}}$,

$$p(k|\bar{\phi}) = \mathrm{Tr}[\rho_{\bar{\phi}}\Pi_k], \tag{174}$$

now we have all the requirements for the assessment of Fisher Information matrix,

$$F_{ij} = \sum_k p(k|\bar{\phi}) \left(\frac{\partial \ln p(k|\bar{\phi})}{\partial \varphi_i}\right) \left(\frac{\partial \ln p(k|\bar{\phi})}{\partial \varphi_j}\right) \tag{175}$$

and Quantum Fisher Information matrix,

$$Q_{ij} = \frac{1}{2}\mathrm{Tr}[\rho_{\bar{\phi}} L_i L_j + L_j L_i] \tag{176}$$

where $L_{i,j}$ are the SLD operators introduced in the Chapter 3, with the introduction of the parameter vector $\bar{\phi} = \{\phi_0, \phi_1\}$, in

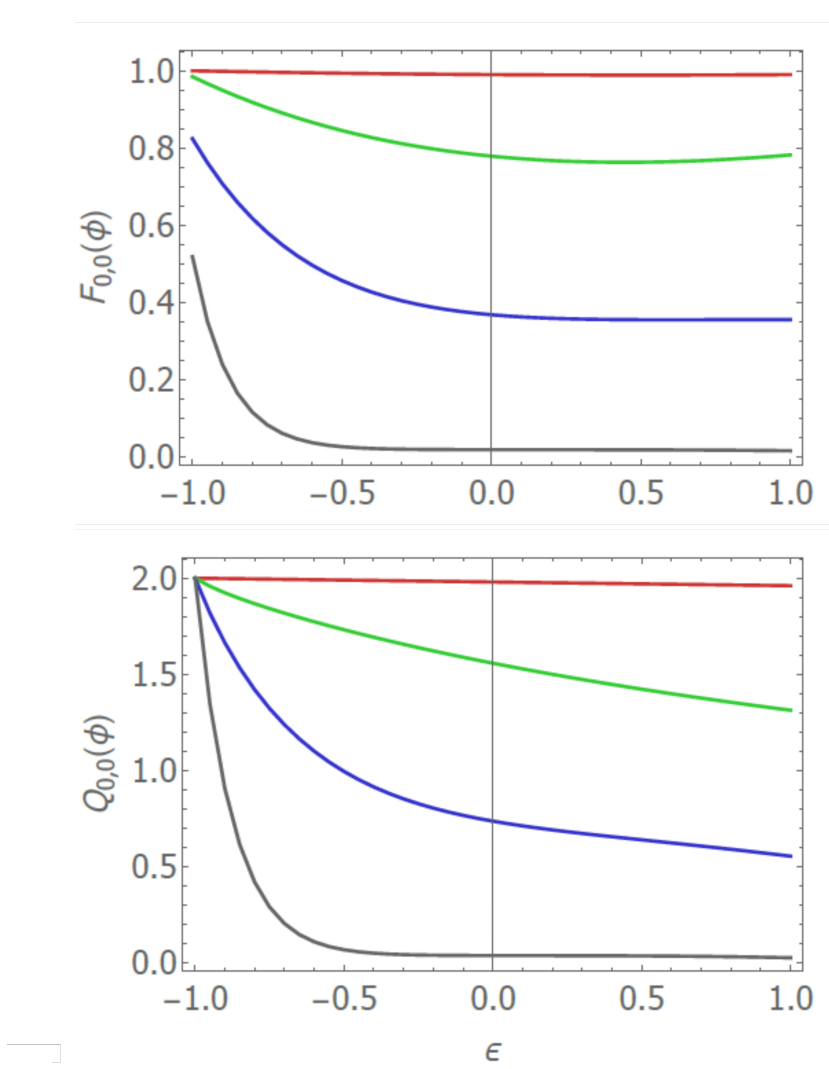

Figure 38: FI and QFI elements F_{00} and Q_{00} on the parameter ϕ_0 as a function on the spectral correlation degree ϵ.

order to estimate the average phase-shift value ϕ_0 and dephasing parameter ϕ_1, which are defined by Taylor expanding the phase-shift $\phi(\omega_j)$ up to the first order,

$$\phi(\omega_j) \approx \phi_0 + \phi_1(\omega_j - \Omega_p/2). \tag{177}$$

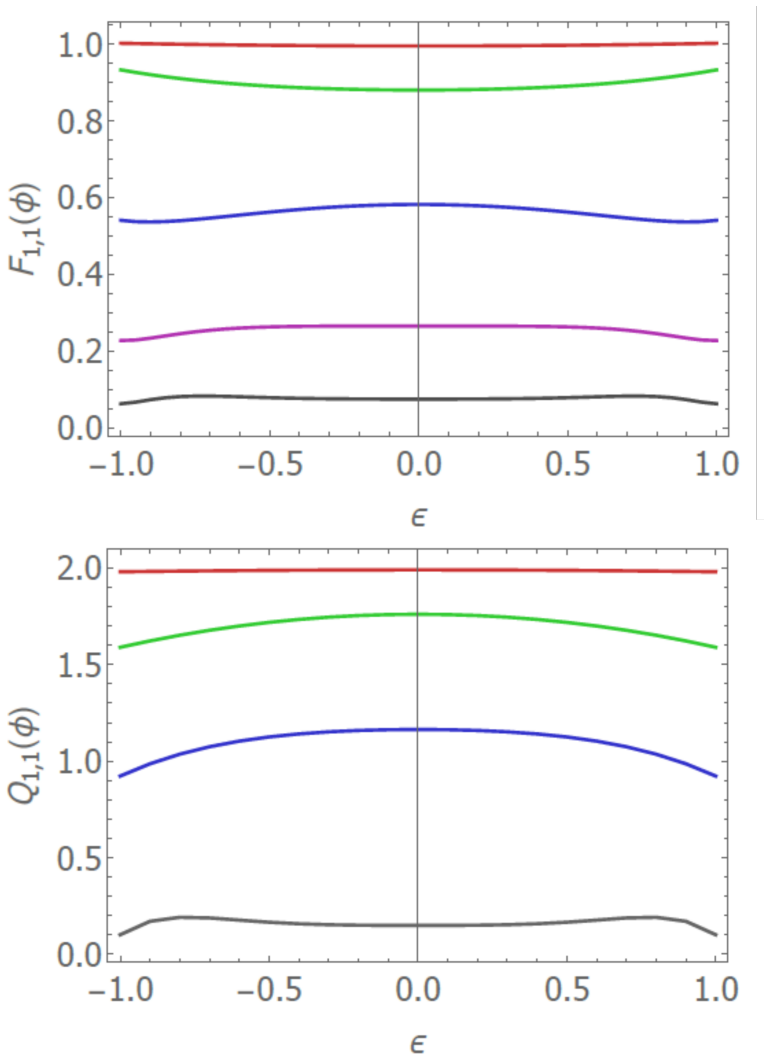

Figure 39: FI and QFI elements F_{11} and Q_{11} on the parameter ϕ_1 as a function on the spectral correlation degree ϵ.

In Fig. 38 it is sketched the analytical investigation of the FI (F_{00}) and QFI (Q_{00}) associated to the ϕ_0 parameter as a function of ϵ, restricting to the case of $\sigma^2 = 1$ and $\phi_0 = n\pi/4$ ($n \in \mathbb{Z}$) which allows us to neglect the off-diagonal elements of such matrices, and for four different values of dephasing ($\phi_1 = \{0.1, 0.5, 1, 2\}$ from top to the bottom); the contributions of both information matrices

respect on the ϕ_1 parameter (F_{11} and Q_{11}) are then reported in Fig. 39.

From the graphs it is possible to observe, especially for the main shift parameter, the strong dependence of the FI and QFI matrices that suggests us to use anti-correlated photons ($\epsilon < 0$) in order to find the highest amount of ϕ_0-information, which coincides with the dispersion cancellation conjectures described above, while for no correlation or for positive correlation F_{00} and Q_{00} collapse significantly to zero; furthermore, the dephasing information functions F_{11} and Q_{11} seem to be less sensitive to the presence of spectral correlation, even if they exhibit a symmetrical behavior with a ridge on ϵ for low values of dephasing. However, very interesting considerations could be made by observing the graph of the trade-off function Υ in Fig. 40 whose expression has been mentioned in Eq.76.

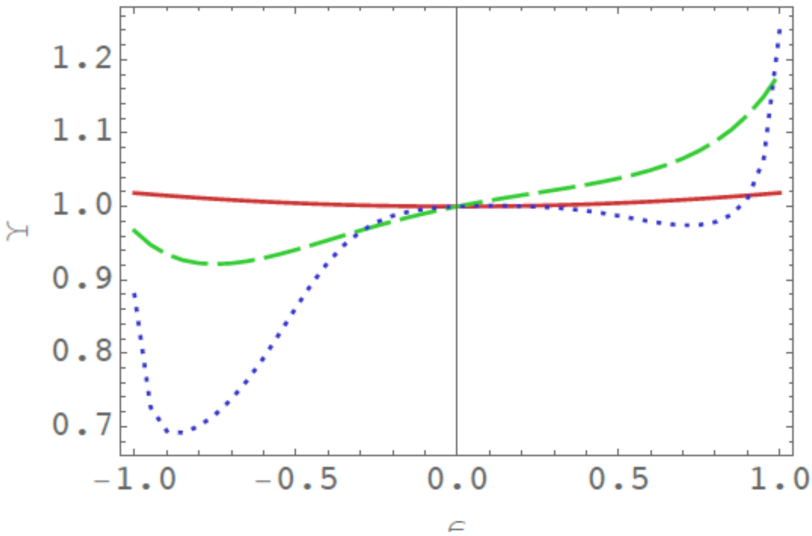

Figure 40: Trade-off function Υ as a function on the spectral correlation degree ϵ for different values of dephasing: red-solid line, $\phi_1 = 0.1$; green-dashed line, $\phi_1 = 1$; blue-dotted line, $\phi_1 = 2$.

From the graph, we observe a very different behavior compared to the singular contributions of FI and QFI functions; here we

notice that as the amount of spectral degree increase, also it is possible to extrapolate from the system, with the chosen POVM measurement, even more information for phase and dephasing estimation, moving more closely to the saturation of the Quantum Cramer-Rao bound. Differently from the previous plots, which suggest that the more informative state can be reached using anti-correlated photons, in this regime we are far from saturating the QCRB, highlighting again the big difference between the FI and QFI matrices and the Υ.

CONCLUSIONS AND OUTLOOK

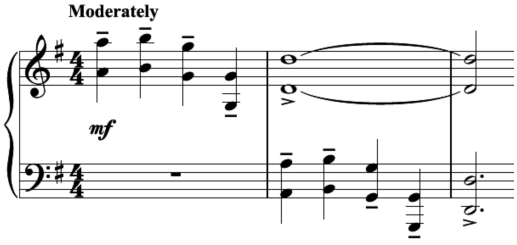

— Theme of close encounters of the third kind, J. Williams

Since single photons constitute the fundamental engine of quantum photonics platforms, the complete characterisation and control of their generation is a matter of interest that will open new paths in the quantum technology era. As witnessed in last decade, such interest has not only provided methods to inspect the characterics of a photon source, but it has also helped establish a novel way of encoding information with photons, *i.e.* the spectral/temporal degree of freedom.

In this thesis we faced this necessity, first exploring the most utilised methods which exploit spectrally resolving devices, such as spectrometers, looking at the spectral wave-function profile, with the JSI analysis, establishing the spectral correlation strength, by calculating the auto-correlation function $g^{(2)}(\tau)$. These strategies offer a truly complete approach to the investigation of the spectral behavior of the photon pair, but may suffer from the difficulties of detecting spectral correlations over much smaller scales than the typical spectral resolution, of the order of nanometers.

In this thesis we found a different approach to this issue, exploring the fundamentals of *metrology* and *quantum metrology*. This *modus operandi*, which aims at finding the optimal way exploiting measured resources, makes quantum metrology a useful starting

point that fits the needs of spectral correlation assessment. The necessary extention respect to standard metrology is to include noise in a multi parameter approach; an experimental exploration of this quantum multi parameter estimation constitutes the core of this thesis.
The multi parameter approach has been investigated with two experiments: in the first one we observed the estimation enhancement of a collective measurement strategy compared to the individual one. In the second one we studied a noisy measurement apparatus, whose efficiency changes while testing the chirality of some sugar solutions.
The link between the assessment of spectral correlation and quantum metrology methods involves the exploration of the dispersion cancellation effect, that discriminates against uncorrelation and correlation photon-pair states by a dephasing measurements on a dispersive sample, giving a bound on the spectral entanglement strength of the two-photon probe.

Such *close encounter* may start the development of future works connected to a more extensive use of quantum metrology on spectral based architectures in quantum communication and information. Indeed, despite this novel encoding of quantum information constitutes a very innovative approach for the future of quantum technologies, however it requires a variety of instrumental methods in order to constantly control all the experimental steps. In this scenario, quantum metrology seems to comply with part of this request, and, by monitoring the measurement process, could go beyond current physical impediments.

Part I

APPENDIX

A

EVOLUTION OF THE TWO-PHOTON STATE UNDER PHASE ROTATION

The aim of this section is to obtain the detection probabilities from a two-photon N00N state with limited visibility, following a phase shift ϕ. The combination of a beam splitter (BS), a phase shift ϕ, and a second BS can be modelled as an unbalanced BS with transmission $\cos(\phi/2)$. Since we use the polarization degree of freedom of a single spatial mode, the phase shift can be implemented as a polarization rotation by means of a half wave plate (HWP), as in the calibration phase, or of an optically active solution. The mode mixing performs the transformation:

$$\begin{aligned} \hat{a}_H^\dagger &\to \cos(\phi/2)\hat{a}_H^\dagger + \sin(\phi/2)\hat{a}_V^\dagger, \\ \hat{a}_V^\dagger &\to \cos(\phi/2)\hat{a}_V^\dagger - \sin(\phi/2)\hat{a}_H^\dagger. \end{aligned} \tag{178}$$

The first step considers perfectly indistinguishable photons in the two-photon state $|\Psi_0\rangle_{in} = \hat{a}_H^\dagger \hat{a}_V^\dagger |0\rangle$, which evolve following the phase shift:

$$\begin{aligned} |\Psi_\phi\rangle_{in} &= \left[\cos\left(\frac{\phi}{2}\right)\hat{a}_H^\dagger + \sin\left(\frac{\phi}{2}\right)\hat{a}_V^\dagger\right]\left[\cos\left(\frac{\phi}{2}\right)\hat{a}_V^\dagger - \sin\left(\frac{\phi}{2}\right)\hat{a}_H^\dagger\right]|0\rangle \\ &= \left[\cos(\phi)\hat{a}_H^\dagger\hat{a}_V^\dagger - \sin(\phi)\frac{(\hat{a}_H^{\dagger 2} - \hat{a}_V^{\dagger 2})}{2}\right]|0\rangle. \end{aligned} \tag{179}$$

An HWP is then inserted, and set at an angle θ with respect to the horizontal; its effect on the two-photon state delivers the expression

$$|\Psi_{\theta;\phi}\rangle_{in} = \cos(\phi)\left[-\cos(4\theta)\hat{a}_H^\dagger\hat{a}_V^\dagger + \frac{1}{2}\sin(4\theta)(\hat{a}_H^{\dagger 2} - \hat{a}_V^{\dagger 2})\right]|0\rangle + \\ -\sin(\phi)\left[\sin(4\theta)\hat{a}_H^\dagger\hat{a}_V^\dagger + \frac{1}{2}\cos(4\theta)(\hat{a}_H^{\dagger 2} - \hat{a}_V^{\dagger 2})\right]|0\rangle, \tag{180}$$

from which the following probabilities can be obtained:

$$\begin{aligned} p^{in}(1|\theta;\phi) &= \frac{1}{2}(1+\cos(8\theta-2\phi)), \\ p^{in}(2|\theta;\phi) &= \frac{1}{2}\sin^2(4\theta-\phi), \end{aligned} \tag{181}$$

where we separate the contributions that occur from the probability of photon coincidence, having the state expression $|1_H\rangle|1_V\rangle$, with $p^{in}(1|\theta;\phi)$, and the one of finding two photons on the same arm, $(|2_H\rangle|0_V\rangle - |0_H\rangle|2_V\rangle)\sqrt{2}$, with $p^{in}(2|\theta;\phi)$.
Using the same approach, it is possible to calculate the evolution of quantum state $|\Psi_0\rangle_{dis} = \hat{a}_H^\dagger\hat{b}_V^\dagger|0\rangle$ for two distinguishable photons: here we also need considering two extra modes a_V and b_H, initially in the vacuum state, to define transformations similar to the ones in Eq.178. These then give an expression for the state as:

$$\begin{aligned} |\Psi_\phi\rangle_{dis} &= \left[\cos\left(\frac{\phi}{2}\right)\hat{a}_H^\dagger + \sin\left(\frac{\phi}{2}\right)\hat{a}_V^\dagger\right]\left[\cos\left(\frac{\phi}{2}\right)\hat{b}_V^\dagger - \sin\left(\frac{\phi}{2}\right)\hat{b}_H^\dagger\right]|0\rangle \\ &= \left[\cos\left(\frac{\phi}{2}\right)^2\hat{a}_H^\dagger\hat{b}_V^\dagger - \sin\left(\frac{\phi}{2}\right)^2\hat{a}_V^\dagger\hat{b}_H^\dagger - \sin(\phi)\frac{(\hat{a}_H^\dagger\hat{b}_H^\dagger - \hat{a}_V^\dagger\hat{b}_V^\dagger)}{2}\right]|0\rangle. \end{aligned} \tag{182}$$

and then, including the HWP, the probabilities for the distinguishable case reads,

$$\begin{aligned} p^{dis}(1|\theta;\phi) &= \frac{1}{4}(3+\cos(8\theta-2\phi)) \\ p^{dis}(2|\theta;\phi) &= \frac{1}{4}\sin^2(4\theta-\phi). \end{aligned} \tag{183}$$

These have been obtained considering detectors unable to distinguish between the modes $\hat{a}^\dagger$ and $\hat{b}^\dagger$.
In the general case, the initial mode $\hat{b}_V^\dagger$ could possess a component mode $\hat{a}_V^\dagger$, which is indistinguishable from $\hat{a}_H^\dagger$ in all other degrees of freedom, and a distinguishable component $\hat{q}_V^\dagger$; so that, such mode can be written as,

$$\hat{b}_V^\dagger = \sqrt{1-\epsilon^2}\hat{a}_V^\dagger + \epsilon\hat{q}_V^\dagger, \tag{184}$$

with ϵ as a degree of distinguishability.
As before, we need to introduce extra vacuum modes; the combined probabilities considering the degree of distinguishability will be given by the weighted sums:

$$\begin{aligned} p(1|\theta;\phi,\epsilon) &= \frac{1-\epsilon^2}{2}(1+\cos(8\theta-2\phi)) + \frac{\epsilon^2}{4}(3+\cos(8\theta-2\phi)) \\ p(2|\theta;\phi,\epsilon) &= \frac{1-\epsilon^2}{2}\sin^2(4\theta-\phi) + \frac{\epsilon^2}{4}\sin^2(4\theta-\phi). \end{aligned} \tag{185}$$

These expressions can be cast in more compact form by introducing a visibility parameter ν of the predicted fringes as $\nu = (2-\epsilon^2)/(2+\epsilon^2)$:

$$\begin{aligned} p(1|\theta;\phi,\nu) &= \frac{1}{1+\nu}(1+\nu\cos(8\theta-2\phi)) \\ p(2|\theta;\phi,\nu) &= \frac{\nu}{1+\nu}\sin^2(4\theta-\phi) \end{aligned} \tag{186}$$

B

TWO-PHOTON STATE EVOLUTION FOR DEGREE OF CORRELATION ESTIMATION

Considering the quantum state of the photon couple generated by parametric down conversion source,

$$|\Psi\rangle = \int d\omega_s d\omega_i f(\omega_s, \omega_i) \hat{a}_H^\dagger(\omega_s) \hat{a}_V^\dagger(\omega_i) |0\rangle, \tag{187}$$

where $f(\omega_s, \omega_i)$ is the spectral function of the photon pair. Introducing a half wave plate (HWP) and a dispersive material inducing a rotation θ and a phase $\phi(\omega)$ to the state respectively, $|\Psi\rangle$ evolves

$$|\Psi\rangle \to \int d\omega_s d\omega_i f(\omega_s, \omega_i) \left[\cos\left(2\theta + \frac{\phi(\omega_s)}{2}\right) \hat{a}_H^\dagger(\omega_s) + \sin\left(2\theta + \frac{\phi(\omega_s)}{2}\right) \hat{a}_V^\dagger(\omega_s) \right] \times \\ \times \left[-\sin\left(2\theta + \frac{\phi(\omega_i)}{2}\right) \hat{a}_H^\dagger(\omega_i) + \sin\left(2\theta + \frac{\phi(\omega_i)}{2}\right) \hat{a}_V^\dagger(\omega_i) \right] |0\rangle. \tag{188}$$

Considering the propagation of the photons to the detector 1 at time t_1 and to the detector 2 at time t_2 ,

$$\int d\omega_s d\omega_i f(\omega_s, \omega_i) \left[\varphi_S(\omega_s, \omega_i) e^{i\omega_s t_s + i\omega_i t_i} - \varphi_C(\omega_s, \omega_i) e^{i\omega_s t_i + i\omega_i t_s} \right] \\ = \tilde{\varphi}_S(t_s, t_i) - \tilde{\varphi}_C(t_i, t_s) = A(t_s, t_i), \tag{189}$$

where

$$\varphi_S(\omega_s,\omega_i) = g(\omega_s)g(\omega_i)\cos\left(2\theta+\frac{\phi(\omega_s)}{2}\right)\cos\left(2\theta+\frac{\phi(\omega_i)}{2}\right)$$
$$\varphi_C(\omega_s,\omega_i) = g(\omega_s)g(\omega_i)\sin\left(2\theta+\frac{\phi(\omega_i)}{2}\right)\sin\left(2\theta+\frac{\phi(\omega_s)}{2}\right). \tag{190}$$

The solution of the FT state in Eq.189 can be found as

$$\int dt_s dt_i |A(t_s,t_i)|^2 = \int dt_s dt_i |\tilde{\varphi}_S(t_s,t_i)|^2 + \int dt_s dt_i |\tilde{\varphi}_C(t_i,t_s)|^2 - \\ -2\mathrm{Re}\int dt_s dt_i \tilde{\varphi}_S^*(t_s,t_i)\tilde{\varphi}_C(t_i,t_s) \tag{191}$$

Using the Parseval theorem, we solve the integral on the frequency space

$$\int d\omega_s d\omega_i |g(\omega_s)|^2|g(\omega_i)|^2|f(\omega_s,\omega_i)|^2\cos^2\left(2\theta+\frac{\phi(\omega_s)}{2}\right)\cos^2\left(2\theta+\frac{\phi(\omega_i)}{2}\right) \\ + \int d\omega_s d\omega_i |g(\omega_i)|^2|g(\omega_s)|^2|f(\omega_i,\omega_s)|^2\sin^2\left(2\theta+\frac{\phi(\omega_s)}{2}\right)\sin^2\left(2\theta+\frac{\phi(\omega_i)}{2}\right) \\ -2\mathrm{Re}\int dt_s dt_i \tilde{\varphi}_S^*(t_s,t_i)\tilde{\varphi}_C(t_i,t_s) \tag{192}$$

Defining $\theta_s \equiv 2\theta + \phi(\omega_s)/2$ and $\theta_i \equiv 2\theta + \phi(\omega_i)/2$ we can utilise the relations:

$$\cos^2\theta_s\cos^2\theta_i + \sin^2\theta_s\sin^2\theta_i = \frac{1}{2}\left(\cos^2(\theta_s-\theta_i)+\cos^2(\theta_s+\theta_i)\right). \tag{193}$$

Expanding the third integral of the Eq.192,

$$\int dt_s dt_i \tilde{\varphi}_S^*(t_s,t_i)\tilde{\varphi}_C(t_i,t_s) = \int d\omega_s d\omega_i d\nu_s d\nu_i e^{-i\omega_s t_s - i\omega_i t_i} e^{i\nu_s t_i + i\nu_i t_s} \times \\ \times\, g(\omega_s)g(\omega_i)f^*(\omega_s,\omega_i)\cos\theta_s\cos\theta_i f(\nu_s)f(\nu_i)f(\nu_s,\nu_i)\sin\theta_s\sin\theta_i = \\ = \frac{1}{4}\int d\omega_s d\omega_i |g(\omega_s)|^2|g(\omega_i)|^2 f^*(\omega_s,\omega_i)f(\omega_i,\omega_s)\sin(2\theta_s)\sin(2\theta_i) \tag{194}$$

So, the probability of the system is

$$P(\theta) = \int d\omega_s d\omega_i |g(\omega_s)|^2 |g(\omega_i)|^2 |f(\omega_s, \omega_i)|^2 \frac{1}{2}\big(\cos^2(\theta_s - \theta_i) + \cos^2(\theta_s + \theta_i)\big) + \\ - \frac{1}{2} \mathrm{Re} \int d\omega_s d\omega_i |g(\omega_s)|^2 |g(\omega_i)|^2 f^*(\omega_s, \omega_i) f(\omega_i, \omega_s) \sin(2\theta_s) \sin(2\theta_i). \tag{195}$$

Neglecting the dispersion of the source with the phase-matching condition, $f^*(\omega_s, \omega_i) = f(\omega_s, \omega_i) = f(\omega_i, \omega_s)$, the Eq.195 become,

$$P(\theta) = \frac{1}{2} \int d\omega_s d\omega_i |g(\omega_s)|^2 |g(\omega_i)|^2 |f(\omega_s, \omega_i)|^2 \times \\ \times \big[\cos^2(\theta_s - \theta_i) + \cos^2(\theta_s + \theta_i) - \sin(2\theta_s)\sin(2\theta_i)\big] = \frac{1}{2}\big(1 + \cos(\gamma)\big), \tag{196}$$

Introducing the efficiency of the NooN apparatus ν,

$$P(\theta) = \frac{1}{2}\big(1 + e^{-\sigma^2/2}\cos(\gamma)\big), \tag{197}$$

where $\sigma^2 = -2\log(\nu)$ and $\gamma = 8\theta + 2\phi(\Omega_p/2)$.

BIBLIOGRAPHY

[1] Max Planck. "Ueber irreversible Strahlungsvorgänge." In: *Annalen der Physik* 306.1 (1900), pp. 69–122. DOI: 10.1002/andp.19003060105. URL: https://doi.org/10.1002/andp.19003060105.

[2] Bruce R. Wheaton. "Philipp Lenard and the Photoelectric Effect, 1889-1911." In: *Historical Studies in the Physical Sciences* 9 (Jan. 1978), pp. 299–322. DOI: 10.2307/27757381. URL: https://doi.org/10.2307/27757381.

[3] A. Einstein. "Über einen die Erzeugung und Verwandlung des Lichtes betreffenden heuristischen Gesichtspunkt." In: *Annalen der Physik* 322.6 (1905), pp. 132–148. DOI: 10.1002/andp.19053220607. URL: https://doi.org/10.1002/andp.19053220607.

[4] P. A. M. Dirac. "The Quantum Theory of the Emission and Absorption of Radiation." In: *Proceedings of the Royal Society A: Mathematical, Physical and Engineering Sciences* 114.767 (Mar. 1927), pp. 243–265. DOI: 10.1098/rspa.1927.0039. URL: https://doi.org/10.1098/rspa.1927.0039.

[5] R. HANBURY BROWN and R. Q. TWISS. "A Test of a New Type of Stellar Interferometer on Sirius." In: *Nature* 178.4541 (Nov. 1956), pp. 1046–1048. DOI: 10.1038/1781046a0. URL: https://doi.org/10.1038/1781046a0.

[6] T. H. MAIMAN. "Stimulated Optical Radiation in Ruby." In: *Nature* 187.4736 (Aug. 1960), pp. 493–494. DOI: 10.1038/187493a0. URL: https://doi.org/10.1038/187493a0.

[7] John F. Clauser. "Experimental distinction between the quantum and classical field-theoretic predictions for the photoelectric effect." In: *Physical Review D* 9.4 (Feb. 1974), pp. 853–860. DOI: 10.1103/physrevd.9.853. URL: https://doi.org/10.1103/physrevd.9.853.

[8] C. K. Hong, Z. Y. Ou, and L. Mandel. "Measurement of subpicosecond time intervals between two photons by interference." In: *Physical Review Letters* 59.18 (Nov. 1987), pp. 2044–2046. DOI: 10.1103/physrevlett.59.2044. URL: https://doi.org/10.1103/physrevlett.59.2044.

[9] P Grangier, G Roger, and A Aspect. "Experimental Evidence for a Photon Anticorrelation Effect on a Beam Splitter: A New Light on Single-Photon Interferences." In: *Europhysics Letters (EPL)* 1.4 (Feb. 1986), pp. 173–179. DOI: 10.1209/0295-5075/1/4/004. URL: https://doi.org/10.1209/0295-5075/1/4/004.

[10] Oliver Benson et al. "Regulated and Entangled Photons from a Single Quantum Dot." In: *Physical Review Letters* 84.11 (Mar. 2000), pp. 2513–2516. DOI: 10.1103/physrevlett.84.2513. URL: https://doi.org/10.1103/physrevlett.84.2513.

[11] M. Müller et al. "On-demand generation of indistinguishable polarization-entangled photon pairs." In: *Nature Photonics* 8.3 (Feb. 2014), pp. 224–228. DOI: 10.1038/nphoton.2013.377. URL: https://doi.org/10.1038/nphoton.2013.377.

[12] Daniel Huber et al. "Strain-Tunable GaAs Quantum Dot: A Nearly Dephasing-Free Source of Entangled Photon Pairs on Demand." In: *Physical Review Letters* 121.3 (July 2018). DOI: 10.1103/physrevlett.121.033902. URL: https://doi.org/10.1103/physrevlett.121.033902.

[13] B. F. Polkovnikov. "Parametric and polariton scattering in noncentrosymmetric crystals." In: *Journal of Soviet Laser Research* 13.5 (1992), pp. 323–353. DOI: 10.1007/bf01124888. URL: https://doi.org/10.1007/bf01124888.

[14] David C. Burnham and Donald L. Weinberg. "Observation of Simultaneity in Parametric Production of Optical Photon Pairs." In: *Physical Review Letters* 25.2 (July 1970), pp. 84–87. DOI: 10.1103/physrevlett.25.84. URL: https://doi.org/10.1103/physrevlett.25.84.

[15] Xiongfeng Ma, Chi-Hang Fred Fung, and Hoi-Kwong Lo. "Quantum key distribution with entangled photon sources." In: *Physical Review A* 76.1 (July 2007). DOI: 10.1103/physreva.76.012307. URL: https://doi.org/10.1103/physreva.76.012307.

[16] D Achilles, E Rogacheva, and A Trifonov. "Fast quantum key distribution with decoy number states." In: *Journal of Modern Optics* 55.3 (Feb. 2008), pp. 361–373. DOI: 10.1080/09500340701441293. URL: https://doi.org/10.1080/09500340701441293.

[17] Valerio Scarani et al. "Quantum Cryptography Protocols Robust against Photon Number Splitting Attacks for Weak Laser Pulse Implementations." In: *Physical Review Letters* 92.5 (Feb. 2004). DOI: 10.1103/physrevlett.92.057901. URL: https://doi.org/10.1103/physrevlett.92.057901.

[18] Antonio Acin, Nicolas Gisin, and Valerio Scarani. "Coherent-pulse implementations of quantum cryptography protocols resistant to photon-number-splitting attacks." In: *Physical Review A* 69.1 (Jan. 2004). DOI: 10.1103/physreva.69.012309. URL: https://doi.org/10.1103/physreva.69.012309.

[19] Hoi-Kwong Lo, Xiongfeng Ma, and Kai Chen. "Decoy State Quantum Key Distribution." In: *Physical Review Letters* 94.23 (June 2005). DOI: 10.1103/physrevlett.94.230504. URL: https://doi.org/10.1103/physrevlett.94.230504.

[20] Marco Barbieri et al. "What Hong-Ou-Mandel interference says on two-photon frequency entanglement." In: *Scientific Reports* 7.1 (Aug. 2017). DOI: 10.1038/s41598-017-07555-4. URL: https://doi.org/10.1038/s41598-017-07555-4.

[21] Ilaria Gianani et al. "Hong–Ou–Mandel control through spectral shaping." In: *Journal of Optics* 20.8 (July 2018), p. 085201. DOI: 10.1088/2040-8986/aad01a. URL: https://doi.org/10.1088/2040-8986/aad01a.

[22] T. Gerrits et al. "Spectral correlation measurements at the Hong-Ou-Mandel interference dip." In: *Physical Review A* 91.1 (Jan. 2015). DOI: 10.1103/physreva.91.013830. URL: https://doi.org/10.1103/physreva.91.013830.

[23] Thomas Gerrits et al. "Generation of degenerate, factorizable, pulsed squeezed light at telecom wavelengths." In: *Optics Express* 19.24 (Nov. 2011), p. 24434. DOI: 10.1364/oe.19.024434. URL: https://doi.org/10.1364/oe.19.024434.

[24] N. Bruno et al. "Pulsed source of spectrally uncorrelated and indistinguishable photons at telecom wavelengths." In: *Optics Express* 22.14 (July 2014), p. 17246. DOI: 10.1364/oe.22.017246. URL: https://doi.org/10.1364/oe.22.017246.

[25] Barak Dayan et al. "Spectral polarization and spectral phase control of time-energy entangled photons." In: *Physical Review A* 75.4 (Apr. 2007). DOI: 10.1103/physreva.75.043804. URL: https://doi.org/10.1103/physreva.75.043804.

[26] Rodney Loudon and Thomas von Foerster. "The Quantum Theory of Light." In: *American Journal of Physics* 42.11 (Nov. 1974), pp. 1041–1042. DOI: 10.1119/1.1987930. URL: https://doi.org/10.1119/1.1987930.

[27] Richard P. Feynman. "Simulating physics with computers." In: *International Journal of Theoretical Physics* 21.6-7 (June 1982), pp. 467–488. DOI: 10.1007/bf02650179. URL: https://doi.org/10.1007/bf02650179.

[28] P.W. Shor. "Algorithms for quantum computation: discrete logarithms and factoring." In: *Proceedings 35th Annual Symposium on Foundations of Computer Science*. IEEE Comput. Soc. Press. DOI: 10.1109/sfcs.1994.365700. URL: https://doi.org/10.1109/sfcs.1994.365700.

[29] Peter W. Shor. "Polynomial-Time Algorithms for Prime Factorization and Discrete Logarithms on a Quantum Computer." In: *SIAM Journal on Computing* 26.5 (Oct. 1997), pp. 1484–1509. DOI: 10.1137/s0097539795293172. URL: https://doi.org/10.1137/s0097539795293172.

[30] Lov K. Grover. "A Fast Quantum Mechanical Algorithm for Database Search." In: *ANNUAL ACM SYMPOSIUM ON THEORY OF COMPUTING*. ACM, 1996, pp. 212–219.

[31] Michael A. Nielsen and Isaac L. Chuang. "Introduction to the Tenth Anniversary Edition." In: *Quantum Computation and Quantum Information*. Cambridge University Press, pp. xvii–xviii. DOI: 10.1017/cbo9780511976667.001. URL: https://doi.org/10.1017/cbo9780511976667.001.

[32] R. Simon. "Peres-Horodecki Separability Criterion for Continuous Variable Systems." In: *Physical Review Letters* 84.12 (Mar. 2000), pp. 2726–2729. DOI: 10.1103/physrevlett.84.2726. URL: https://doi.org/10.1103/physrevlett.84.2726.

[33] M. PLANCK. "On the Theory of the Energy Distribution Law of the Normal Spectrum." In: *The Old Quantum Theory*. Elsevier, 1967, pp. 82–90. DOI: 10.1016/b978-0-08-012102-4.50013-9. URL: https://doi.org/10.1016/b978-0-08-012102-4.50013-9.

[34] B. Lounis and W. E. Moerner. "Single photons on demand from a single molecule at room temperature." In: *Nature* 407.6803 (Sept. 2000), pp. 491–493. DOI: 10.1038/35035032. URL: https://doi.org/10.1038/35035032.

[35] M Hennrich et al. "Photon statistics of a non-stationary periodically driven single-photon source." In: *New Journal of Physics* 6 (July 2004), pp. 86–86. DOI: 10.1088/1367-2630/6/1/086. URL: https://doi.org/10.1088/1367-2630/6/1/086.

[36] Axel Kuhn, Markus Hennrich, and Gerhard Rempe. "Deterministic Single-Photon Source for Distributed Quantum Networking." In: *Physical Review Letters* 89.6 (July 2002). DOI: 10.1103/physrevlett.89.067901. URL: https://doi.org/10.1103/physrevlett.89.067901.

[37] J. McKeever. "Deterministic Generation of Single Photons from One Atom Trapped in a Cavity." In: *Science* 303.5666 (Mar. 2004), pp. 1992–1994. DOI: 10.1126/science.1095232. URL: https://doi.org/10.1126/science.1095232.

[38] Mathias Steiner et al. "Highly efficient, tunable single photon source based on single molecules." In: *Applied Physics Letters* 90.18 (Apr. 2007), p. 183122. DOI: 10.1063/1.2736294. URL: https://doi.org/10.1063/1.2736294.

[39] J. Kim et al. "A single-photon turnstile device." In: *Nature* 397.6719 (Feb. 1999), pp. 500–503. DOI: 10.1038/17295. URL: https://doi.org/10.1038/17295.

[40] F. De Martini, G. Di Giuseppe, and M. Marrocco. "Single-Mode Generation of Quantum Photon States by Excited Single Molecules in a Microcavity Trap." In: *Physical Review Letters* 76.6 (Feb. 1996), pp. 900–903. DOI: 10.1103/physrevlett.76.900. URL: https://doi.org/10.1103/physrevlett.76.900.

[41] Christian Brunel et al. "Triggered Source of Single Photons based on Controlled Single Molecule Fluorescence." In: *Physical Review Letters* 83.14 (Oct. 1999), pp. 2722–2725. DOI: 10.1103/physrevlett.83.2722. URL: https://doi.org/10.1103/physrevlett.83.2722.

[42] Christian Maurer et al. "A single-photon source based on a single Ca+ ion." In: *New Journal of Physics* 6 (July 2004), pp. 94–94. DOI: 10.1088/1367-2630/6/1/094. URL: https://doi.org/10.1088/1367-2630/6/1/094.

[43] B. B. Blinov et al. "Observation of entanglement between a single trapped atom and a single photon." In: *Nature* 428.6979 (Mar. 2004), pp. 153–157. DOI: 10.1038/nature02377. URL: https://doi.org/10.1038/nature02377.

[44] Matthias Keller et al. "Continuous generation of single photons with controlled waveform in an ion-trap cavity system." In: *Nature* 431.7012 (Oct. 2004), pp. 1075–1078. DOI: 10.1038/nature02961. URL: https://doi.org/10.1038/nature02961.

[45] Satoshi Kako et al. "A gallium nitride single-photon source operating at 200 K." In: *Nature Materials* 5.11 (Oct. 2006), pp. 887–892. DOI: 10.1038/nmat1763. URL: https://doi.org/10.1038/nmat1763.

[46] Andrew J. Shields. "Semiconductor quantum light sources." In: *Nature Photonics* 1.4 (Apr. 2007), pp. 215–223. DOI: 10.1038/nphoton.2007.46. URL: https://doi.org/10.1038/nphoton.2007.46.

[47] Stefan Strauf et al. "High-frequency single-photon source with polarization control." In: *Nature Photonics* 1.12 (Nov. 2007), pp. 704–708. DOI: 10.1038/nphoton.2007.227. URL: https://doi.org/10.1038/nphoton.2007.227.

[48] T Gaebel et al. "Stable single-photon source in the near infrared." In: *New Journal of Physics* 6 (July 2004), pp. 98–98. DOI: 10.1088/1367-2630/6/1/098. URL: https://doi.org/10.1088/1367-2630/6/1/098.

[49] E Wu et al. "Room temperature triggered single-photon source in the near infrared." In: *New Journal of Physics* 9.12 (Dec. 2007), pp. 434–434. DOI: 10.1088/1367-2630/9/12/434. URL: https://doi.org/10.1088/1367-2630/9/12/434.

[50] Stuart J. Freedman and John F. Clauser. "Experimental Test of Local Hidden-Variable Theories." In: *Physical Review Letters* 28.14 (Apr. 1972), pp. 938–941. DOI: 10.1103/physrevlett.28.938. URL: https://doi.org/10.1103/physrevlett.28.938.

[51] Alain Aspect, Philippe Grangier, and Gérard Roger. "Experimental Tests of Realistic Local Theories via Bell's Theorem." In: *Physical Review Letters* 47.7 (Aug. 1981), pp. 460–463. DOI: 10.1103/physrevlett.47.460. URL: https://doi.org/10.1103/physrevlett.47.460.

[52] S. Friberg, C. K. Hong, and L. Mandel. "Measurement of Time Delays in the Parametric Production of Photon Pairs." In: *Physical Review Letters* 54.18 (May 1985), pp. 2011–2013. DOI: 10.1103/physrevlett.54.2011. URL: https://doi.org/10.1103/physrevlett.54.2011.

[53] Robert W. Boyd and Barry R. Masters. "Nonlinear Optics, Third Edition." In: *Journal of Biomedical Optics* 14.2 (2009), p. 029902. DOI: 10.1117/1.3115345. URL: https://doi.org/10.1117/1.3115345.

[54] Harishankar Jayakumar et al. "Deterministic Photon Pairs and Coherent Optical Control of a Single Quantum Dot." In: *Physical Review Letters* 110.13 (Mar. 2013). DOI: 10.1103/physrevlett.110.135505. URL: https://doi.org/10.1103/physrevlett.110.135505.

[55] Simona Checcucci et al. "Beaming light from a quantum emitter with a planar optical antenna." In: *Light: Science & Applications* 6.4 (Dec. 2016), e16245–e16245. DOI: 10.1038/lsa.2016.245. URL: https://doi.org/10.1038/lsa.2016.245.

[56] Peter J. Mosley et al. "Direct Measurement of the Spatial-Spectral Structure of Waveguided Parametric Down-Conversion." In: *Physical Review Letters* 103.23 (Dec. 2009). DOI: 10.1103/physrevlett.103.233901. URL: https://doi.org/10.1103/physrevlett.103.233901.

[57] Andreas Christ et al. "Probing multimode squeezing with correlation functions." In: *New Journal of Physics* 13.3 (Mar. 2011), p. 033027. DOI: 10.1088/1367-2630/13/3/033027. URL: https://doi.org/10.1088/1367-2630/13/3/033027.

[58] O A Ivanova et al. "Multiphoton correlations in parametric down-conversion and their measurement in the pulsed regime." In: *Quantum Electronics* 36.10 (Oct. 2006), pp. 951–956. DOI: 10.1070/qe2006v036n10abeh013300. URL: https://doi.org/10.1070/qe2006v036n10abeh013300.

[59] Jeremie Fulconis et al. "Nonclassical Interference and Entanglement Generation Using a Photonic Crystal Fiber Pair Photon Source." In: *Physical Review Letters* 99.12 (Sept. 2007). DOI: 10.1103/physrevlett.99.120501. URL: https://doi.org/10.1103/physrevlett.99.120501.

[60] S. Tanzilli et al. "Highly efficient photon-pair source using periodically poled lithium niobate waveguide." In: *Electronics Letters* 37.1 (2001), p. 26. DOI: 10.1049/el:20010009. URL: https://doi.org/10.1049/el:20010009.

[61] Harald Herrmann et al. "Post-selection free, integrated optical source of non-degenerate, polarization entangled photon pairs." In: *Optics Express* 21.23 (Nov. 2013), p. 27981. DOI: 10.1364/oe.21.027981. URL: https://doi.org/10.1364/oe.21.027981.

[62] Peter J. Mosley et al. "Heralded Generation of Ultrafast Single Photons in Pure Quantum States." In: *Physical Review Letters* 100.13 (Apr. 2008). DOI: 10.1103/physrevlett.100.133601. URL: https://doi.org/10.1103/physrevlett.100.133601.

[63] Yu He et al. "Time-Bin-Encoded Boson Sampling with a Single-Photon Device." In: *Physical Review Letters* 118.19 (May 2017). DOI: 10.1103/physrevlett.118.190501. URL: https://doi.org/10.1103/physrevlett.118.190501.

[64] B. Brecht et al. "Photon Temporal Modes: A Complete Framework for Quantum Information Science." In: *Physical Review X* 5.4 (Oct. 2015). DOI: 10.1103/physrevx.5.041017. URL: https://doi.org/10.1103/physrevx.5.041017.

[65] Benjamin Brecht et al. "From quantum pulse gate to quantum pulse shaper—engineered frequency conversion in nonlinear optical waveguides." In: *New Journal of Physics* 13.6 (June 2011), p. 065029. DOI: 10.1088/1367-2630/13/6/065029. URL: https://doi.org/10.1088/1367-2630/13/6/065029.

[66] Vahid Ansari et al. "Temporal-mode measurement tomography of a quantum pulse gate." In: *Physical Review A* 96.6 (Dec. 2017). DOI: 10.1103/physreva.96.063817. URL: https://doi.org/10.1103/physreva.96.063817.

[67] U. M. Titulaer and R. J. Glauber. "Density Operators for Coherent Fields." In: *Physical Review* 145.4 (May 1966), pp. 1041–1050. DOI: 10.1103/physrev.145.1041. URL: https://doi.org/10.1103/physrev.145.1041.

[68] C. K. Law, I. A. Walmsley, and J. H. Eberly. "Continuous Frequency Entanglement: Effective Finite Hilbert Space and Entropy Control." In: *Physical Review Letters* 84.23 (June

2000), pp. 5304–5307. DOI: 10.1103/physrevlett.84.5304. URL: https://doi.org/10.1103/physrevlett.84.5304.

[69] Peter P. Rohde. "Boson sampling with photons of arbitrary spectral structure." In: *Physical Review A* 91.1 (Jan. 2015). DOI: 10.1103/physreva.91.012307. URL: https://doi.org/10.1103/physreva.91.012307.

[70] He-Liang Huang et al. "Statistical Analysis for Collision-free Boson Sampling." In: *Scientific Reports* 7.1 (Nov. 2017). DOI: 10.1038/s41598-017-15596-y. URL: https://doi.org/10.1038/s41598-017-15596-y.

[71] Antoine Monmayrant, Sébastien Weber, and Béatrice Chatel. "A newcomer's guide to ultrashort pulse shaping and characterization." In: *Journal of Physics B: Atomic, Molecular and Optical Physics* 43.10 (May 2010), p. 103001. DOI: 10.1088/0953-4075/43/10/103001. URL: https://doi.org/10.1088/0953-4075/43/10/103001.

[72] Malte Avenhaus et al. "Fiber-assisted single-photon spectrograph." In: *Optics Letters* 34.18 (Sept. 2009), p. 2873. DOI: 10.1364/ol.34.002873. URL: https://doi.org/10.1364/ol.34.002873.

[73] Frank Schlawin, Konstantin E. Dorfman, and Shaul Mukamel. "Entangled Two-Photon Absorption Spectroscopy." In: *Accounts of Chemical Research* 51.9 (Sept. 2018), pp. 2207–2214. DOI: 10.1021/acs.accounts.8b00173. URL: https://doi.org/10.1021/acs.accounts.8b00173.

[74] Rolf Landauer. "Information is Physical." In: *Physics Today* 44.5 (May 1991), pp. 23–29. DOI: 10.1063/1.881299. URL: https://doi.org/10.1063/1.881299.

[75] R. Zamir. "A proof of the Fisher information inequality via a data processing argument." In: *IEEE Transactions on Information Theory* 44.3 (May 1998), pp. 1246–1250. DOI: 10.1109/18.669301. URL: https://doi.org/10.1109/18.669301.

[76] Leonard J. Savage. "On Rereading R. A. Fisher." In: *The Annals of Statistics* 4.3 (May 1976), pp. 441–500. DOI: 10.1214/aos/1176343456. URL: https://doi.org/10.1214/aos/1176343456.

[77] John W. Pratt. "F. Y. Edgeworth and R. A. Fisher on the Efficiency of Maximum Likelihood Estimation." In: *The Annals of Statistics* 4.3 (May 1976), pp. 501–514. DOI: 10.1214/aos/1176343457. URL: https://doi.org/10.1214/aos/1176343457.

[78] D. PETZ and C. GHINEA. "INTRODUCTION TO QUANTUM FISHER INFORMATION." In: *Quantum Probability and Related Topics*. WORLD SCIENTIFIC, Jan. 2011. DOI: 10.1142/9789814338745_0015. URL: https://doi.org/10.1142/9789814338745_0015.

[79] MATTEO G. A. PARIS. "QUANTUM ESTIMATION FOR QUANTUM TECHNOLOGY." In: *International Journal of Quantum Information* 07.supp01 (Jan. 2009), pp. 125–137. DOI: 10.1142/s0219749909004839. URL: https://doi.org/10.1142/s0219749909004839.

[80] Carl W. Helstrom. "Quantum detection and estimation theory." In: *Journal of Statistical Physics* 1.2 (1969), pp. 231–252. DOI: 10.1007/bf01007479. URL: https://doi.org/10.1007/bf01007479.

[81] Alexander S. Holevo. *Statistical Structure of Quantum Theory*. Springer Berlin Heidelberg, 2001. DOI: 10.1007/3-540-44998-1. URL: https://doi.org/10.1007/3-540-44998-1.

[82] V. Giovannetti. "Quantum-Enhanced Measurements: Beating the Standard Quantum Limit." In: *Science* 306.5700 (Nov. 2004), pp. 1330–1336. DOI: 10.1126/science.1104149. URL: https://doi.org/10.1126/science.1104149.

[83] Vittorio Giovannetti, Seth Lloyd, and Lorenzo Maccone. "Quantum Metrology." In: *Physical Review Letters* 96.1 (Jan. 2006). DOI: 10.1103/physrevlett.96.010401. URL: https://doi.org/10.1103/physrevlett.96.010401.

[84] Jose Andrade-Garda, ed. *Basic Chemometric Techniques in Atomic Spectroscopy*. Royal Society of Chemistry, 2013. DOI: 10.1039/9781849739344. URL: https://doi.org/10.1039/9781849739344.

[85] R Whittaker et al. "Absorption spectroscopy at the ultimate quantum limit from single-photon states." In: *New Journal of Physics* 19.2 (Feb. 2017), p. 023013. DOI: 10.1088/1367-2630/aa5512. URL: https://doi.org/10.1088/1367-2630/aa5512.

[86] Jonathan P. Dowling. "Quantum optical metrology – the lowdown on high-NooN states." In: *Contemporary Physics* 49.2 (Mar. 2008), pp. 125–143. DOI: 10.1080/00107510802091298. URL: https://doi.org/10.1080/00107510802091298.

[87] Rafal Demkowicz-Dobrzański, Marcin Jarzyna, and Jan Kołodyński. "Quantum Limits in Optical Interferometry." In: *Progress in Optics*. Elsevier, 2015, pp. 345–435. DOI: 10.1016/bs.po.2015.02.003. URL: https://doi.org/10.1016/bs.po.2015.02.003.

[88] Jonathan P. Dowling and Kaushik P. Seshadreesan. "Quantum Optical Technologies for Metrology, Sensing, and Imaging." In: *Journal of Lightwave Technology* 33.12 (June 2015), pp. 2359–2370. DOI: 10.1109/jlt.2014.2386795. URL: https://doi.org/10.1109/jlt.2014.2386795.

[89] G.M D'Ariano, C Macchiavello, and M.F Sacchi. "On the general problem of quantum phase estimation." In: *Physics Letters A* 248.2-4 (Nov. 1998), pp. 103–108. DOI: 10.1016/s0375-9601(98)00702-6. URL: https://doi.org/10.1016/s0375-9601(98)00702-6.

[90] G. J. Milburn, Wen-Yu Chen, and K. R. Jones. "Hyperbolic phase and squeeze-parameter estimation." In: *Physical Review A* 50.1 (July 1994), pp. 801–804. DOI: 10.1103/physreva.50.801. URL: https://doi.org/10.1103/physreva.50.801.

[91] G M DrquotAriano, M G A Paris, and P Perinotti. "To take a (binary) decision yourquotd better use entanglement." In: *Journal of Optics B: Quantum and Semiclassical Optics* 4.4

(Aug. 2002), S277–S280. DOI: 10.1088/1464-4266/4/4/305. URL: https://doi.org/10.1088/1464-4266/4/4/305.

[92] Zhengfeng Ji et al. "Parameter Estimation of Quantum Channels." In: *IEEE Transactions on Information Theory* 54.11 (Nov. 2008), pp. 5172–5185. DOI: 10.1109/tit.2008.929940. URL: https://doi.org/10.1109/tit.2008.929940.

[93] Akio Fujiwara. "Quantum channel identification problem." In: *Physical Review A* 63.4 (Mar. 2001). DOI: 10.1103/physreva.63.042304. URL: https://doi.org/10.1103/physreva.63.042304.

[94] *Theory of Point Estimation*. Springer-Verlag, 1998. DOI: 10.1007/b98854. URL: https://doi.org/10.1007/b98854.

[95] Hugo Leiva. "A Generalization of Cramer's Rule." In: *Advances in Linear Algebra and Matrix Theory* 05.04 (2015), pp. 156–166. DOI: 10.4236/alamt.2015.54016. URL: https://doi.org/10.4236/alamt.2015.54016.

[96] Alexander Holevo. *Probabilistic and Statistical Aspects of Quantum Theory*. Edizioni della Normale, 2011. DOI: 10.1007/978-88-7642-378-9. URL: https://doi.org/10.1007/978-88-7642-378-9.

[97] Samuel L. Braunstein and Carlton M. Caves. "Statistical distance and the geometry of quantum states." In: *Physical Review Letters* 72.22 (May 1994), pp. 3439–3443. DOI: 10.1103/physrevlett.72.3439. URL: https://doi.org/10.1103/physrevlett.72.3439.

[98] Samuel L. Braunstein, Carlton M. Caves, and G.J. Milburn. "Generalized Uncertainty Relations: Theory, Examples, and Lorentz Invariance." In: *Annals of Physics* 247.1 (Apr. 1996), pp. 135–173. DOI: 10.1006/aphy.1996.0040. URL: https://doi.org/10.1006/aphy.1996.0040.

[99] Manuel Gessner, Luca Pezzè, and Augusto Smerzi. "Efficient entanglement criteria for discrete, continuous, and hybrid variables." In: *Physical Review A* 94.2 (Aug. 2016). DOI: 10.1103/physreva.94.020101. URL: https://doi.org/10.1103/physreva.94.020101.

[100] Luca Pezzé and Augusto Smerzi. "Entanglement, Nonlinear Dynamics, and the Heisenberg Limit." In: *Physical Review Letters* 102.10 (Mar. 2009). DOI: 10.1103/physrevlett.102.100401. URL: https://doi.org/10.1103/physrevlett.102.100401.

[101] Manuel Gessner, Luca Pezzè, and Augusto Smerzi. "Resolution-enhanced entanglement detection." In: *Physical Review A* 95.3 (Mar. 2017). DOI: 10.1103/physreva.95.032326. URL: https://doi.org/10.1103/physreva.95.032326.

[102] Richard D. Gill and Serge Massar. "State estimation for large ensembles." In: *Physical Review A* 61.4 (Mar. 2000). DOI: 10.1103/physreva.61.042312. URL: https://doi.org/10.1103/physreva.61.042312.

[103] Sammy Ragy, Marcin Jarzyna, and Rafał Demkowicz-Dobrzański. "Compatibility in multiparameter quantum metrology." In: *Physical Review A* 94.5 (Nov. 2016). DOI: 10.1103/physreva.94.052108. URL: https://doi.org/10.1103/physreva.94.052108.

[104] Richard D. Gill and Mădălin I. Guţă. "On asymptotic quantum statistical inference." In: *Institute of Mathematical Statistics Collections*. Institute of Mathematical Statistics, 2013, pp. 105–127. DOI: 10.1214/12-imscoll909. URL: https://doi.org/10.1214/12-imscoll909.

[105] Mihai D. Vidrighin et al. "Joint estimation of phase and phase diffusion for quantum metrology." In: *Nature Communications* 5.1 (Sept. 2014). DOI: 10.1038/ncomms4532. URL: https://doi.org/10.1038/ncomms4532.

[106] Matteo Altorio et al. "Metrology with Unknown Detectors." In: *Physical Review Letters* 116.10 (Mar. 2016). DOI: 10.1103/physrevlett.116.100802. URL: https://doi.org/10.1103/physrevlett.116.100802.

[107] C. Helstrom and R. Kennedy. "Noncommuting observables in quantum detection and estimation theory." In: *IEEE Transactions on Information Theory* 20.1 (Jan. 1974), pp. 16–24. DOI: 10.1109/tit.1974.1055173. URL: https://doi.org/10.1109/tit.1974.1055173.

[108] H. Yuen and M. Lax. "Multiple-parameter quantum estimation and measurement of nonselfadjoint observables." In: *IEEE Transactions on Information Theory* 19.6 (Nov. 1973), pp. 740–750. DOI: 10.1109/tit.1973.1055103. URL: https://doi.org/10.1109/tit.1973.1055103.

[109] G Chiribella, G M D'Ariano, and M F Sacchi. "Joint estimation of real squeezing and displacement." In: *Journal of Physics A: Mathematical and General* 39.9 (Feb. 2006), pp. 2127–2142. DOI: 10.1088/0305-4470/39/9/009. URL: https://doi.org/10.1088/0305-4470/39/9/009.

[110] Yu Watanabe, Takahiro Sagawa, and Masahito Ueda. "Optimal Measurement on Noisy Quantum Systems." In: *Physical Review Letters* 104.2 (Jan. 2010). DOI: 10.1103/physrevlett.104.020401. URL: https://doi.org/10.1103/physrevlett.104.020401.

[111] Alex Monras and Fabrizio Illuminati. "Measurement of damping and temperature: Precision bounds in Gaussian dissipative channels." In: *Physical Review A* 83.1 (Jan. 2011). DOI: 10.1103/physreva.83.012315. URL: https://doi.org/10.1103/physreva.83.012315.

[112] Philip J. D. Crowley et al. "Tradeoff in simultaneous quantum-limited phase and loss estimation in interferometry." In: *Physical Review A* 89.2 (Feb. 2014). DOI: 10.1103/physreva.89.023845. URL: https://doi.org/10.1103/physreva.89.023845.

[113] M. G. Genoni et al. "Optimal estimation of joint parameters in phase space." In: *Physical Review A* 87.1 (Jan. 2013). DOI: 10.1103/physreva.87.012107. URL: https://doi.org/10.1103/physreva.87.012107.

[114] K Matsumoto. "A new approach to the Cramér-Rao-type bound of the pure-state model." In: *Journal of Physics A: Mathematical and General* 35.13 (Mar. 2002), pp. 3111–3123. DOI: 10.1088/0305-4470/35/13/307. URL: https://doi.org/10.1088/0305-4470/35/13/307.

[115] Cyril Vaneph, Tommaso Tufarelli, and Marco G. Genoni. "Quantum estimation of a two-phase spin rotation." In: *Quantum Measurements and Quantum Metrology* 1 (Jan. 2013). DOI: 10.2478/qmetro-2013-0003. URL: https://doi.org/10.2478/qmetro-2013-0003.

[116] Berihu Teklu, Stefano Olivares, and Matteo G A Paris. "Bayesian estimation of one-parameter qubit gates." In: *Journal of Physics B: Atomic, Molecular and Optical Physics* 42.3 (Jan. 2009), p. 035502. DOI: 10.1088/0953-4075/42/3/035502. URL: https://doi.org/10.1088/0953-4075/42/3/035502.

[117] Stefano Olivares and Matteo G A Paris. "Bayesian estimation in homodyne interferometry." In: *Journal of Physics B: Atomic, Molecular and Optical Physics* 42.5 (Feb. 2009), p. 055506. DOI: 10.1088/0953-4075/42/5/055506. URL: https://doi.org/10.1088/0953-4075/42/5/055506.

[118] Magdalena Szczykulska, Tillmann Baumgratz, and Animesh Datta. "Reaching for the quantum limits in the simultaneous estimation of phase and phase diffusion." In: *Quantum Science and Technology* 2.4 (Aug. 2017), p. 044004. DOI: 10.1088/2058-9565/aa7fa9. URL: https://doi.org/10.1088/2058-9565/aa7fa9.

[119] Christian Schmid et al. "Quantum teleportation and entanglement swapping with linear optics logic gates." In: *New Journal of Physics* 11.3 (Mar. 2009), p. 033008. DOI: 10.1088/0031-8949/11/3/033008. URL: https://doi.org/10.1088/0031-8949/11/3/033008.

[120] N. K. Langford et al. "Demonstration of a Simple Entangling Optical Gate and Its Use in Bell-State Analysis." In: *Physical Review Letters* 95.21 (Nov. 2005). DOI: 10.1103/physrevlett.95.210504. URL: https://doi.org/10.1103/physrevlett.95.210504.

[121] T Nagata et al. "Analysis of experimental error sources in a linear-optics quantum gate." In: *New Journal of Physics* 12.4 (Apr. 2010), p. 043053. DOI: 10.1088/1367-2630/12/4/043053. URL: https://doi.org/10.1088/1367-2630/12/4/043053.

[122] J. S. Lundeen et al. "Tomography of quantum detectors." In: *Nature Physics* 5.1 (Nov. 2008), pp. 27–30. DOI: 10.1038/nphys1133. URL: https://doi.org/10.1038/nphys1133.

[123] C. A. Parvin. "An Introduction to Multivariate Statistical Analysis, 3rd ed. T.W. Anderson. Hoboken, NJ: John Wiley & Sons, 2003, 742 pp., 99.95, hardcover.ISBN0 – 471 – 36091 – 0.." In: *Clinical Chemistry* 50.5 (May 2004), pp. 981–982. DOI: 10.1373/clinchem.2003.025684. URL: https://doi.org/10.1373/clinchem.2003.025684.

[124] J. D. Franson. "Nonlocal cancellation of dispersion." In: *Physical Review A* 45.5 (Mar. 1992), pp. 3126–3132. DOI: 10.1103/physreva.45.3126. URL: https://doi.org/10.1103/physreva.45.3126.

[125] J. D. Franson. "Nonclassical nature of dispersion cancellation and nonlocal interferometry." In: *Physical Review A* 80.3 (Sept. 2009). DOI: 10.1103/physreva.80.032119. URL: https://doi.org/10.1103/physreva.80.032119.

[126] So-Young Baek, Young-Wook Cho, and Yoon-Ho Kim. "Nonlocal dispersion cancellation using entangled photons." In: *Optics Express* 17.21 (Oct. 2009), p. 19241. DOI: 10.1364/oe.17.019241. URL: https://doi.org/10.1364/oe.17.019241.

[127] S. Kullback and R. A. Leibler. "On Information and Sufficiency." In: *The Annals of Mathematical Statistics* 22.1 (Mar. 1951), pp. 79–86. DOI: 10.1214/aoms/1177729694. URL: https://doi.org/10.1214/aoms/1177729694.